CENTRO DE INVESTIGACIÓN Y DE ESTUDIOS AVANZADOS
DEL INSTITUTO POLITÉCNICO NACIONAL

Unidad Zacatenco

Departamento de Control Automático

"Diseño y control cooperativo de vehículos cudrirotor para el transporte de una carga"

TESIS

Que presenta

Jossué Cariño Escobar

Para obtener el grado de

Doctor en Ciencias

EN LA ESPECIALIDAD DE

Control Automático

Directores de Tesis:

Dr. Rogelio Lozano Leal

Dr. Moisés Bonilla Estrada

Ciudad de México **Enero, 2020**

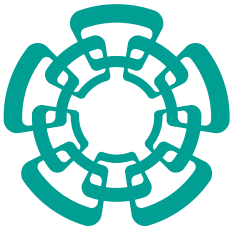

CENTRO DE INVESTIGACIÓN Y DE ESTUDIOS AVANZADOS
DEL INSTITUTO POLITÉCNICO NACIONAL

Unidad Zacatenco

Submitted to the Department of Automatic Control

"Design and Cooperative Control of Quadcopter Vehicles for the Translation of a Load"

THESIS

Presented by

Jossué Cariño Escobar

in partial fulfillment of the requirements for the degree of

Doctor of Philosophy in Automatic Control

Thesis supervisors:

Rogelio Lozano Leal
Director of UMI-LAFMIA Laboratory

Moisés Bonilla Estrada
Associate Professor

México City **January, 2020**

Agradecimientos

Le agradezco al Consejo Nacional de Ciencia y Tecnología (CONACYT) por haberme brindado su apoyo en recursos económicos para la realización de éste posgrado y una estancia de investigación. Sin su programa de becas, tanto nacionales como de movilidad, no podría haber terminado éste doctorado.

También agradezco al Centro de Investigación y de Estudios Avanzados del Instituto Politécnico Nacional (CINVESTAV) por su apoyo económico y en recursos para la estancia de invectigación realizada en el extranjero.

Le estoy muy agradecido al Doctor Rogelio Lozano Leal, por haberme tenido tanta paciencia durante mis primeras publicaciones y por darme ánimos cuándo más los necesito. También por tener la sabiduría de saberme dar mi espacio cuándo era necesario, y de enfocarme cuándo era preciso.

Al Doctor Moisés Bonilla Estrada le agradezco por haberme acogido en el departamento de Control Automático y por haberme apoyado durante éste trayecto.

Al Doctor Pedro Castillo García, por no haber perdido el contacto y siempre estar dispuesto a impulsarme para destacar, a las buenas o a las malas. También me gustaría agradezer la confianza que me ha brindado a lo largo de los años, y espero que éste sea un pilar más que demuestre que ésta bien posicionada.

Le agradezco a mi madre, María Leonor Escobar Escobar, que me ha ayudado a encontrar éste camino, a veces de formas menos directas que otras, pero simepre con las mejores de las intenciones.

Le agradezco a mi padre, Rubén Isaac Cariño Garay por haberme mostrado de dónde proviene la verdadera fortaleza de una persona y de dónde sacar esa infinidad de paciencia que siempre lo ha caracterizado.

A mi hermano, Rodrigo Cariño Escobar, por ser mi compañero por todos éstos años y espero que se la siga pasando viajando y buscando su propia fortuna a dónde los vientos de su espíritu lo lleven.

A mi hermano, Rubén Isaac Cariño Escobar, por todos los consejos que me ha dado y para que siga excarvando su propio lugar en ésta tierra tan llena de oportunidades.

A mi amada, María Fernanda Martínez Fernández de Castro, por haber hecho de éstos años los más significativos de mi vida. Mientras me ayudabas a desenvolver mis ideas para que el mundo las pudiera ver, también me ayudaste a revelar mi carácter y decidimos juntos atarnos a ésta vida. Yo creí en ti y ahora tú crees en mí, mi amor.

Para mis amigos, que me gustaría dedicarles a cada uno una línea en éste texto, que de una u otra forma fue la semilla de dónde salieron las ideas entre conversaciones y risa. Que su camino sea menos turbulento que el mío y con más alegría de ser posible.

Careful. We don't want to learn from this.

Bill Watterson, Calvin and Hobbes

"Do you know, I always thought Unicorns were fabulous monsters, too? I never saw one alive before"
"Well, now that we have seen each other," said the Unicorn, "If you'll believe in me, I'll believe in you."

Lewis Carroll, Through the Looking-Glass

“Diseño y control cooperativo de vehículos cudrirotor para el transporte de una carga”

Que presenta

Jossué Cariño Escobar

Sometido al departamento de Control automático

para obtener el grado de Doctor en Ciencias

EN LA ESPECIALIDAD DE

Control Automático

Resumen

El presente trabajo propone una nueva e innovadora forma para transportar una carga usando vehículos aéreos no tripulados (UAV) en un esquema de control cooperativo. La configuración elegida es la suspención de la carga usando cables debido a su facilidad de implementación y a su bajo peso agregado.

El diseño del controlador cooperativo se basa en la teoría de pasividad de sistemas dinámicos y sus propiedades energéticas. Ésto permite un amplio rango de opciones de diseño, incluyendo comunicación implícita, un control descentralizado y algunas garantías en caso de un fallo en la red de comunicación y sensores. Los vehículos utilizados sólo requieren ser capaces de seguir una trayectoria basada en la fuerza del agente. Un controlador para un sistema de aterrizaje y despegue vertical en un plano (PVTOL) también es propuesto para ser implementado en el control cooperativo.

Los resultados han sido corroborados usando simulaciones numéricas y con una validación experimental.

Palabras Clave

UAV, Control cooperativo, Control basado en pasividad, Comunicación implícita, Manipulación aérea

Design and Cooperative Control of Quadcopter Vehicles for the Translation of a Load

by

Jossué Cariño Escobar

Submitted to the Department of Automatic Control
on January 1, 2020, in partial fulfillment of the
requirements for the degree of
Doctor of Philosophy in Automatic Control

Abstract

This thesis proposes an innovative way of transporting a load using unmanned aerial vehicles (UAVs) in a cooperative control scheme. A slung-load configuration is chosen because of its ease of implementation and low weight.

The cooperative controller design is based on passivity and energy properties of the system. It allows for a wide range of design options, including implicit communication, decentralized control and some fail-safe guarantees in case the communication/sensor network stops working. The vehicles used only need to be able to track a force trajectory. A controller for a PVTOL system is also proposed in order to implement it with the proposed cooperative control scheme if required.

The results are corroborated using numerical simulations and with an experimental validation.

Keywords

UAV, Cooperative Control, Passivity-based Control, Implicit Communication, Aerial Manipulation

Thesis Supervisor: Rogelio Lozano Leal
Title: Director of UMI-LAFMIA Laboratory

Thesis Supervisor: Moisés Bonilla Estrada
Title: Associate Professor

Contents

List of Figures

List of Tables

Notation

$a \in \mathbb{R}_+$	A non-negative scalar
$g \in \mathbb{R}_+$	The acceleration of the gravity in scalar form
$\vec{a}_. \in \mathbb{R}^n$	A vector of size n
$\vec{g}_. \in \mathbb{R}^2$	The gravity in vector form in two dimensions
$\vec{g}_. \in \mathbb{R}^3$	The gravity in vector form in three dimensions
$\vec{a}_. \in \mathbb{R}^n \rightarrow a_{i,.}$	The component i of a vector of size n
$\vec{0}_n \in \mathbb{R}^n$	A vector of size n whose elements are all 0
$A \in \mathbb{R}^{m \times n}$	A matrix of size $m \times n$
$I_n \in \mathbb{R}^{n \times n}$	An identity matrix of size $n \times n$
$diag\{a_0, a_1, ..., a_n\} \in \mathbb{R}^{n \times n}$	A square matrix of size $n \times n$ whose diagonal elements are $\{a_0, a_1, ..., a_n\}$
$\overline{0}_{m \times n} \in \mathbb{R}^{m \times n}$	A matrix of size $m \times n$ whose elements are all 0
$q \in \mathbb{H}$	A quaternion variable
$:=$	Definition
$\Omega_.$	A vector space set
$m_.$	Mass of a vehicle or an object
$\omega_.$	Angular velocity or a motor, rigid body, etc.
$k_.$	A gain, usually positive and used in control laws
$k_{m.,.}$	A positive motor gain, used to calculate the thrust of motors w.r.t. their speed
$K \in \mathbb{R}_+^{m \times n}$	A matrix of size $m \times n$ that contains positive gain parameters

$\dot{a} := \frac{d}{dt}a(t)$	Differentiation with respect to time
$\ddot{a} := \frac{d^2}{dt^2}a(t)$	Second differentiation with respect to time
$a^{(n)} := \frac{d^n}{dt^n}a(t)$	N-th differentiation with respect to time
$\frac{\partial}{\partial b}a$	Partial differentiation of a with respect to variable $b \in \mathbb{R}^n$
$\frac{\partial^2}{\partial b^2}a$	Second partial differentiation of a with respect to variable $b \in \mathbb{R}^n$

Acronyms

UAV	Unmanned Aerial Vehicles
DoF	Degree of Freedom
PVTOL	Planar Vertical Take-Off and Landing
LQR	Linear-Quadratic Regulator
IMU	Inertial Measurement Unit
3D	Three Dimensional
2D	Two Dimensional
w.r.t.	[...]with respect to[...]

Chapter 1

Introduction

The problem of transportation and logistics has always played a central role in society and economics. The fact is that there exists a wide variety of means of transportation. From ground vehicles like trucks and trains, to maritime transportation using freighters and ships, to aerial transportation in planes and helicopters. Even rockets can be considered a means of displacing objects from one place to another. This bears to ask the question, why are there so many of them? The easiest answer is that society has different needs and different constraints, and the means of transportation are as diverse as the things we are trying to transport. It is not the same to displace a letter from one country to another than millions of people from their homes to their works. The fact is that society will always have a need to ship something in different times and through different places.

This work presents yet another way to transfer objects from one point to another. However, the method presented here takes advantage of some technological achievements that have been developing in recent times in order to present an innovative way of doing it in the hopes that it will be used in one of the many other methods there are for the advancement of humanity. All this starts with one of the most interesting technologies of our time, unmanned aerial vehicles.

1.1 Unmanned Aerial Vehicles

The term unmanned aerial vehicle (UAV) has a very specific meaning in the context of automatic control research, but it can be substituted by the word "drone" for the general public. In effect, most people think of those small toys that one can buy in almost any store nowadays, but they do not realize that drones have permeated many of the layers of industrial automation in recent years. This type of autonomous vehicles has seen a rise in popularity, and not only as a didactic novelty. There has been a growing interest in many different types of field for their use, like law enforcement or disaster relief to name a few [Valavanis and Vachtsevanos, 2015]. This in turn makes this kind of vehicles a popular option for the development of innovative control strategies.

UAVs can be divided into two main categories depending on their wing configuration: rotary-wing and fixed-wing drones. Examples of fixed-winged drones include airplanes in all kinds of configurations. These type of UAV are good to travel long distances consuming a minimal amount of energy, but at the expense of longer landing and take-off zones and decreased maneuverability. Rotary-wing drones, on the other hand, include examples such as helicopters and multirotors, which include quadcopters, hexacopters, octacopters, etc. These types of UAVs have excellent maneuverability and can take-off and land in constrained spaces, but at the expense of requiring more energy even to just stay in one place. Depending on the task at hand is the kind of vehicle that is usually used, and there has even been research done in order to make a hybrid vehicle that combines the best characteristics of both of these vehicles without any of the drawbacks, like the works of [Cronin, 2019], [Joshi et al., 2019] and [Belokon et al., 2019], to name a few.

However, recent areas of research for UAV applications has focused on expanding the range of tasks that already existing platforms can achieve. One such territory is the aerial manipulation field, which includes, perching, grasping, positioning tasks, among others. These types of applications have seen a lot of interest in recent years because it encourages physical interaction of the UAV with its surrounding environment [Khamseh et al., 2018], which enables them to be used in a wider and more complex variety of tasks.

1.2 Aerial Manipulation and Transportation using UAVs

Recent advances in electronic sensors, power storage and electric motor efficiency have contributed to the idea that drones should be used in tasks than involve physical interaction with their surroundings. The fact that UAVs do not require extra equipment dedicated to the safety of a pilot means that they can potentially go into hazardous or unreachable places without compromising the safety of any human life and at a potential lower cost. This is the main focus of the field of aerial manipulation.

Some examples of aerial manipulation are as simple as a stick protruding from the drone in order to touch and move objects, to something as complex as kinematic chains made out of extremely precise motors.

The fact that UAVs do not require extra equipment dedicated to the safety of a pilot means that more weight capacity can be used for lifting and transporting the load. The interest of using UAVs in commercial and industrial applications has been focused on the passive perception and monitoring of the environment, like inspection, video capture, surveillance, ... Recent research for UAV applications has focused on expanding this range of tasks like the aerial manipulation field, which includes, perching, grasping and positioning tasks, among others. These types of applications have seen a lot of interest in recent years because it encourages physical interaction of the UAV with its surrounding environment [Khamseh et al., 2018], which enables them to be used in a wider variety of tasks. However, the most common solutions to the aerial manipulation problem usually mount a gripper or robotic arm to the UAV[Ruggiero et al., 2018]. Some examples of this can be seen in works where the problem of grasping and perching are addressed using light-weight and low complexity grippers [Mellinger et al., 2011] [Backus et al., 2014]. Another way to address the problem is by means of bio-inspired designs manipulator arms for aerial griping [Thomas et al., 2014] [ASME, 2013]. There are many works that propose a solution to manipulation tasks using a robotic arm attached to quadcopters [Kim et al., 2013] [Orsag et al., 2014] [Ramon Soria et al., 2019]. Some tasks require more complexity for the kind of manipulation required, in which case a common solution is to add more manipulators [Yu et al., 2019] [Suarez et al., 2019] or more complex ones [Danko and Oh,

2013] [Cano et al., 2013] [Suarez et al., 2015] [Heredia et al., 2019]. There are others that propose unique platforms designed from the ground-up with aerial manipulation in mind [Nikou et al., 2015]. The advantage of using a dedicated manipulation mechanism is that it adds dexterity to the the aerial manipulation task at the expense of weight. This ultimately increases battery consumption and lowers flight time. In contrast, the use of cables or tether mechanisms, like the ones in [Cruz and Fierro, 2014] [Cruz and Fierro, 2017] and [Foehn et al., 2017], offer an alternative to aerial manipulation tasks with minimal weight gain at the expense of almost non-existent dexterity. For the problem at hand, which is the transportation of a load from one point to another, there is no need for a fine-tuned manipulation, which makes the cable mechanisms a more attractive solution. The configuration that is more widely used is denominated as "slung-load", and consists of carrying the load below the vehicles using a single cable, or a tether mechanism.

1.3 Cooperative Transportation using UAVs

Figure 1-1: An example of a position-based control of a swarm of drones

One of the first questions that arises when dealing with a slung-load transport system comes from the choice of using a single vehicle like in [Pereira et al., 2016] [Cruz and Fierro, 2014] [Notter et al., 2016] [Cruz and Fierro, 2017] [Foehn et al., 2017] or multiple vehicles like in [Maza et al., 2009] [Aghdam et al., 2016] [SAYYAADI and SOLTANI,

2018] or [Shirani et al., 2019]. The single vehicle approach allows a simpler control strategy to be used at the expense of flexibility, as this types of vehicles are often designed with a very specific type of load in mind. A cooperative approach has the advantage that the number of agents can be chosen depending on the characteristics of the load, and not the other way around. The drawback is that the interaction and cooperation makes for more complex control schemes in general. An example of the position control of various vehicles (called swarm in this case) can be seen in Figure 1-1

Figure 1-2: An example of a cooperative scheme to build a structure. Each agent has a simple gripper mechanism and the work is distributed among the agents.

Cooperative schemes can be be classified into centralized and decentralized algorithms. Centralized control algorithms, like the ones presented in [Sreenath and Kumar, 2013] [Masone et al., 2016] and [Manubens et al., 2013], have the advantage that most of the computational resources can be concentrated into a single dedicated vehicle or ground control station. However, this type of configuration heavily relies on the communication among the agents. Figure 1-2 shows an example of a centralized algorithm controlling a group of drones.

Figure 1-3: An example of a cooperative scheme to transport and deploy a cable structure.

On the other hand, decentralized algorithms, like the ones in [Mellinger et al., 2013] and [Rezaee and Abdollahi, 2013], can be considered to be more robust against errors in communication and may even be able to rely on sensors in order to gather information of other agents. This explicit way of exchanging information is known as a sensing and communication network according to [Qu, 2009]. Figure 1-3 shows a couple of quadcopters deploying a cable structure. Recently, there has been a tendency to take advantage of the cable's connection of the agents to the load by considering the effects of this physical interaction as a form of implicit communication, like it was presented in [Tagliabue et al., 2017], [Tognon et al., 2018] and [Gabellieri et al., 2018]. Some examples where implicit

communication could be applied are shown in Figures 1-4 and 1-5. The main advantage of implicit communication is that the control algorithm of each vehicle does not depend directly on the state of the other vehicles, which makes this type of schemes even more robust.

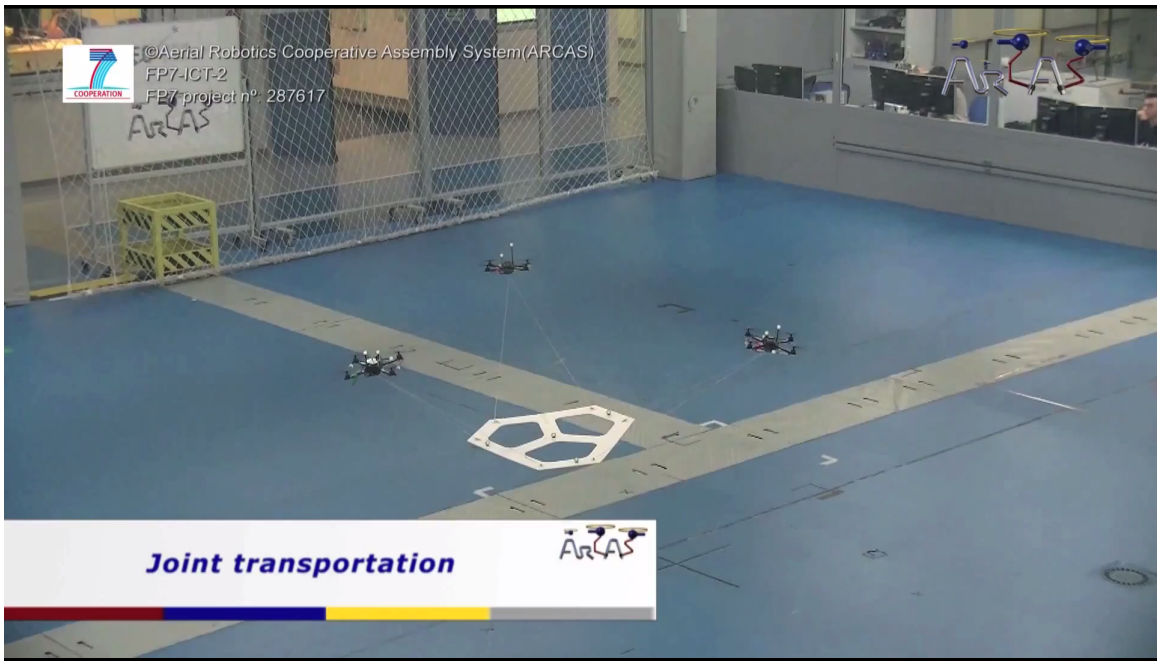

Figure 1-4: An example of aerial manipulation using a tethering mechanism and cables.

Because of its ability to be used for implicit communication, low weight and its simple arrangement, the so called "slung-load" configuration is the method of choice to be used to solve the cooperative transport of a load.

1.4 Objective

The relevance of the transportation problem is being addressed in this work. It was shown how using UAVs for the aerial manipulation is a very attractive research topic because of all the possible applications that could be solved. Some solutions have already been mentioned, but most of them do not take advantage of the modular approach that comes from using a cooperative control scheme. Some works of autonomous cooperative transport were mentioned, but most of them rely on a centralized control center or in a sen-

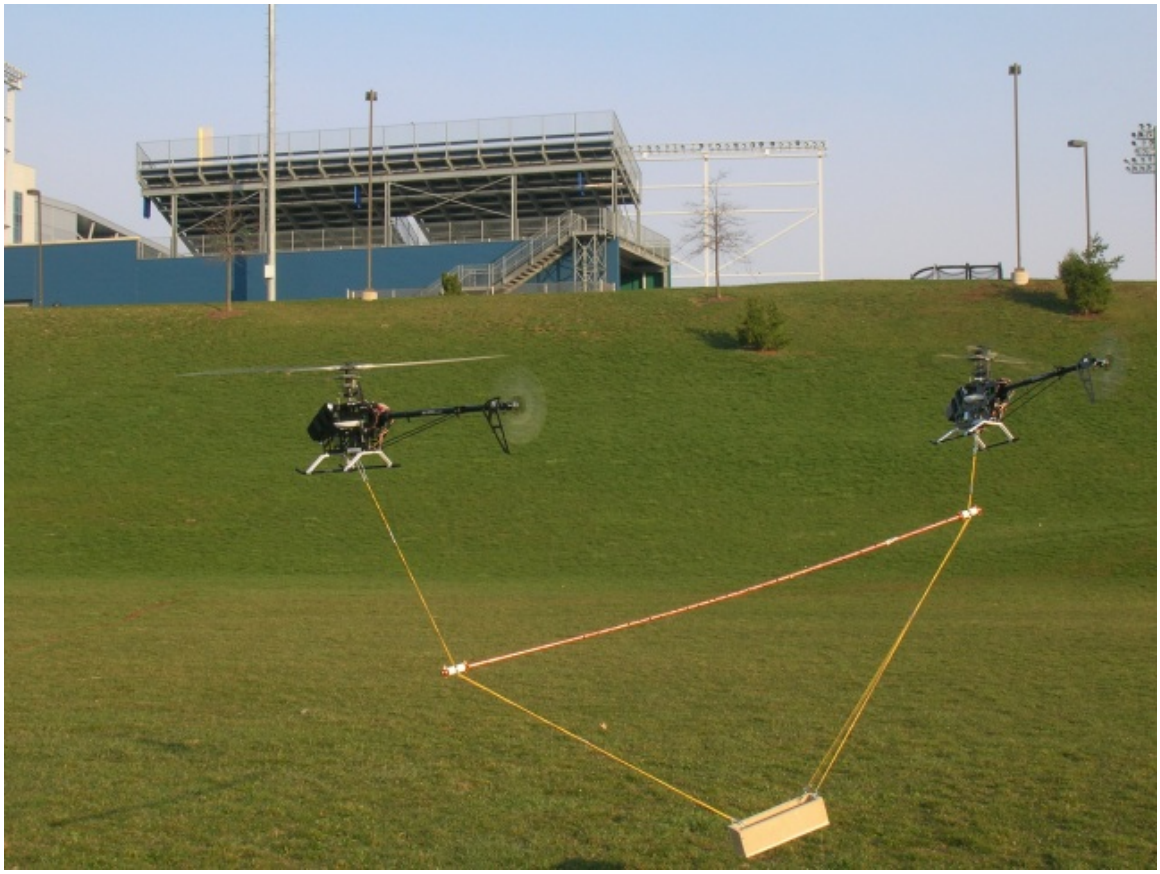

Figure 1-5: An example of a cooperative scheme to transport a load using a cable mechanism with a bar.

sor/communication network. However, the fact of having a physical connection with the load that is transported can have an advantage that not many cooperative transport algorithms use, and that is the possibility of using implicit communication. Almost all of the works that use implicit communication depend on estimating some physical parameters online in order to compensate for them, most notably the ones based on mechanical impedance control.

This work proposes a solution to the cooperative slung-load problem with implicit communication using a passivity-based approach. The design presented here is innovative in that it does not rely on the estimation of online parameters in order to work, its design strategy has a modular approach and was proven to work in a physical system of two quadcopter vehicles.

In Chapter 2, the load transportation scheme is translated into three specific cooperative

control objectives.

The design and corroboration of the main cooperative control scheme is presented in Chapter 4, which assumes that the agents are either fully actuated or its position dynamics are able to be regulated.

In order to comply with this assumption, Chapter 3 presents a control law for the PV-TOL platform that meets all these requirements and can be used in case the need arises to implement such a controller. The proposed cooperative control was implemented on an experimental platform consisting of two quadcopter vehicles and a load in the form of a bar.

The results of the experiment has been displayed and analyzed in Chapter 5.

Finally, the conclusions and future work are shown in Chapter 6

Chapter 2

Problem Statement

The previous chapter introduced the different approaches that have been used in order to solve the transportation problem. In its most basic form, it can be addressed as carrying a load from one point to the other. This simple objective is the basis of many aerial navigation algorithms. However, its implementation can quickly increase in complexity by taking into account various factors like the type of carrying configuration, the shape and weight of the load itself and even the number and type of agents involved. The focus of this chapter is to synthesize and present the transportation problem in such a way that it can later be solved in the following chapters. Chapter 5 shows an experimental validation of the proposed conditions and is a testament of the validity of the hypotheses and simplifications made here.

2.1 Cooperative Control Objective

The type of vehicle considered in this work are quadcopters, which are an underactuated type of UAV that can move in a 3D space. The chosen mechanism is a slung-load configuration and the form of the load considered can be arbitrary, as well as the anchor point for the cables on the load. A free body diagram of this type of arrangement can be seen in Figure 2-1.

The first assumption that is going to be made is that the distance from the center of mass of the load to each anchor point (the $\vec{d}_{\{1,2,\ldots,n\}}$ vectors in Figure 2-1) is not zero. This

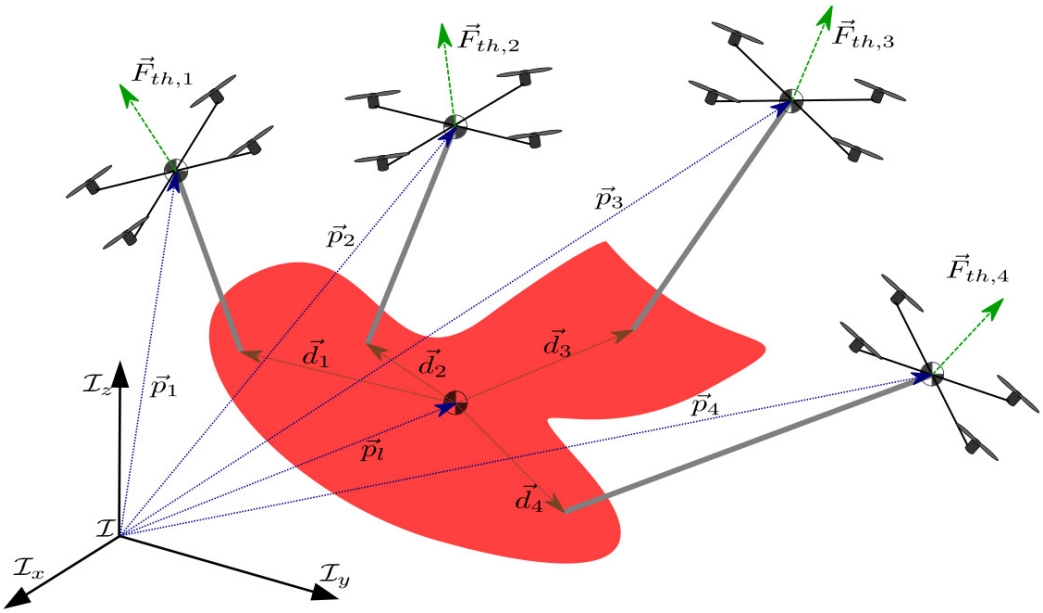

Figure 2-1: Free body diagram of the general form of a cooperative slung-load transport in 3D space using quadcopters with four agents

implies that there is no anchor point at the center of mass of the load. In practice, the configuration of the anchor points can be chosen *a priori* if one uses a tether mechanism in order to help avoid collisions.

Using Figure 2-1 as a reference , the control objective can be stated according to the load's position $\vec{p}_l$ w.r.t. an inertial reference frame $\mathscr{I}$ as

$$t \to \infty \implies \begin{cases} \vec{p}_l \to & \vec{p}_{l,d} \\ \dot{\vec{p}}_l \to & \vec{0} \end{cases} \tag{2.1}$$

Because of the configuration of the slung-load mechanism, the control objective (2.1) can be achieved from the perspective of individual agents. If it can be ensured that the agents converge to a desired position, the load will tends towards a specific position. This can be stated as

$$t \to \infty \implies \begin{cases} \vec{p}_j \to & \vec{p}_{j,d} \\ \dot{\vec{p}}_i \to & \vec{0} \\ \dot{\vec{p}}_l \to & \vec{0} \end{cases} \tag{2.2}$$

for all $i \in \{1,2,...,n\} \setminus \Omega_j$ and for all $j \in \Omega_j \subset \{1,2,...,n\}$ for some nonempty set Ω_j of at least three elements (because of the three dimensions of movement).

The previous definitions are restrictive in the sense that they only allow for a single possible configuration of the final state. Sometimes, it is better to consider that the system arrives to a region of interest. Even the load's orientation is not as relevant, only the position of the center of mass. In these cases, it is better to have an objective *set* instead of a punctual desired state for the control design. The control objective in this case can be generalized in a 3D environment as

Control Objective 2.1.1. *Let $\vec{p}_l \in \mathbb{R}^3$ be the position of the load in the inertial frame $\mathscr{I}$; $\vec{p}_i \in \mathbb{R}^3$ is the position of each agent in the inertial frame $\mathscr{I}$ for all $i \in \{1,2,...,n\}$ agents; $\dot{\vec{p}}_l, \dot{\vec{p}}_i \in \mathbb{R}^3$ is the load's and agent's velocities, respectively; and let $\Omega_d \subset \mathbb{R}^{3+3n}$ be a desired system position set. The objective is to make the load and agent's position converge asymptotically to the desired position set with zero velocity as time tends towards infinity, namely:*

$$t \to \infty \implies \begin{cases} \begin{bmatrix} \vec{p}_l \\ \vec{p}_i \end{bmatrix} \to \Omega_d \\ \begin{bmatrix} \dot{\vec{p}}_l \\ \dot{\vec{p}}_i \end{bmatrix} \to \vec{0} \end{cases} \tag{2.3}$$

□

2.2 Problem Simplification

The transport problem for objective (2.3) can become quite complicated because: the load's swing effects may eventually produce instability in the system as a whole; and it is difficult to estimate the state of the load, like position and velocity, from an external agent's point of

view. In this section some assumptions are made in order to synthesize the system model in a way that will allow a simpler controller design in Chapter 4.

2.2.1 Planar Movement

Moving from an initial point $\vec{p}_{\cdot,0}$ to a desired point $\vec{p}_{\cdot,d}$ in a 3D space can be seen as moving in a plane that is collinear with both points and perpendicular to the ground plane ($\mathscr{I}_x - \mathscr{I}_y$ from Figure 2-1) of the inertial frame. An example of this plane can be seen in Figure 2-2. In this way, the problem can be restated but in a 2D perspective.

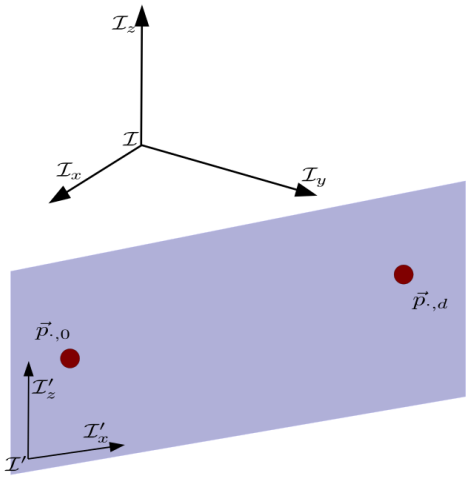

Figure 2-2: Collinear plane for points $\vec{p}_{\cdot,0}$ and $\vec{p}_{\cdot,d}$ w.r.t. the inertial frame $\mathscr{I}$

The quadcopter agents can be modeled as PVTOL vehicles by restricting their movement in this plane. The new inertial plane can be defined as $\mathscr{I}'$.

2.2.2 Rigid Ideal Cables

Cables in aerial manipulation problems can be modeled in many ways, like kinematic chains composed of many rigid links. However, a key aspect of cooperative schemes that use cables is ensuring that the cables stay tense for all agents. Otherwise, the weight of the load is not distributed among the agents. One way of ensuring this by considering or enforcing that the agents and the load's velocity is small enough.

In this work, the cables are modeled as if they were rigid bodies but with despicable mass (practically mass-less). The consequence of choosing the model this way, along with restricting it to a plane as mention in Section 2.2.1, is that the more agents there are, the interaction among them is less realistic as the cables will tend to have forces that tend to compress them. If this would happen in a practical implementation, the cables would sack leaving the connection of the agent with the load "severed". This is the main reason of using two agents instead of more for all the planar implementations of cooperative aerial manipulation.

2.2.3 Bar Load

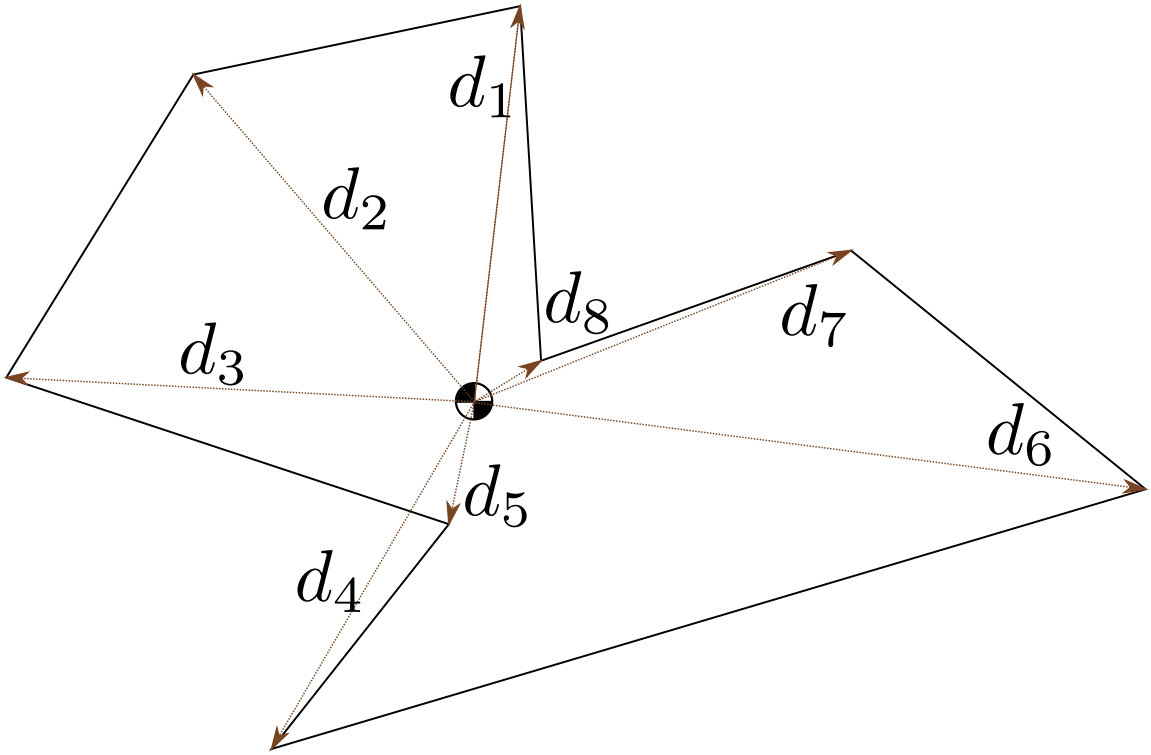

Figure 2-3: Load synthesis diagram using just the anchor points and the center of mass

The load presented on Figure 2-1 has an arbitrary shape. However, there are various ways in which it can be simplified for modeling and control purposes. One such approach is to consider it as a polygon form using just the anchor points and its center of mass. Figure 2-3 shows an example of this kind of synthesis.

Section 2.2.2 presents a compelling argument for using only two agents. With just two anchor points, the load model can be simplified into a bar. In practice, a bar can be used as a tethering mechanism to force this configuration, as can be seen in Image 1-5

2.2.4 Ideal Conditions

The proposed conditions presented in the mathematical models and the external conditions are proposed to be in controlled environments. In this case, the most notable change is the absence of wind or aerodynamic effects like drag. This is done in order to keep the analysis in the cooperative control, as robust and wind effects are better suited for their own consideration. In practical terms, this implies that the results can be used seamlessly in interior or calm environments, but should have a more special consideration in more hostile ones.

2.2.5 Planar Cooperative Control Objective

Using the simplifications proposed above, the objective 2.1.1 can be simplified into

Control Objective 2.2.1. *Let $\vec{p}_l \in \mathbb{R}^2$ be the position of the load in the plane $\mathscr{I}'$ as seen in Figure 2-2; $\vec{p}_i \in \mathbb{R}^2$ is the position of each agent in the inertial frame $\mathscr{I}'$ for all $i \in \{1,2,...,n\}$ agents; $\dot{\vec{p}}_l, \dot{\vec{p}}_i \in \mathbb{R}^2$ is the load's and agent's velocities, respectively; and let $\Omega_d \subset \mathbb{R}^{2+2n}$ be a desired system position set. The objective is to make the load and agent's position converge asymptotically to a desired position set with zero velocity as time tends towards infinity, namely:*

$$t \to \infty \implies \begin{cases} \begin{bmatrix} \vec{p}_l \\ \vec{p}_i \end{bmatrix} \to \Omega_d \\ \begin{bmatrix} \dot{\vec{p}}_l \\ \dot{\vec{p}}_i \end{bmatrix} \to \vec{0} \end{cases} \tag{2.4}$$

□

2.3 Planar Vertical Take-Off and Landing (PVTOL) Control Objective

The cooperative control objective (2.4) does not explicitly include the orientation of each of the agents. In the system presented if Figure 2-1, the direction of the thrust force acting on the PVTOL depends directly on its orientation, and its magnitude is a control input. In order to achieve objective (2.4) in this situation, the following complementary control objective is introduced.

Control Objective 2.3.1. *Let $\vec{F}_{th,i} \in \mathbb{R}^2$ be the thrust of each agent as seen in Figure 2-1 in the inertial frame $\mathscr{I}'$ shown in Figure 2-2; $F_{th,i} \in \mathbb{R}_+$ is the thrust's magnitude for each agent i and is a control input; let u_i be a desired control input force for each agent. The objective is to make the thrust force of each agent converge towards a desired control input force as time tends towards infinity, namely:*

$$t \to \infty \implies \vec{F}_{th,i} \to u_i \tag{2.5}$$

for some desired control input force $u_i \in \mathbb{R}^2$ □

2.4 Summary

In this chapter, the cooperative control problem for a slung-load transportation has been divided into achieving two separate control objectives presented in (2.4) and (2.5). A diagram of the overall control strategy can be seen on Figure 2-4.

The proposed solution for objective (2.5) will be developed in Chapter 3 and then a solution to the control objective (2.4) will be proposed in Chapter 4.

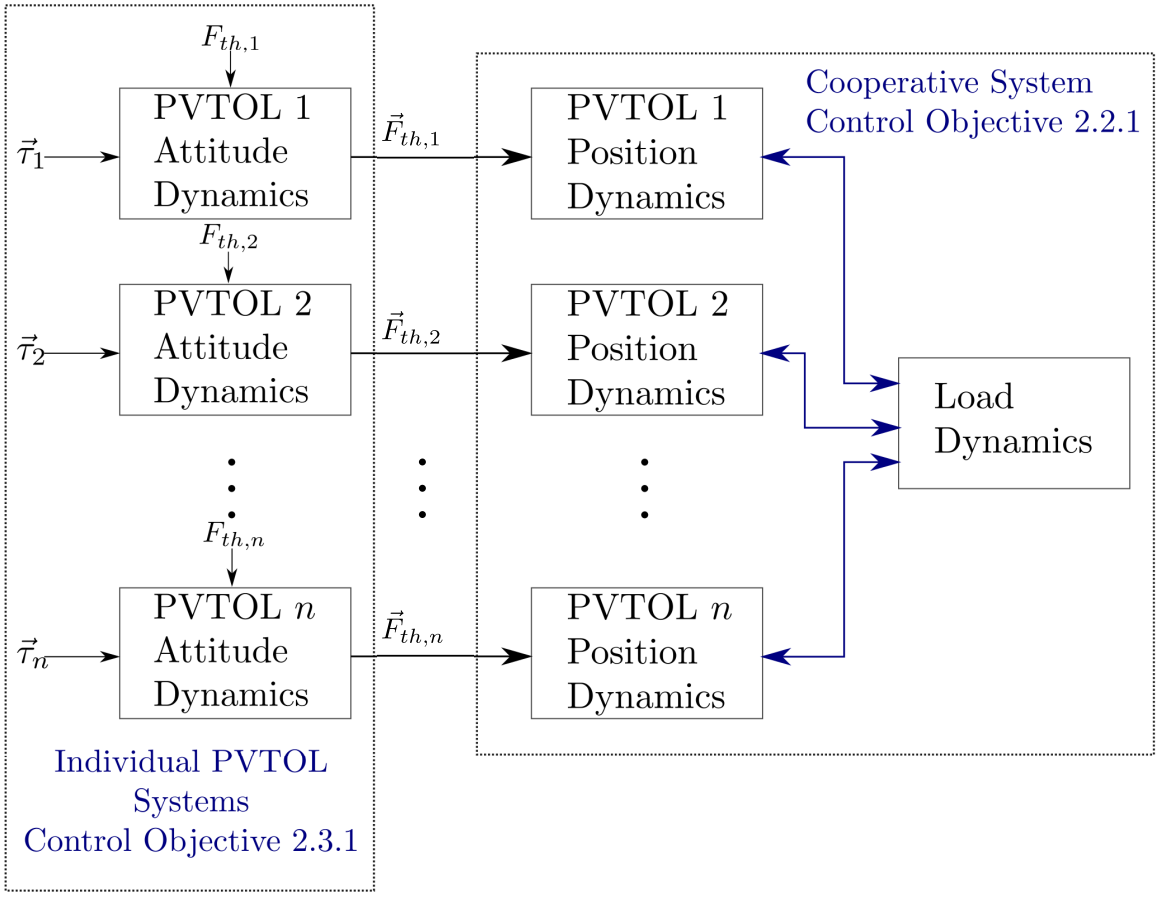

Figure 2-4: A block diagram that shows how the cooperative control using PVTOLs global objective can be separated into two different specific control objectives

Chapter 3

PVTOL Control

In this chapter, a control for the PVTOL platform is presented. The method used is based on the control technique of feedback linearization [Khalil, 2002, Chapter 13]. This is a nonlinear control technique that allows the system to be transformed into a linear system using a feedback function. The advantage of this technique is that it becomes easier to solve the regulation problem for the force of the PVTOL. In other words, this control allows us to shape the form of the force acting on the PVTOL.

This chapter is meant to be used as a complement to the theory and results presented in Chapter 4. However, they are not essential as the cooperative system control can be synthesized with any kind of agent as long as Objective 2.3.1is achieved. A more thorough discussion can be seen on Chapter 4.

This chapter is divided in four main sections. Section 3.1 presents the PVTOL model that is used throughout the controller design and numerialc validations. The control is presented in section 3.2, which in turn separates the design into various parts. In section 3.2.1 the regulation problem to be solved is introduced. Section 3.2.2 extends the model presented in section 3.1 in order to allow the use of an exact linearization methodology as presented in [Khalil, 2015, Chapter 13]. In section 3.2.3, a state feedback control is proposed to solve the regulation problem. In section 3.3 an academic example is presented using a numerical simulation. Finally, section 3.4 is used to present the final thoughts of the presented PVTOL control and make some remarks on how to implement it for the theory presented in Chapter 4. All the proofs of the theorems shown in this chapter can be

addressed in Appendix A

3.1 PVTOL System Model

The PVTOL is considered to behave like a rigid body. The external forces acting on the system are considered to be just the effects of the motors and the gravity. It is considered that the speed is small enough that any aerodynamic effects, such as drag, is negligible in the model. The free body diagram of all the forces considered is shown in figure 3-1 and explained further in this section.

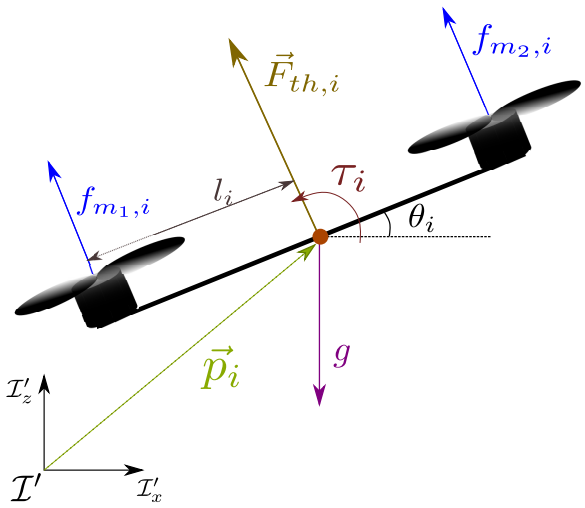

Figure 3-1: The PVTOL free body diagram.

The position of the vehicle $\vec{p}_i := \begin{bmatrix} x & z \end{bmatrix}^T \in \mathbb{R}^2$ and its attitude $\theta_i \in \mathbb{R}$ are referenced w.r.t. the inertial frame $\mathscr{I}'$. The mass of the vehicle m_i and the effect of the gravity g are positive constants.

It is assumed that the velocity of each motor $\omega_j \quad \forall j \in \{1,2\}$ is controllable. The thrust that each motor generates $f_{m_j,i} \in \mathbb{R}_+$ is proportional to the square of the propellers' speed, that is

$$f_{m_i} = k_{m_j}\,\omega_i^2 \qquad \forall i \in \{1,2\} \tag{3.1}$$

for some real constant $k_{m_i} > 0$.

In order to simplify the design and analysis of the control law, the control inputs will be considered as

$$\begin{aligned} u &= f_{m_1} + f_{m_2} \\ \tau &= l\,(f_{m_2} - f_{m_1}) \end{aligned} \tag{3.2}$$

which are the PVTOL thrust force and torque, respectively.

The PVTOL model can the be described by applying a Newton-Euler method to obtain

$$m\ddot{x} = -u\sin\theta \tag{3.3}$$

$$m\ddot{z} = u\cos\theta - mg \tag{3.4}$$

$$J\ddot{\theta} = \tau \tag{3.5}$$

where $J \in \mathbb{R}$ is a positive constant that represents the second inertia moment.

More information about this model can be obtained from [Castillo et al., 2005].

3.2 PVTOL Control Design

In this section, the control for the PVTOL is designed in a four part procedure. The first part explains the objective that the designed control should reach and which will guide the rest of the design process. An extension is given for the PVTOL model presented in section 3.1 in order to transform the higher derivatives of equations (3.3) and (3.4) into an affine system. The altitude dynamics are then extracted from this system and will be used in the stability proof. The next part proposes a feedback linearization control for the new affine system and gives the conditions in which the control strategy is valid. The last part presents a state feedback control in order to stabilize the vehicle in a trajectory tracking scheme and it will be shown that the control algorithm locally stabilizes the PVTOL system.

3.2.1 PVTOL Control Problem Statement

The problem addressed in this work is known as the tracking problem. In order to present a better understanding of it from a theoretical point of view the following definition is needed

The state of the PVTOL vehicle is defined as

$$\hat{\xi} := \begin{bmatrix} x & \dot{x} & z & \dot{z} & \theta & \dot{\theta} \end{bmatrix}^T \tag{3.6}$$

The control objective is then presented as

Control Objective 3.2.1. *Design the control inputs u and τ in equations* (3.3) - (3.5) *such that*

$$\lim_{t\to\infty} \left|\left| \hat{\xi} - \hat{\xi}_d(t) \right|\right| = 0 \tag{3.7}$$

where $\hat{\xi}_d(t) : \mathbb{R} \to \mathbb{R}^6$ is a function that represents the desired trajectory of the vehicle.

If objective 3.2.1 is accomplished, it means that the vehicle is capable of tracking the state $\hat{\xi}_d(t)$.

3.2.2 System Model Extension

The control input u in (3.3) and (3.4) can be extended to include higher order derivatives. In order to do this, the following remark is used.

Remark 3.2.1. *The control input u is considered to be a C^2 function. This implies that $\dot{u}, \ddot{u}$ exist and are continuous.*

Taking into consideration Remark 3.2.1, the differentiation of equations (3.3) and (3.4) w.r.t. time results in

$$m x^{(3)} = m x^{(3)}(u, \theta, \dot{u}, \dot{\theta}) = \quad -\dot{u}\sin\theta - u\dot{\theta}\cos\theta \tag{3.8}$$

$$m z^{(3)} = m z^{(3)}(u, \theta, \dot{u}, \dot{\theta}) = \quad \dot{u}\cos\theta - u\dot{\theta}\sin\theta \tag{3.9}$$

It should be noted that the differentiation presented in (3.9) does not contain a term related to the gravity of the system mg, but equation (3.4) does take it into account for the system model. Equations (3.8) and (3.9) can be differentiated once again w.r.t. time, which results in

$$mx^{(4)} = -\ddot{u}\sin\theta - 2\dot{u}\dot{\theta}\cos\theta - u\ddot{\theta}\cos\theta + u\dot{\theta}^2\sin\theta \tag{3.10}$$

$$mz^{(4)} = \ddot{u}\cos\theta - 2\dot{u}\dot{\theta}\sin\theta - u\ddot{\theta}\sin\theta - u\dot{\theta}^2\cos\theta \tag{3.11}$$

Substituting $\ddot{\theta}$, given in (3.5), into (3.10) and (3.11) results in

$$mx^{(4)} = -\ddot{u}\sin\theta - 2\dot{u}\dot{\theta}\cos\theta - \frac{u\tau\cos\theta}{J} + u\dot{\theta}^2\sin\theta \tag{3.12}$$

$$mz^{(4)} = \ddot{u}\cos\theta - 2\dot{u}\dot{\theta}\sin\theta - \frac{u\tau\sin\theta}{J} - u\dot{\theta}^2\cos\theta \tag{3.13}$$

which can be rewritten in matrix form as

$$m\begin{bmatrix} x^{(4)} \\ z^{(4)} \end{bmatrix} = \begin{bmatrix} -\sin\theta & -\frac{u\cos\theta}{J} \\ \cos\theta & -\frac{u\sin\theta}{J} \end{bmatrix}\begin{bmatrix} \ddot{u} \\ \tau \end{bmatrix} + \begin{bmatrix} -2\dot{\theta}\cos\theta & u\dot{\theta}\sin\theta \\ -2\dot{\theta}\sin\theta & -u\dot{\theta}\cos\theta \end{bmatrix}\begin{bmatrix} \dot{u} \\ \dot{\theta} \end{bmatrix} \tag{3.14}$$

Define $E(u,\theta)$ and $F\left(u,\dot{u},\theta,\dot{\theta}\right)$ as

$$E(u,\theta) \coloneqq \begin{bmatrix} -\sin\theta & -\frac{u\cos\theta}{J} \\ \cos\theta & -\frac{u\sin\theta}{J} \end{bmatrix} \tag{3.15}$$

$$F\left(u,\dot{u},\theta,\dot{\theta}\right) \coloneqq \begin{bmatrix} -2\dot{\theta}\cos\theta & u\dot{\theta}\sin\theta \\ -2\dot{\theta}\sin\theta & -u\dot{\theta}\cos\theta \end{bmatrix}\begin{bmatrix} \dot{u} \\ \dot{\theta} \end{bmatrix} \tag{3.16}$$

Then (3.14) can be written as

$$m \begin{bmatrix} x^{(4)} \\ z^{(4)} \end{bmatrix} = E(u,\theta) \begin{bmatrix} \ddot{u} \\ \tau \end{bmatrix} + F\left(u,\dot{u},\theta,\dot{\theta}\right) \tag{3.17}$$

which is in an affine control form.

3.2.3 PVTOL Feedback Linearization

The control inputs of the system presented in (3.17) are $\ddot{u}$ and τ. The nonlinearity in equation (3.17) is due to matrix $E(u,\theta)$ and the term $F\left(u,\dot{u},\theta,\dot{\theta}\right)$. The control inputs $\ddot{u}$ and τ can compensate for the matrix $E(u,\theta)$ by using its inverse, but its domain will be restricted by the conditions under which the matrix is not singular. The following corollary is used to obtain this domain.

Remark 3.2.2. *Matrix $E(u,\theta)$ is not singular iff $u \neq 0$. This can be deduced from the fact that*

$$det\left[E(u,\theta)\right] = \frac{u}{J} \tag{3.18}$$

□

The nonlinear term $F\left(u,\dot{u},\theta,\dot{\theta}\right)$ can be canceled by subtraction. The control inputs $\ddot{u}$ and τ are defined as

$$\begin{bmatrix} \ddot{u} \\ \tau \end{bmatrix} := E^{-1}(u,\theta) \left(m \begin{bmatrix} u_{tra} \\ u_{att} \end{bmatrix} - F\left(u,\dot{u},\theta,\dot{\theta}\right) \right) \tag{3.19}$$

where $u_{tra}, u_{att} \in \mathbb{R}$ are new control inputs for the resulting linear system and $E^{-1}(u,\theta)$ has the form

$$E^{-1}(u,\theta) = \begin{bmatrix} -\sin\theta & \cos\theta \\ -\dfrac{J\cos\theta}{u} & -\dfrac{J\sin\theta}{u} \end{bmatrix} \tag{3.20}$$

Introducing (3.19) into (3.17) leads to

$$\begin{bmatrix} x^{(4)} \\ z^{(4)} \end{bmatrix} = \begin{bmatrix} u_{tra} \\ u_{att} \end{bmatrix} \tag{3.21}$$

In order to design a state feedback control law, the state of the system is defined as

$$\xi := \left[\begin{array}{c|c|c|c|c|c|c|c} x & z & \dot{x} & \dot{z} & \ddot{x} & \ddot{z}+g & x^{(3)} & z^{(3)} \end{array} \right]^T \tag{3.22}$$

Note that most control design techniques for the PVTOL define the state as shown in (3.6), which are the variables that could be obtained from the sensors and most state estimators. However, according to (3.3), (3.4), (3.8) and (3.9), the derivatives $\ddot{x}, \ddot{z}, x^{(3)}$ and $z^{(3)}$ can be obtained from the vehicle's variables $m, \theta, \dot{\theta}, u$ and $\dot{u}$. The following corollary can be obtained from this fact.

Corollary 3.2.1. *There exists a transformation $T(\cdot)$ that changes the state presented in* (3.6) *into the one in* (3.22)

$$\xi = T\left(\hat{\xi}, u, \dot{u}\right) = \begin{bmatrix} x \\ z \\ \dot{x} \\ \dot{z} \\ -\dfrac{u \sin\theta}{m} \\ \dfrac{u \cos\theta}{m} \\ \dfrac{-\dot{u}\sin\theta - u\dot{\theta}\cos\theta}{m} \\ \dfrac{\dot{u}\cos\theta - u\dot{\theta}\sin\theta}{m} \end{bmatrix} \tag{3.23}$$

□

Using the state vector (3.22), equation (3.4) and the system (3.21), the PVTOL system can be expressed as the following linear system

$$\dot{\xi} = \begin{bmatrix} \overline{0}_{6\times 2} & I_{6\times 6} \\ \overline{0}_{2\times 2} & \overline{0}_{2\times 6} \end{bmatrix} \xi + \begin{bmatrix} \overline{0}_{6\times 2} \\ I_2 \end{bmatrix} \begin{bmatrix} u_{tra} \\ u_{att} \end{bmatrix} + \begin{bmatrix} \overline{0}_{3\times 1} \\ -g \\ \overline{0}_{4\times 1} \end{bmatrix} \tag{3.24}$$

Equation (3.24) shows that the PVTOL system has been transformed into a linear representation with a gravity term. The control input $\begin{bmatrix} u_{tra} & u_{att} \end{bmatrix}^T$ will be used to compensate the gravity and stabilize the system.

Following the lead from Chapter 2, the PVTOL system can be separated into two independent dynamical systems. The first one is the PVTOL position dynamics and the second one is the PVTOL's attitude dynamics. Both will be address in the following sections.

PVTOL Position Dynamical System

The translational dynamics are obtained from system (3.24). The system presented here will be used in the following sections to help prove the local stability of the system.

The state vector of the lateral position dynamic system is defined as

$$\xi_{tra} \coloneqq \begin{bmatrix} x & \dot{x} & \ddot{x} & x^{(3)} \end{bmatrix}^T \tag{3.25}$$

Taking into account system (3.24), the differentiation of ξ_{tra} w.r.t. time is

$$\dot{\xi}_{tra} = A\,\xi_{tra} + B\,u_{tra} \tag{3.26}$$

with the matrices A and B defined as

$$A \coloneqq \begin{bmatrix} \overline{0}_{3\times 1} & I_3 \\ 0 & \overline{0}_{1\times 3} \end{bmatrix}, \qquad B \coloneqq \begin{bmatrix} \overline{0}_{3\times 1} \\ 1 \end{bmatrix} \tag{3.27}$$

PVTOL Altitude Dynamical System

The altitude dynamics are obtained from system (3.24) so that it may later be used for the stability analysis and the calculation of the region of attraction.

The state vector of the altitude system is defined as

$$\xi_{alt} \coloneqq \left[\begin{array}{c|c|c|c} z & \dot{z} & \ddot{z}+g & z^{(3)} \end{array}\right]^T \tag{3.28}$$

Taking into account system (3.24), the differentiation of ξ_{alt} w.r.t. time is

$$\dot{\xi}_{alt} = A\,\xi_{alt} + B\,u_{alt} + \gamma_{alt} \tag{3.29}$$

The constant vector γ_{alt} is the effect that the gravity has on system (3.29), with the following definition

$$\gamma_{alt} \coloneqq \begin{bmatrix} 0 & -g & 0 & 0 \end{bmatrix}^T \tag{3.30}$$

3.2.4 State Feedback Control Design

The proposed control algorithm in this work for system (3.24) is a state feedback control. Its description and the stability analysis are shown in the following definition and theorem.

Definition 3.2.1. *Let us define two gain vectors $K_{tra}, K_{att} \in \mathbb{R}^{1\times 4}$, which are chosen in order to comply with the Lyapunov equations*

$$P_{tra}\,(A - B\,K_{tra}) + (A - B\,K_{tra})^T\,P_{tra} = -Q_{tra} \tag{3.31}$$

$$P_{alt}\,(A - B\,K_{alt}) + (A - B\,K_{alt})^T\,P_{alt} = -Q_{alt} \tag{3.32}$$

where $Q_{tra}, P_{tra}, Q_{alt}, P_{alt} \in \mathbb{R}^{4\times 4}$ are positive definite symmetric matrices. □

Theorem 3.2.1. *The proposed control law is*

$$\begin{bmatrix} u_{tra} \\ u_{alt} \end{bmatrix} = \begin{bmatrix} -K_{tra}\,\xi_{tra} \\ -K_{alt}\,(\xi_{alt} - \gamma_u) \end{bmatrix} \tag{3.33}$$

where

$$\gamma_u \coloneqq \begin{bmatrix} \overline{0}_{1\times 2} & g & 0 \end{bmatrix}^T \tag{3.34}$$

The control law (3.33) *locally stabilizes system* (3.24) *to the state*

$$\xi^* = \begin{bmatrix} \overline{0}_{5\times 1} \\ g \\ \overline{0}_{2\times 1} \end{bmatrix} \tag{3.35}$$

□

Theorem 3.2.1 provides the basis to achieve the control objective 3.2.1. In order to complete the control algorithm the desired trajectory needs to be transformed into the new state coordinates.

Corollary 3.2.2. *The desired trajectory presented in* (3.7) *can be transformed into a desired trajectory in the new state vector as*

$$\xi_d(t) \coloneqq \xi_d \coloneqq T\left(\hat{\xi}_d(t), u, \dot{u}\right) \tag{3.36}$$

It is assumed that this trajectory is continuous and smooth and that $u \neq 0$*. Also, its differentiation w.r.t. time is also assumed to have the form (see Corollary 3.2.1)*

$$\dot{\xi}_d = \begin{bmatrix} \overline{0}_{6\times 2} & I_{6\times 6} \\ \overline{0}_{2\times 2} & \overline{0}_{2\times 6} \end{bmatrix} \xi_d \tag{3.37}$$

□

Corollary 3.2.3. *It follows from Corollary 3.2.2 and definitions 3.25 and 3.28 that the trajectories for the translation and altitude systems can be obtained as*

$$\xi_{tra,d} \coloneqq \begin{bmatrix} x_d & \dot{x}_d & \ddot{x}_d & x_d^{(3)} \end{bmatrix}^T \tag{3.38}$$

$$\xi_{alt,d} \coloneqq \begin{bmatrix} z_d & \dot{z}_d & \ddot{z}_d & z_d^{(3)} \end{bmatrix}^T \tag{3.39}$$

Also from Corollary 3.2.2, the trajectories for each subsystem have the form

$$\dot{\xi}_{tra,d} = A\,\xi_{tra,d} \tag{3.40}$$

$$\dot{\xi}_{alt,d} = A\,\xi_{alt,d} \tag{3.41}$$

□

The following theorem is the result of using corollary 3.2.2 and the control law presented in theorem 3.2.1.

Theorem 3.2.2. *The control law*

$$\begin{bmatrix} u_{tra} \\ u_{alt} \end{bmatrix} = \begin{bmatrix} -K_{tra}\left(\xi_{tra} - \xi_{tra,d}\right) \\ -K_{alt}\left(\xi_{alt} - \xi_{alt,d} - \gamma_u\right) \end{bmatrix} \tag{3.42}$$

makes system (3.24) *be locally asymptotically stable to the state*

$$\xi^* = \xi_d + \begin{bmatrix} \overline{0}_{5\times 1} \\ g \\ \overline{0}_{2\times 1} \end{bmatrix} \tag{3.43}$$

□

Even though the linear system (3.24) has been proven to be asymptotically exponentially stable around the desired state ξ_d using Theorem 3.2.2, the fact that the inverse (3.20) was used means that the stability is local according to Remark 3.2.2. The approach taken in this work is to calculate a region of attraction for which the stability analysis of the proposed control law is still valid. As the system was separated into an altitude and a translation system, and this singularity only affects the altitude dynamics, the translation dynamics are still globally asymptotically stable.

Theorem 3.2.3. *The region of attraction of system* (3.24) *with control* (3.33) *can be defined as*

$$\Omega := \left\{ \xi \in \mathbb{R}^8 \middle| \, ||\xi_{alt}|| < g \right\} \tag{3.44}$$

□

Theorem 3.2.4. *The region of attraction of system* (3.24) *with control* (3.42) *can be defined as*

$$\Omega := \left\{ \xi \in \mathbb{R}^8 \middle| \, ||\xi_{alt}|| < \left| \frac{u_d \cos\theta_d}{m} + g \right| \right\} \tag{3.45}$$

□

From equations (3.15), (3.19), (3.20), (3.25), (3.28), (3.34), (3.38) and (3.42), and definition 3.2.1, the control inputs $\ddot{u}$ and τ are completely defined as

$$\begin{bmatrix} \ddot{u} \\ \tau \end{bmatrix} = \begin{bmatrix} -\sin\theta & \cos\theta \\ -\dfrac{J\cos\theta}{u} & -\dfrac{J\sin\theta}{u} \end{bmatrix} \left\{ m \begin{bmatrix} -K_{tra}\left(\xi_{tra} - \xi_{tra,d}\right) \\ -K_{alt}\left(\xi_{alt} - \xi_{alt,d} - \gamma_u\right) \end{bmatrix} - \begin{bmatrix} -2\dot{\theta}\cos\theta & u\dot{\theta}\sin\theta \\ -2\dot{\theta}\sin\theta & -u\dot{\theta}\cos\theta \end{bmatrix} \begin{bmatrix} \dot{u} \\ \dot{\theta} \end{bmatrix} \right\} \tag{3.46}$$

3.2.5 PVTOL Force Regulation

The presented theorems are useful to control the complete state ξ of the PVTOL platform. However, in order to comply with the Control Objective 2.3.1, it is only necessary at this point to control just the thrust vector force

$$F_{th,i} = \begin{bmatrix} \xi_{5,i} \\ \xi_{6,i} \end{bmatrix} \tag{3.47}$$

This can be done without loss of generality by adapting the control law presented in Theorem 3.2.2, as stated in the following corollary

Corollary 3.2.4. *The control law*

$$\begin{bmatrix} u_{tra} \\ u_{alt} \end{bmatrix} = \begin{bmatrix} -K_{tra,13}\left(\ddot{x}_i - \ddot{x}_{i,d}\right) - K_{tra,14}\, x_i^{(3)} \\ -K_{alt,13}\left(\ddot{z}_i - \ddot{z}_{i,d}\right) - K_{alt,14}\, z_i^{(3)} \end{bmatrix} \tag{3.48}$$

makes system (3.24) *be locally asymptotically stable to the state*

$$\xi^* = \begin{bmatrix} \overline{0}_{4\times 1} \\ \xi_{5,d,i} \\ \xi_{6,d,i} \\ \overline{0}_{2\times 1} \end{bmatrix} + \begin{bmatrix} \overline{0}_{5\times 1} \\ g \\ \overline{0}_{2\times 1} \end{bmatrix} \tag{3.49}$$

□

3.3 PVTOL Control Academic Example

According to Definition 3.2.1, two state feedback gains K_{tra} and K_{alt} are needed in order to implement the proposed PVTOL control law. These matrices can be obtained using many different methods like pole placement [Chen, 1998, Chapter 9] or root locus [Dorf and Bishop, 2011, Chapter 7], the only restriction is that they need to satisfy the Lyapunov algebraic equations (3.31) and (3.32).

For the example presented here, these gains will be obtained using a LQR approach. The parameters used to solve the algebraic Riccati equation were

$$Q_{LQR} = diag\begin{Bmatrix} 1 & 1 & 0.1 & 0.01 \end{Bmatrix} \tag{3.50}$$

is the state-cost weighted matrix[1]and

$$R_{LQR} = I_2 \tag{3.51}$$

is the input-cost weighted matrix[2].

The control law (3.46) was simulated numerically with the following state feedback gain

[1]The matrix Q_{LQR} was selected in this way to ensure that the position and velocity states converge faster to the desired state. The higher-order terms are not as important because they either depend on the attitude state, which is assumed to have fast dynamics, or on the numerical integration of the thrust force, which are extended states.

[2]The matrix R_{LQR} was selected in this simple way because the input-cost is not as important as the design of Q_{LQR}.

$$K_{tra} = K_{alt} = \begin{bmatrix} 1 & 2.91712925 & 3.75482154 & 2.74219676 \end{bmatrix} \tag{3.52}$$

m	$1.8 \quad kg$	J	$0.79 \quad kg \cdot m^2$
g	$9.81 \quad m/s^2$	t_0	$0 \quad s$
Δt	$0.01 \quad s$	t_f	$30 \quad s$
x_d	$-1 \quad m$	z_d	$1.5 \quad m$
$\dot{x}_d$	$0 \quad m/s$	$\dot{z}_d$	$0 \quad m/s$
θ_d	$0 \quad rad$	$\dot{\theta}_d$	$0 \quad rad/s$
u_d	$mg \quad N$	$\dot{u}_d$	$0 \quad N/s$
x_0	$0 \quad m$	z_0	$0 \quad m$
$\dot{x}_0$	$0 \quad m/s$	$\dot{z}_0$	$0 \quad m/s$
θ_0	$0 \quad rad$	$\dot{\theta}_0$	$0 \quad rad/s$
u_0	$0.01m \quad N$	$\dot{u}_0$	$0 \quad N/s$

Table 3.1: Academic example simulation parameters for the proposed PVTOL control law

From these parameters, the maximum value of the region of attraction is

$$\left| \frac{u_d \cos\theta_d}{m} + g \right| = |g| \tag{3.53}$$

and the norm of the initial parameters vector $\xi_{alt,0}$ is obtained using (3.23)

$$\left|\left|\xi_{alt,0}\right|\right| = \left|\left| \frac{0.01\,m\cos 0}{m} - g \right|\right| = 9.8 < g \tag{3.54}$$

which implies that the initial conditions of the system are inside the region of attraction (3.45).

In order to proof the robustness of the proposed control, a crosswind perturbation was added to the simulation as described in [Munoz et al., 2010], with random bounded parameters

$$w_1 \sim \mathscr{U}(-5,5) \tag{3.55}$$

and

$$w_2 \sim \mathscr{U}(-0.01,0.01) \tag{3.56}$$

The results of the simulation can be seen in figures 3-2 through 3-11.

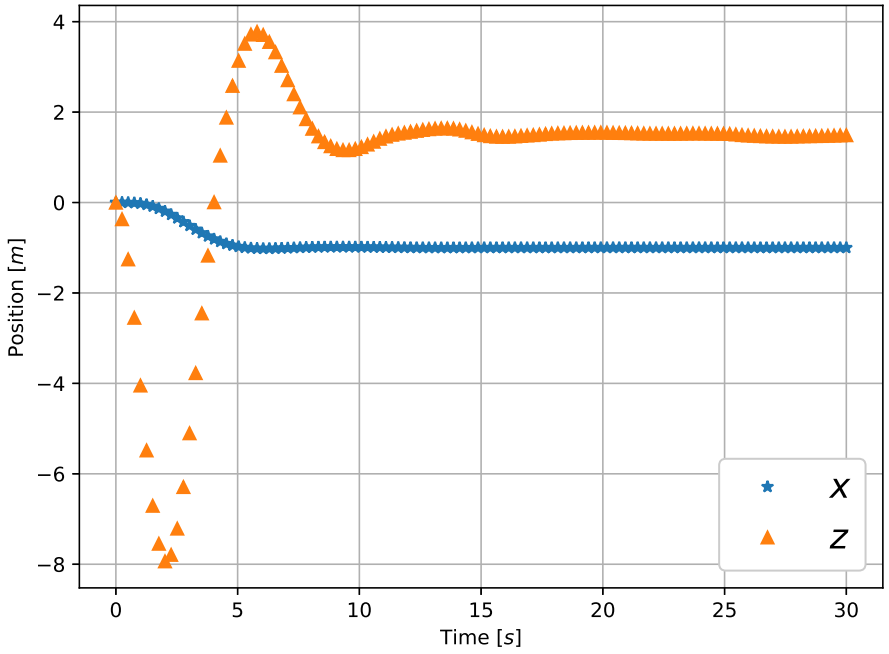

Figure 3-2: PVTOL control academic example position

Figure 3-2 shows the x_i and z_i position of the PVTOL. Because of the initial conditions, the altitude drops significantly in the first seconds of the simulation due to the effect of the gravity. On both figure 3-2 and 3-3 the effect of the crosswind does not allow the state to fully reach the desired state, but it can be seen in figures 3-4 and 3-5 that the error is bounded.

The change of attitude of the vehicle is reflected in figure 3-6. It can be seen that it has a jump at the start due to the initial conditions and the desired position. The angular velocity is shown in figure 3-7. Both of these plots have small angles changes, but it is enough to have an effect on the translational dynamics.

Figure 3-8 shows the input torque and figure 3-9 shows the thrust vector magnitude. In figure 3-8 the input torque τ is bounded near zero because of the crosswind perturbation. It can be seen in figure 3-9 that the thrust vector u does not pass through zero, which avoids the singularity in the control algorithm presented.

Figures 3-9-3-11 show the dynamics of the thrust vector system. Because the thrust vector u is a control input, the initial conditions of the thrust vector's dynamic system can

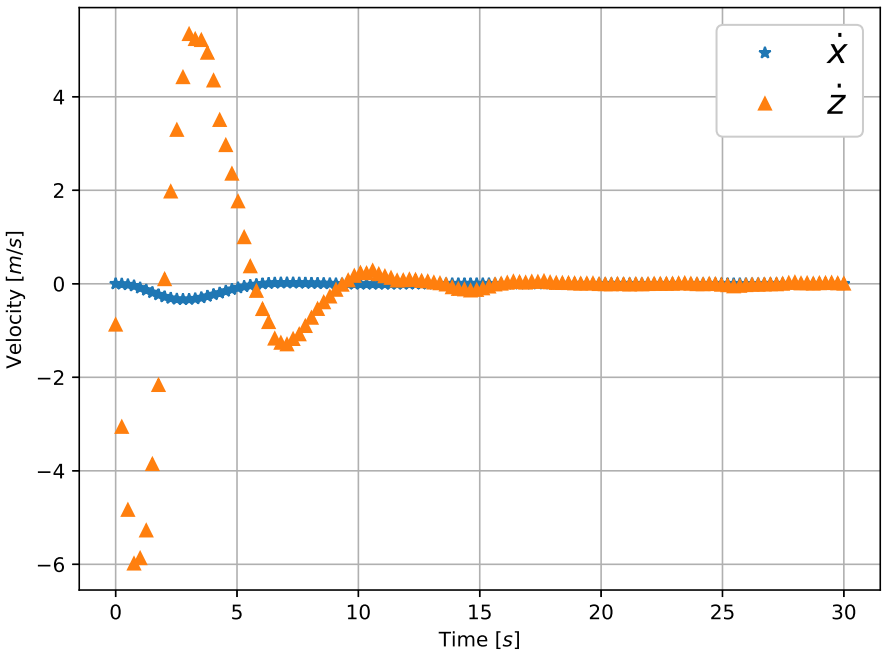

Figure 3-3: PVTOL control academic example velocity

be initialized at any arbitrary value. The thrust does not come close to zero since the initial conditions satisfy (3.44) and (3.45)

3.4 Summary

Even though the PVTOL platform model presented in equations (3.3)-(3.5) is well known, the control input u can be extended in order to make the platform behave like a linear system. In contrast with other non linear control techniques, like the ones presented in [Aguilar-Ibañez, 2017], [Aguilar-Ibañez et al., 2018] and [Hernández-Castañeda et al., 2018], the advantage of this approach is that the control design and stability analysis is easier for the linear system than for the original model. A state feedback control was used and proven to be able to solve the tracking problem. However, this is just one of the possible controls that can be used with this linearized system.

Feedback linearization has been applied to the PVTOL platform before, mostly by extending the state of the system's thrust force F_{th}. However, the feedback linearization in all these controllers can only be local, as the feedback function has a singularity when $F_{th} = 0$.

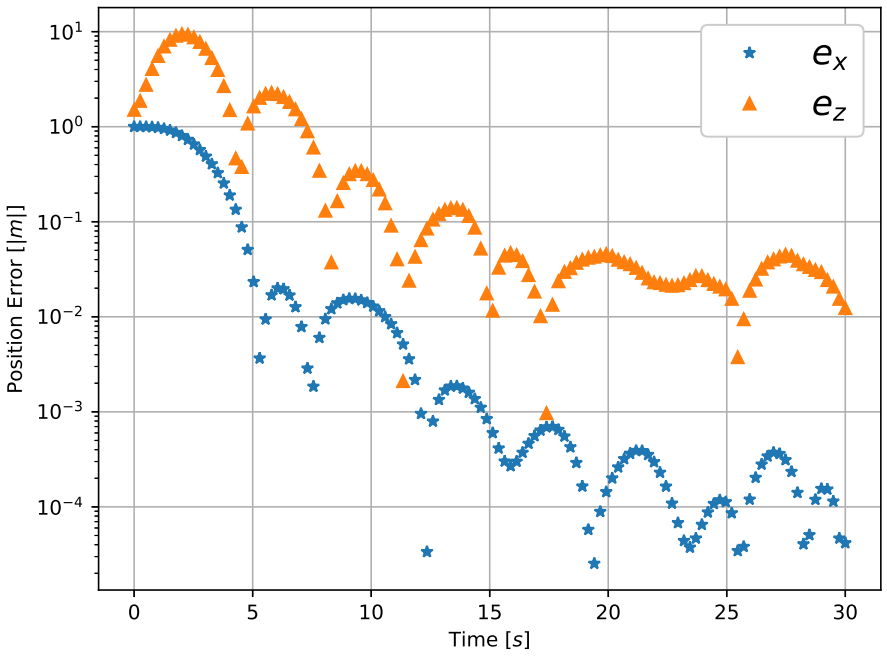

Figure 3-4: PVTOL control academic example absolute position error

This is because the inverse of the matrix $E(F_{th}, \theta)$ is used to make the feedback linearization possible, and it becomes singular at this particular point, which is explained in Remark 3.2.2. The singularity for this model is unavoidable, but most of these works only acknowledge it, and [Aguilar-Ibanez et al., 2019] even mentions that the thrust of the vehicle is always positive in practice. Even if the physical system does have the limitation that the thrust force should always remain positive, that is not a guarantee that the control scheme implemented may not at some point pass through the singularity. In [Puga et al., 2015], the range of action of the control is limited to a region, which could be used to prevent the state of the vehicle from reaching the singularity, but that is not the main objective of these authors.

Finally, the controller presented here solves Control Objective 2.3.1 by using Corollary 3.2.4 (see Figure 2-4). Control Objective 2.2.1 will be solved in the next chapter with the aid of this result.

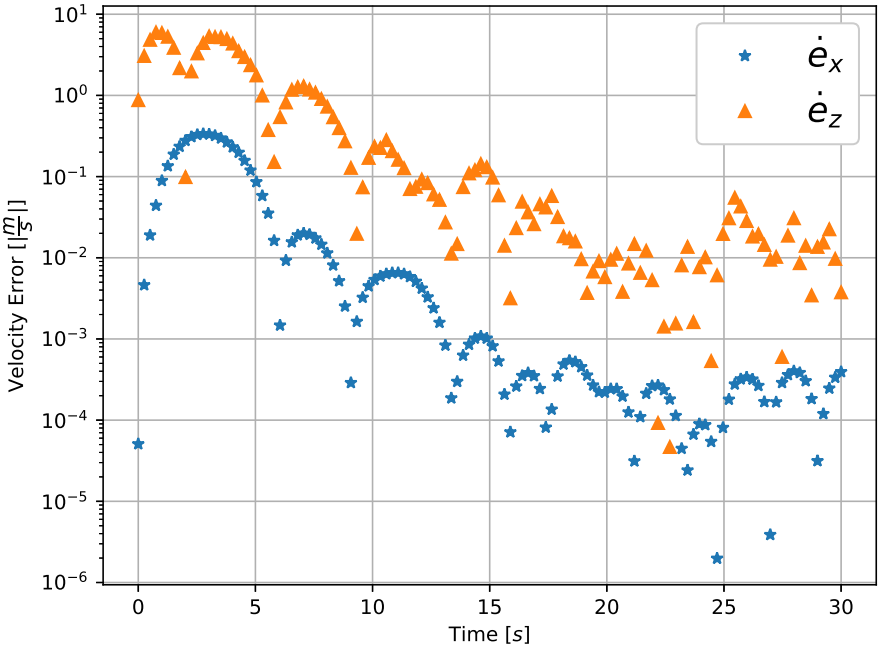

Figure 3-5: PVTOL control academic example absolute velocity error

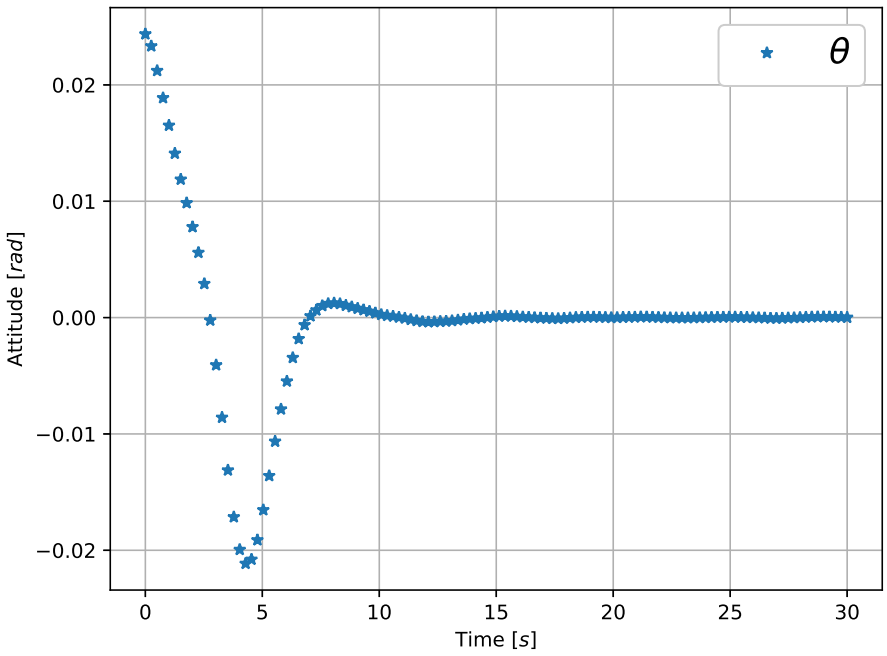

Figure 3-6: PVTOL control academic example attitude

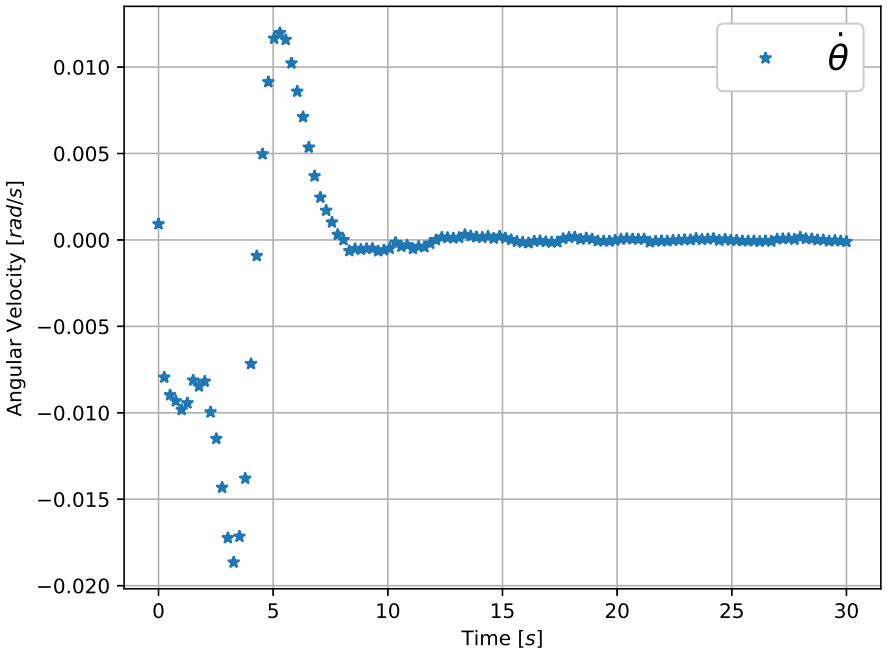

Figure 3-7: PVTOL control academic example angular velocity

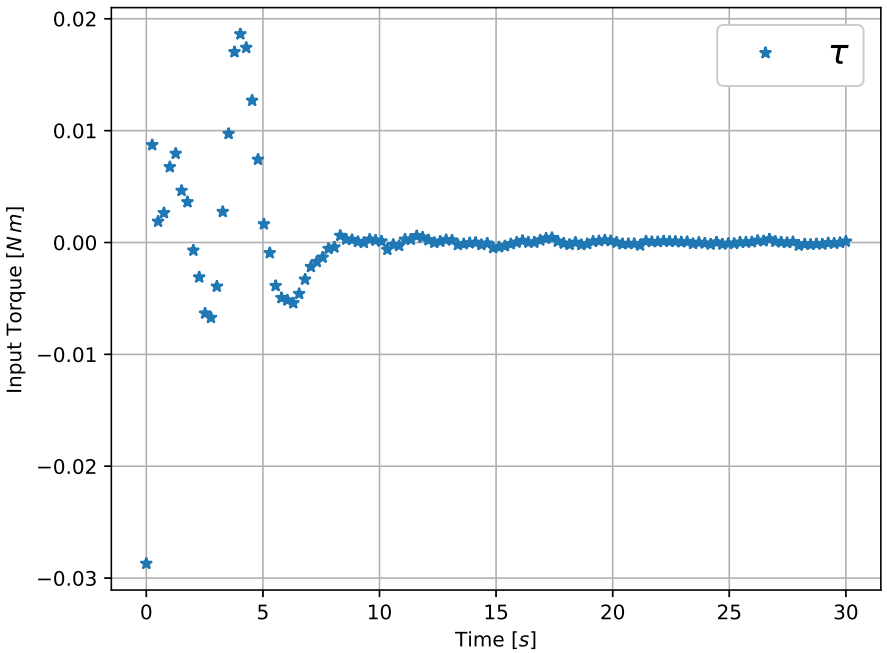

Figure 3-8: PVTOL control academic example input torque τ

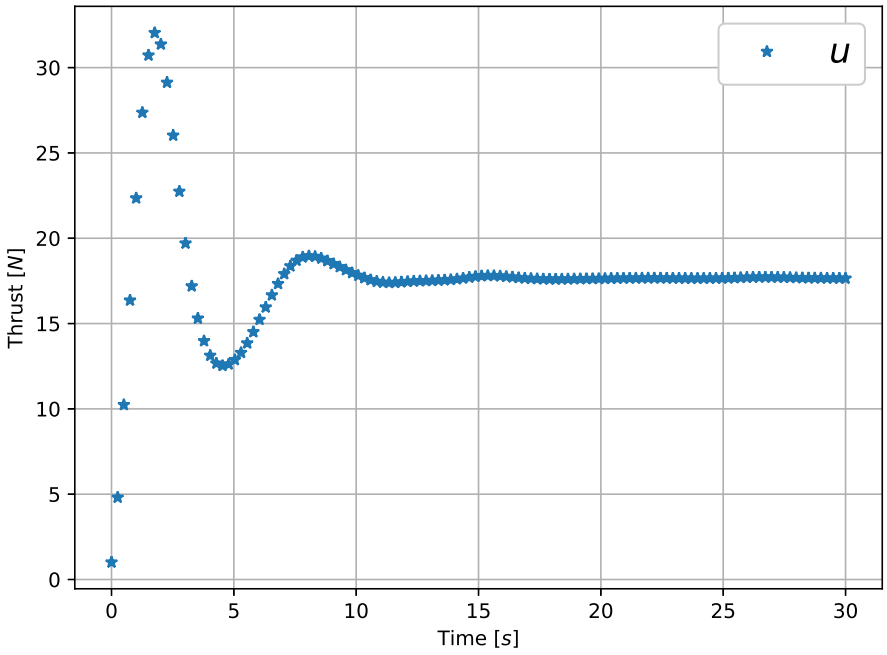

Figure 3-9: PVTOL control academic example position F_{th}

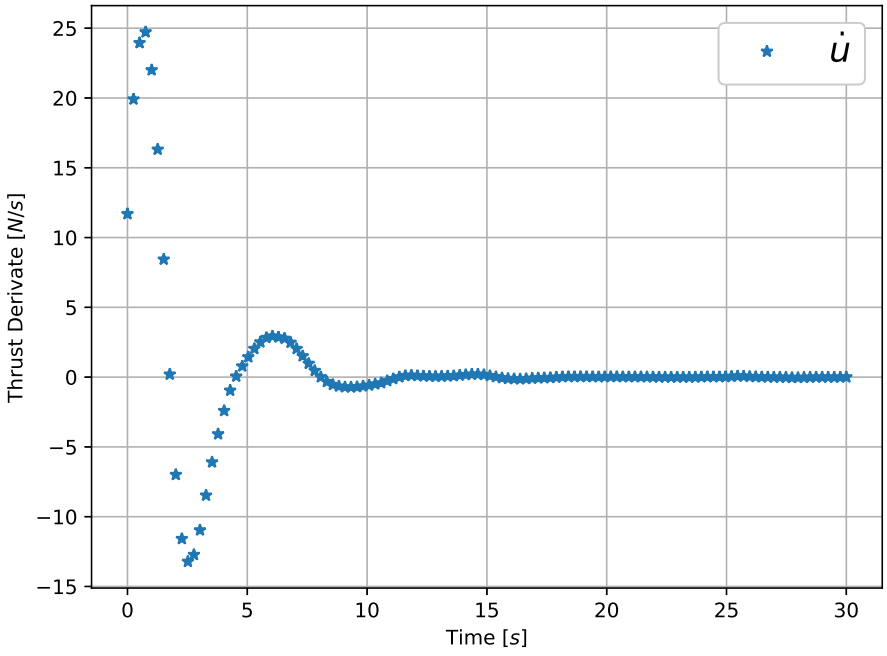

Figure 3-10: PVTOL control academic example thrust vector differentiation w.r.t. time $\dot{F}_{th}$

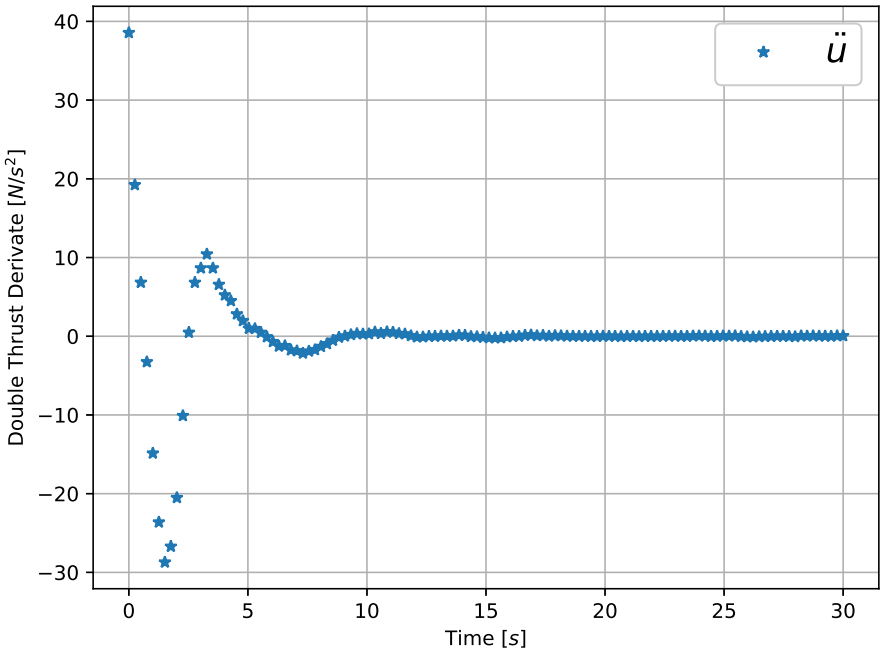

Figure 3-11: PVTOL control academic example thrust vector double differentiation w.r.t. time $\ddot{F}_{th}$

Chapter 4

Cooperative Slung-Load Transport Control

This chapter presents the main theoretical results in order to achieve Control Objective 2.2.1, which results in a decentralized cooperative control law (see Figure 2-4). The main contributions come from the properties of the proposed design approach. The system is guaranteed to be locally asymptotically stable towards a desired state set Ω_d using very little system information, unlike similar approaches like the ones in [Tognon et al., 2018] [Tagliabue et al., 2017] [Tagliabue et al., 2019] and [Gabellieri et al., 2018]. The algorithm in its minimum expression only requires the velocity information of each vehicle and can be extended to include even traditional cooperation schemes. Like the works in [Guerrero et al., 2015] and [Valk and Keviczky, 2018], the proposed approach is based on passivity, which adds robustness to the system by modifying the point of minimal mechanical energy.

The chapter is divided in four main sections. Section 4.1.1 presents a more thorough description of the cooperative system model than the one presented in Chapter 2, along with its dynamic equations. Section 4.2 shows the design approach based on an objective function and the theorems that prove the stability of the proposed control law. Section 4.3 displays the results of an academic example. The control law that was developed is compared with another one based on mechanical impedance control using a numeric simulation. Finally, a summary of the presented design process can be found in Section 4.4. The main theorems of the passivity theory that are going to be used are defined in Appendix B.

The proof of the presented theorems can be seen in Appendix C

4.1 Cooperative Slung-Load Transport Dynamic Model

This section presents a system as the one presented in Figure 2-1, but with all the considerations listed in Section 2.2. The cooperative system is compromised of two agents and a slung-load in the form of a bar. A visualization of the system's configuration and parameters can be seen in Figure 4-1. The variables are described in this section and the dynamics equations are then obtained using the Euler-Lagrange methodology.

4.1.1 System Description

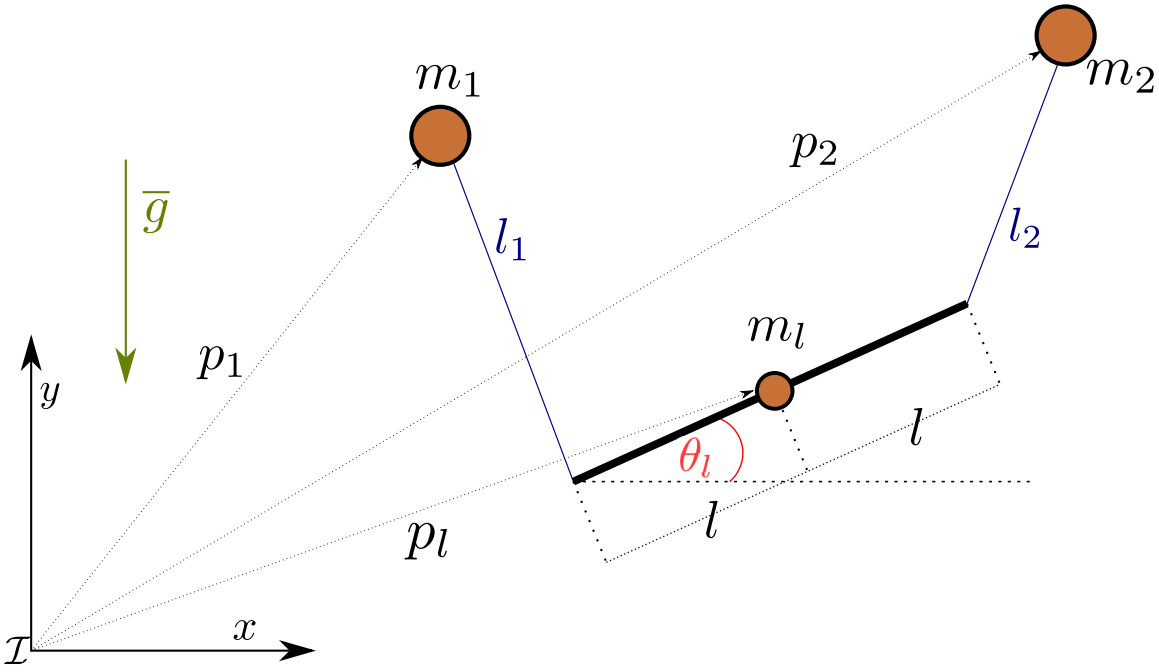

Figure 4-1: The free body diagram of the vehicles with the bar attached

Figure 4-1 shows the system's free body diagram. The variables are defined as:

- $\mathscr{I}'$ is the inertial reference frame.
- x, z are the horizontal and vertical axis, respectively.
- $\overline{g} \coloneqq \begin{bmatrix} 0 & -g \end{bmatrix}^T \in \mathbb{R}^2$ is the effect of the gravity, and $g \in \mathbb{R}$ is its value.

- $m_l \in \mathbb{R}$ is the load's mass.
- $\vec{p}_l \coloneqq \begin{bmatrix} x_l & y_l \end{bmatrix}^T \in \mathbb{R}^2$ is the load's position w.r.t. the inertial reference frame $\mathscr{I}'$.
- $\theta_l \in \mathbb{R}$ is the load's attitude.
- $l \in \mathbb{R}$ is the length from the load's center of mass to each of the cables.
- $m_i \in \mathbb{R} \quad \forall i \in \{1,2\}$ are the individual masses of each vehicle.
- $\vec{p}_i \coloneqq \begin{bmatrix} x_i & y_i \end{bmatrix}^T \in \mathbb{R}^2 \quad \forall i \in \{1,2\}$ are the positions of each vehicle w.r.t. the inertial reference frame $\mathscr{I}'$.
- $l_i \in \mathbb{R} \quad \forall i \in \{1,2\}$ are the cable's length for each vehicle.

The dynamic model of a PVTOL was presented in Chapter 3. In this chapter, it is assumed that the thrust force $\vec{F}_{th,i}$ of each PVTOl is a control input of the system. This can be accomplished by using Corollary 3.2.4. The cables are assumed to be attached to the center of mass of each vehicle.

4.1.2 Dynamic Equations

The method used to obtain the model is the Euler-Lagrange formulation. The reason behind this is that the close relationship of the system Lagrangian with the energy of the system. This fact will be used later on to develop the passivity and stability tests. The state of generalized coordinates $q \in \mathbb{R}^7$ used for the equations is defined as

$$q \coloneqq \begin{bmatrix} p_l \\ \theta_l \\ p_1 \\ p_2 \end{bmatrix} \tag{4.1}$$

and the full space state of the system $x \in \mathbb{R}^{14}$ can be defined as

$$x \coloneqq \begin{bmatrix} q \\ \dot{q} \end{bmatrix} \tag{4.2}$$

System's Kinetic Energy

The total kinetic energy of the system is the sum of the load's kinetic energy and the vehicles' kinetic energy. The load's kinetic energy is calculated by adding the effects of its linear velocity $\dot{p}_l \in \mathbb{R}^2$ and angular velocity $\dot{\theta}_l \in \mathbb{R}$

$$T_l := \frac{m_l \dot{p}_l^T \dot{p}_l}{2} + \frac{J_l \dot{\theta}_l^2}{2} \tag{4.3}$$

where $J_l \in \mathbb{R}$ is the inertia matrix.

The kinetic energy for each vehicle can be calculated as

$$T_i := \frac{m_i \dot{p}_i^T \dot{p}_i}{2} \tag{4.4}$$

where $\dot{p}_i \in \mathbb{R}^2$ is the vehicle's velocity.

The total kinetic energy is then obtained as

$$T := T_l + \sum_{i=1}^{2} T_i \tag{4.5}$$

System's Potential Energy

The total potential energy of the system is the sum of the load's potential energy, the vehicles' potential energy and the holonomic constraints terms due to the effects that the presence of the cables has on the system. It is assumed that the potential energy is bounded from below, which implies that $\exists \quad U_{min} \in \mathbb{R}$ such that $U \geq U_{min}$. The load's potential energy is calculated as

$$U_l := m_l y_l g \tag{4.6}$$

The potential energy for each vehicle can be obtained as

$$U_i \coloneqq m_i y_i g + \lambda_i \left(e_i^T e_i - l_i^2 \right) \tag{4.7}$$

where the term $\lambda_i \left(e_i^T e_i - l_i^2 \right)$ takes into account the effects that the presence of the cables have on the system's potential energy, and will be described next.

Holonomic Constraints

The terms λ_i in equation (4.7) are Lagrange multipliers and the terms e_i are the distances between each vehicle and the load w.r.t. the system's state q. They are defined as

$$\begin{aligned} e_1 \coloneqq \begin{bmatrix} e_{1,x} \\ e_{1,y} \end{bmatrix} &\coloneqq -p_1 + p_l - l \begin{bmatrix} \cos\theta_l \\ \sin\theta_l \end{bmatrix} \\ e_2 \coloneqq \begin{bmatrix} e_{2,x} \\ e_{2,y} \end{bmatrix} &\coloneqq -p_2 + p_l + l \begin{bmatrix} \cos\theta_l \\ \sin\theta_l \end{bmatrix} \end{aligned} \tag{4.8}$$

In order for the distances l_i to remain constant the following equality, which defines the holonomic constraints, must be enforced

$$e_i^T e_i - l_i^2 = 0 \tag{4.9}$$

The total potential energy is obtained as

$$U \coloneqq U_l + \sum_{i=1}^{2} U_i + \phi\left(q\right)^T \lambda \tag{4.10}$$

where the Lagrange multipliers vector $\lambda \in \mathbb{R}^2$ is defined as

$$\lambda \coloneqq \begin{bmatrix} \lambda_1 \\ \lambda_2 \end{bmatrix} \tag{4.11}$$

and the holonomic constraints vector $\phi\left(q\right)$ as

$$\phi\left(q\right) \coloneqq \begin{bmatrix} e_1^T e_1 - l_1^2 \\ e_2^T e_2 - l_2^2 \end{bmatrix} = \overline{0} \tag{4.12}$$

The system's Lagrangian can be calculated as

$$\begin{aligned}\mathscr{L} = & \quad T - U \\ = & \quad T_l - U_l + \sum_{i=1}^{2} T_i - U_i \\ = & \quad \frac{m_l \dot{p}_l^T \dot{p}_l}{2} + \frac{J_l \dot{\theta}_l^2}{2} + \frac{m_1 \dot{p}_1^T \dot{p}_1}{2} + \frac{m_2 \dot{p}_2^T \dot{p}_2}{2} \\ & -m_l y_l g - m_1 y_1 g - m_2 y_2 g - \phi(q)^T \lambda\end{aligned} \tag{4.13}$$

Differential Equations

The system's dynamic model can be obtained from the Lagrangian as

$$\frac{d}{dt}\frac{\partial \mathscr{L}}{\partial \dot{q}} - \frac{\partial \mathscr{L}}{\partial q} = Q_{n.p.}(u) \tag{4.14}$$

where the vector of non-potential forces is defined as

$$Q_{n.p.}(u) \coloneqq E\,u \tag{4.15}$$

which depends on the control input

$$u \coloneqq \begin{bmatrix} u_1 \\ u_2 \end{bmatrix} \tag{4.16}$$

for each vehicle input vector $u_i \in \mathbb{R}^2$, and the constant matrix

$$E \coloneqq \begin{bmatrix} \overline{0}_{3\times 4} \\ I_4 \end{bmatrix} \tag{4.17}$$

The partial differential equations in (4.14) can be solved for each variable in q as

$$\frac{d}{dt}\frac{\partial \mathscr{L}}{\partial \dot{p}_l} - \frac{\partial \mathscr{L}}{\partial p_l} = m_l \ddot{p}_l - m_l \overline{g} + \begin{bmatrix} e_1 & e_2 \end{bmatrix} \lambda = 0 \tag{4.18}$$

$$\frac{d}{dt}\frac{\partial \mathscr{L}}{\partial \dot{p}_1} - \frac{\partial \mathscr{L}}{\partial p_1} = m_1 \ddot{p}_1 - m_1 \overline{g} + \begin{bmatrix} -e_1 & \overline{0} \end{bmatrix} \lambda = u_1 \tag{4.19}$$

$$\frac{d}{dt}\frac{\partial \mathscr{L}}{\partial \dot{p}_2} - \frac{\partial \mathscr{L}}{\partial p_2} = m_2 \ddot{p}_2 - m_2 \overline{g} + \begin{bmatrix} \overline{0} & -e_2 \end{bmatrix} \lambda = u_2 \tag{4.20}$$

$$\frac{d}{dt}\frac{\partial \mathscr{L}}{\partial \dot{\theta}_l} - \frac{\partial \mathscr{L}}{\partial \theta_l} = J_l\,\ddot{\theta}_l + \left[\begin{array}{c|c} -e_1^T \begin{bmatrix} -\sin\theta_l \\ \cos\theta_l \end{bmatrix} l & e_2^T \begin{bmatrix} -\sin\theta_l \\ \cos\theta_l \end{bmatrix} l \end{array}\right] \lambda = 0 \tag{4.21}$$

The system model can be structured from equations (4.18)-(4.21) in the following matrix form

$$M\,\ddot{q} + A^T(q)\,\lambda + G(q) = E\,u \tag{4.22}$$

where the general inertia matrix is defined as

$$M \coloneqq \mathrm{diag}\{m_l, m_l, J_l, m_1, m_1, m_2, m_2\} \tag{4.23}$$

the effect of the gravity on the system is defined as

$$G(q) \coloneqq \begin{bmatrix} 0 \\ m_l\,g \\ 0 \\ 0 \\ m_1\,g \\ 0 \\ m_2\,g \end{bmatrix} \tag{4.24}$$

and the effect of the constraints on the system is

$$\frac{\partial \phi(q)}{\partial q} \coloneqq A(q) = \left[\begin{array}{c|c|c|c} e_1^T & -e_1^T \begin{bmatrix} -\sin\theta_l \\ \cos\theta_l \end{bmatrix} l & -e_1^T & \overline{0} \\ \hline e_2^T & e_2^T \begin{bmatrix} -\sin\theta_l \\ \cos\theta_l \end{bmatrix} l & \overline{0} & -e_2^T \end{array}\right] \tag{4.25}$$

.

4.2 Control Law and Stability Analysis

The proposed control law is based on passivity and its designed to take the system into a state of minimum energy and into the desired set Ω_d as was seen in Control Objective 2.2.1. Now that the cooperative system model has been completely defined in Section 4.1.1, the desired set Ω_d can be further constrained as

$$\Omega_d \subset \left\{ \left[\begin{array}{ccc} q^T & \dot{q}^T & \lambda^T \end{array} \right]^T \in \mathbb{R}^{16} \middle| \begin{array}{l} \dot{q} = \overline{0}, e_{i,x} = 0, \\ \left\| e_{i,y} \right\| = l_i, \\ \|\lambda_i\| = \dfrac{m_l g}{2 l_i}, \\ e_{i,y} < 0, \lambda_i > 0 \end{array} \right\} \tag{4.26}$$

An auxiliary objective function will be defined in the next section in order to aid the control law design to reach the set Ω_d

4.2.1 Objective Function

Definition 4.2.1. *Following the control design of [Bai et al., 2011], an objective function $\psi(p_1, p_2) \in \mathbb{R}$ is defined such that*

$$\psi(p_1, p_2) \coloneqq \begin{cases} \psi(p_1, p_2) > 0 & , p_i \notin \Omega_d \\ \psi(p_1, p_2) = 0 & , p_i \in \Omega_d \\ \dfrac{\partial \psi(p_1, p_2)}{p_1} + \dfrac{\partial \psi(p_1, p_2)}{p_2} \neq \overline{0} & , p_i \notin \Omega_d \\ \dfrac{\partial \psi(p_1, p_2)}{p_1} + \dfrac{\partial \psi(p_1, p_2)}{p_2} = \overline{0} & , p_i \in \Omega_d \end{cases} \tag{4.27}$$

It is also assumed that $||p_i - p_{i,d}|| \to \infty \implies \psi(p_1, p_2) \to \infty \quad \forall p_{i,d} \in \Omega_d$, which implies that the function $\psi(\cdot)$ is radially unbounded on the error $||p_i - p_{i,d}||$. The third part of the definition is necessary for the stability analysis later on. □

Bounded Objective Function

Definition 4.2.2. *A bounded objective function $\psi_b(p_1, p_2)$ has all the characteristics of an objective function, as stated in definition 4.2.1, but it also has the property*

$$\left\| \frac{\partial \psi_b(p_1, p_2)}{\partial p_i} \right\| < \rho_i \tag{4.28}$$

for some positive $\rho_i \in \mathbb{R}_+$ □

4.2.2 Control Law

The development of a suitable control law is separated in six main results. In Theorem 4.2.1 it was shown how a gravity compensation term can be added to the control input in order to change the potential energy for system (4.22). In Theorem 4.2.2 it was determined that the system is passive with the gravity compensation and, using the Lagrange-Dirichlet Theorem (see Appendix B.3), local asymptotic stability is proved using the Rayleigh dissipation term. In Theorem 4.2.4 asymptotic stability to the desired set is verified with the help of the objective function term and the Krasovskii-LaSalle's invariant set theorem. In Theorem 4.2.5 a saturation function is defined that will be used to bound the control law. In Theorem 4.2.6 the control law for system (4.22) using PVTOL dynamics (3.3), (3.4) and (3.5) is presented.

Theorem 4.2.1. *The control law*

$$u_i \coloneqq \left(m_i + \frac{m_l}{2} \right) \overline{g} + u_{i,p} \tag{4.29}$$

where $u_{i,p} \in \mathbb{R}^2$ *is an additional control input; makes the system* (4.22) *have its minimum potential energy in the set*

$$\begin{bmatrix} q^* \\ \lambda^* \end{bmatrix} \in \Omega_g \coloneqq \left\{ q \in \mathbb{R}^7, \lambda \in \mathbb{R}^2 \;\middle|\; \begin{array}{l} e_{i,x} = 0, \left\| e_{i,y} \right\| = l_i, \\ \left\| \lambda_i \right\| = \dfrac{m_l g}{2 l_i}, \\ e_{i,y} > 0, \\ \lambda_i > 0 \end{array} \right\} \tag{4.30}$$

□

Theorem 4.2.1 allows system (4.22) to have a new point of minimum potential energy

such that $\Omega_d \subset \Omega_g$. Another effect that the gravity compensation has on the system is that it now possesses the passivity property, as stated in the following theorems

Theorem 4.2.2. *The control law*

$$u_i \coloneqq \left(m_i + \frac{m_l}{2}\right) \overline{g} + u_{i,p} \tag{4.31}$$

makes system (4.22) *be passive from the input* $u_{i,p}$ *to the velocity vector* $\begin{bmatrix} \dot{p}_1^T & \dot{p}_2^T \end{bmatrix}^T$ □

One of the advantages of making the system be passive is that feedback interconnections can be added to system (4.22) [Khalil, 2002, Theorem 6.1]. One such connection can be seen in the following theorem

Theorem 4.2.3. *The control law*

$$u_i \coloneqq \left(m_i + \frac{m_l}{2}\right) \overline{g} - k_{v,i}\dot{p}_i + u_{i,\psi} \tag{4.32}$$

where $i \in \{1,2\}$ *and* $k_{v,i} \in \mathbb{R}_+$ *is a positive gain control parameter known as Rayleigh dissipation gain; makes system* (4.22) *be passive from the input* $u_{i,\psi}$ *to the velocity vector* $\begin{bmatrix} \dot{p}_1^T & \dot{p}_2^T \end{bmatrix}^T$ *as seen on Figure 4-2.* □

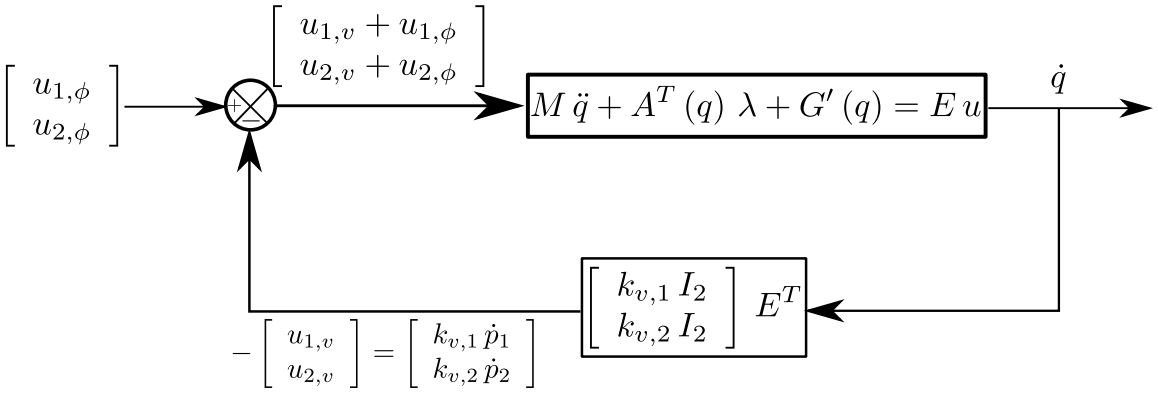

Figure 4-2: Block diagram of system (C.20) showing it is passive.

The Rayleigh dissipation helps to extract kinetic energy from the system in order to drive it into a state of minimum mechanical energy. Also, the gain $k_{v,i}$ can be adjusted to make the system more robust as any perturbation can be seen as increase in the system's

energy. In other words, if the system can be guarantee to always dissipate more mechanical energy than the amount that enters, it adds to its robustness. This is not necessary for the case at hand, but it is worth mentioning it.

Also, other types of feedback interconnections could be added to the system in the same manner as was done in Theorem 4.2.3. The effect that this has is that it changes the minimum of the potential energy. The feedback can also be a passive static nonlinearity (see Definition B.1.2 in Appendix B).

Another use of the passivity property is that stability can be proven by using the Lagrange-Dirichlet theorem as presented in [Lozano et al., 2013, Lemma 7.3], which is shown in Section B.3.

Theorem 4.2.4. *The control law*

$$u_i \coloneqq \left(m_i + \frac{m_l}{2}\right)\overline{g} - k_{v,i}\dot{p}_i - \frac{\partial \psi(p_1,p_2)}{\partial p_i} \tag{4.33}$$

where $i \in \{1,2\}$ *and* $k_{v,i} \in \mathbb{R}_+$ *is a positive gain control parameter; locally asymptotically stabilizes system* (4.22) *towards the set* Ω_d *for any initial condition inside the set*

$$\begin{bmatrix} q_0 \\ \lambda_0 \end{bmatrix} \in \left\{ \begin{bmatrix} q & \dot{q} \end{bmatrix} \in \mathbb{R}^{14}, \lambda \in \mathbb{R}^2 \,\middle|\, e_{i,y} < 0, \lambda_i > 0, T = 0 \right\} \tag{4.34}$$

□

However, this controller assumes that the actuators on the system may output an almost limitless amount of energy, as the control law (4.33) is not bounded. In order to bound it and, therefore, validate the results obtained for a model that is closer to what happens in real-world applications, the control law is bounded using a saturation function.

Definition 4.2.3. *The saturation function is defined for a scalar value* $a \in \mathbb{R}$ *as*

$$\sigma_\beta(a) \coloneqq \begin{cases} a & ,\|a\| < \beta \\ \beta\, sign(a) & ,\|a\| \geq \beta \end{cases} \tag{4.35}$$

where $\beta \in \mathbb{R}_+$ is the saturation limit and sign$(\cdot)$ is the scalar sign function. □

Definition 4.2.4. *The saturation function can be defined for a vector value $v \in \mathbb{R}^n$ as*

$$\overline{\sigma}_\beta(a) := \begin{cases} v & , \|v\| < \beta \\ \beta\, sign(v) & , \|v\| \geq \beta \end{cases} \tag{4.36}$$

where sign$(\cdot) : \mathbb{R}^n \to \mathbb{R}^n$ is the vector sign function and is obtained by applying the scalar sign function element-wise. □

The following theorem shows how a saturation in the control law (4.2.4) still ensures local asymptotic stability for system (4.22).

Theorem 4.2.5. *The control law*

$$u_i := \left(m_i + \frac{m_l}{2}\right)\overline{g} - \overline{\sigma}_{\beta_i}(k_{v,i}\dot{p}_i) - \frac{\partial \psi_b(p_1, p_2)}{\partial p_i} \tag{4.37}$$

$\forall i \in \{1,2\}$ asymptotically stabilizes system (4.22) *towards the set Ω_d for the saturation limits $\beta_i \in \mathbb{R}_+$.* □

It can be seen that the gravity term in the control law (4.37) has not been included in the saturation. The reasoning behind this decision is because the gravity compensation term is constant and therefore allows for the control law to still be bounded without any loss of generality.

4.2.3 Control Law with full PVTOL Dynamics

Theorems 4.2.4 and 4.2.5 give examples of control laws that ensure that the Control Objective 2.2.1 is reached for system (4.22) but do not take explicitly into account the attitude dynamics of each PVTOL vehicle. The following theorem ties in these results with the ones in Chapter 3.

Theorem 4.2.6. *Let there be a control law u_{tra}, u_{alt} that ensures the Control Objective 2.3.1 is enforced on the PVTOL system presented in* (3.24) *with Lyapunov candidate function $V_{att,i}(\xi_i)$, whose differentiation w.r.t. time results in*

$$\dot{V}_{att,i}(\xi_i) = -\upsilon_i\left(\vec{F}_{th,i} - u_i\right) \tag{4.38}$$

where u_i is the desired thrust force as described in Theorem 4.2.4 and $\upsilon_i(\cdot) : \mathbb{R}^2 \to \mathbb{R}_+$ is a positive definite function such that

$$\upsilon_i\left(\vec{F}_{th,i} - u_i\right) > \left\|\dot{\vec{p}}_i\right\| \left\|\vec{F}_{th,i} - u_i\right\| \tag{4.39}$$

Then the control law (4.33) *(or* (4.37)*) locally asymptotically stabilizes the underactuated PVTOL dynamics presented in* (3.3)*,* (3.4) *and* (3.5) *towards the set Ω_d for any initial condition inside the set*

$$\begin{bmatrix} q_0 \\ \lambda_0 \end{bmatrix} \in \left\{ \begin{bmatrix} q & \dot{q} \end{bmatrix} \in \mathbb{R}^{14}, \lambda \in \mathbb{R}^2 \,\middle|\, e_{i,y} < 0, \lambda_i > 0, T = 0 \right\} \tag{4.40}$$

□

4.2.4 Objective Function Design

The choice of using an objective function to guide the system allows control (4.33) to be the basis of more complex control schemes. In this section, some example designs are presented in order to highlight the flexibility of this approach.

Example: Fail-Safe Control

In this case the objective function is defined as $\psi(p_1, p_2) = 0$, which results in $\Omega_d = \Omega_v$. This is considered a fail-safe control because it possess the minimum information necessary in this scheme to accomplish the Control Objective 2.2.1 with an arbitrary desired condition. This control can be used in case the position state of any of the agents is unavailable or if there is a sensor failure. In this case, the final state depends on the initial conditions of the system.

Example: Bounded Altitude Control

The control function for this case is designed in order for the two agents to asymptotically converge to the same altitude using a bounded control. The proposed objective function can be defined as

$$\psi_b(p_1,p_2) = k_{y,1}\ln\left[\cosh\left(y_1-y_d\right)\right] + k_{y,2}\ln\left[\cosh\left(y_2-y_d\right)\right] \tag{4.41}$$

where $k_{y,i} \in \mathbb{R}_+$ and $y_d \in \mathbb{R}$.

This results in

$$\Omega_d = \Omega_v \cap \left\{ \begin{bmatrix} q^T & \dot{q}^T \end{bmatrix}^T \in \mathbb{R}^{14}, \lambda \in \mathbb{R}^2 \middle| y_1 = y_2 = y_d \right\} \tag{4.42}$$

and

$$\frac{\partial \psi_b(p_1,p_2)}{\partial y_i} = k_{y,i}\tanh\left(y_i-y_d\right) \tag{4.43}$$

which has property (4.28) as stated in Definition 4.2.2 for $\rho_i = k_{y,i}$

Example: Passive Formation Control

In this case, the control objective is to stabilize the position of the first agent, which will be denoted as the "leader". The other agent will be forced to follow the leader because of the effect that the physical connection with the load has on the system. The proposed objective function can be defined as

$$\psi(p_1,p_2) = \frac{k_{p,1}\left(p_1-p_{1,d}\right)^T\left(p_1-p_{1,d}\right)}{2} \tag{4.44}$$

where $k_{p,1} \in \mathbb{R}, k_{p,1} > 0$ and $p_{1,d} \in \mathbb{R}^2$.

This results in

$$\Omega_d = \Omega_v \cap \left\{ \begin{bmatrix} q^T & \dot{q}^T \end{bmatrix}^T \in \mathbb{R}^{14}, \lambda \in \mathbb{R}^2 \middle| p_1 = p_{1,d} \right\} \tag{4.45}$$

and $\dfrac{\partial \psi(p_1,p_2)}{\partial p_1} = k_{p,1}\left(p_1-p_{1,d}\right)$. It can easily be seen by using theorem [Khalil, 2002,

Theorem 6.1] that the resulting system with the objective function (4.44) is passive from the input $p_{1,d}$ to the output velocity $\dot{p}_1$. This also highlights how the proposed control design can be used to preserve the passivity of the system while at the same time, reduce the solution space Ω_d.

4.3 Cooperative Control Academic Example and Comparison

In order to demonstrate the control algorithm in action, a numeric simulation is presented. The objective is similar to the passive formation control presented in section 4.2.4, but with an additional altitude reference for the second agent. This section is separated into four parts. Section 4.3.1 describes the objective function used for solving Control Objective 2.2.1. Section 4.3.2 show the parameters used for the simulation and how the gains for the Raleigh dissipation and objective function were chosen. Section 4.3.3 exposes a mechanical impedance-based control that uses the same gains for similar purposes than the presented control law. Finally, Section 4.3.4 displays the results of the numeric simulation with both controllers and exhibits the differences between them.

4.3.1 Objective Function Description

The objective function is defined as

$$\psi(p_1, p_2) := \frac{k_{p,1}\left(p_1 - p_{1,d}\right)^T\left(p_1 - p_{1,d}\right) + k_{p,2}\left(y_2 - y_{2,d}\right)^2}{2} \tag{4.46}$$

where $y_{2,d} \in \mathbb{R}$ and

$$\begin{aligned}\frac{\partial \psi(p_1,p_2)}{\partial p_1} =& k_{p,1}\left(p_1 - p_{1,d}\right)\\ \frac{\partial \psi(p_1,p_2)}{\partial p_1} =& \begin{bmatrix} 0 \\ k_{p,2}\left(y_2 - y_{2,d}\right) \end{bmatrix}\end{aligned} \tag{4.47}$$

4.3.2 Model Parameters

The simulation was made using the data presented in Table 4.1. The control u is designed as in (4.33), with the definition (4.46). The Raleigh dissipation and objective functions gains

$$\begin{aligned} k_{d,1} = \quad k_{d,2} = \quad 3.16227766 \\ k_{p,1} = \quad k_{p,2} = \quad 2.70639157 \end{aligned} \tag{4.48}$$

were chosen using a LQR approach. The model used was a second order particle model with unitary mass ($\ddot{p} = u$) and the parameters used to solve the algebraic Riccati equation were

$$Q_{LQR} = diag\begin{Bmatrix} 10 & 1 \end{Bmatrix} \tag{4.49}$$

is the state-cost weighted matrix[1] and

$$R_{LQR} = I_1 = 1 \tag{4.50}$$

is the input-cost weighted matrix[2].

The simulated control law is described as

[1] The matrix Q_{LQR} was selected in this way to ensure that the position state converges faster to the desired state in order to avoid possible collisions. The velocity is meant to be small in order to more easily allow the implicit communication.

[2] The matrix R_{LQR} was selected in this simple way because the input-cost is not as important as the design of Q_{LQR}.

m_1	$=$	$1.7 \quad kg$	m_2	$=$	$1.62 \quad kg$	m_l	$=$	$0.87 \quad kg$
l_1	$=$	$1.1 \quad m$	l_2	$=$	$0.7 \quad m$	l	$=$	$0.5 \quad m$
t_0	$=$	$0 \quad s$	t_f	$=$	$60 \quad s$	Δt	$=$	$0.1 \quad s$
$x_{1,0}$	$=$	$-1.6 \quad m$	$x_{2,0}$	$=$	$1.2 \quad m$	J_l	$=$	$0.71 \quad kg\,m^2$
$y_{1,0}$	$=$	$0 \quad m$	$y_{2,0}$	$=$	$0 \quad m$	g	$=$	$9.81 \quad m/s^2$
$p_{l,0}$	$=$	$\overline{0} \quad m$	$\theta_{l,0}$	$=$	$0 \quad rad$	$\dot{\theta}_{l,0}$	$=$	$0 \quad rad/s$
$\dot{x}_{1,0}$	$=$	$0 \quad m/s$	$\dot{x}_{2,0}$	$=$	$0 \quad m/s$	$\dot{p}_{l,0}$	$=$	$\overline{0} \quad m/s$
$p_{1,d}$	$=$	$\overline{0} \quad m$	$y_{2,d}$	$=$	$0 \quad m$			

Table 4.1: The parameters used for the simulation

$$
\begin{aligned}
u_1 &:= -k_{p,1}\, p_1 - k_{d,1}\, \dot{p}_1 + \left(m_1 + \frac{m_l}{2}\right) \overline{g} \\
u_2 &:= -k_{p,2} \begin{bmatrix} 0 \\ y_1 \end{bmatrix} - k_{d,2}\, \dot{p}_2 + \left(m_2 + \frac{m_l}{2}\right) \overline{g}
\end{aligned}
\tag{4.51}
$$

The initial conditions of the bar and the vehicles were chosen as one of the most critical states in the problem addressed.

4.3.3 Impedance Control for Comparison

The following impedance control is formulated in order to have comparative simulation results in order to show the superiority of the proposed approach. The control has the same structure as the ones presented in [Villani and De Schutter, 2016, control law 9.16] and [Augugliaro and D'Andrea, 2013, control law 19]

Definition 4.3.1.

$$
\begin{aligned}
u_{1,impedance} &:= -k_{p,1}\, p_1 - k_{d,1}\, \dot{p}_1 + \begin{bmatrix} 0 \\ m_1\, g \end{bmatrix} + e_1\, \lambda_1 \\
u_{2,impedance} &:= -k_{p,2} \begin{bmatrix} x_{d,2} \\ y_1 \end{bmatrix} - k_{d,2}\, \dot{p}_2 + \begin{bmatrix} 0 \\ m_2\, g \end{bmatrix} + e_2\, \lambda_2
\end{aligned}
\tag{4.52}
$$

where $x_{d,2} := 2l \sin\left[\arccos\left(\frac{l_1 - l_2}{2l}\right)\right]$ *is the desired lateral distance for the second vehicle. It was chosen to coincide with the equilibrium point of the objective function in*

(4.46). □

It can be seen that the control inputs in (4.52) depend on not just knowing the desired distance $x_{d,2}$, but also the forces $e_i \lambda_i$ that the presence of the cable and load has on the system. These external forces are assumed to be measured or estimated, like in [Tagliabue et al., 2019].

4.3.4 Simulation Results

In the following section, the simulation results are shown. The proposed control law in (4.51) is plotted on the left side of Figures 4-3 to Figure 4-10. The impedance control (4.52) is plotted on the right side.

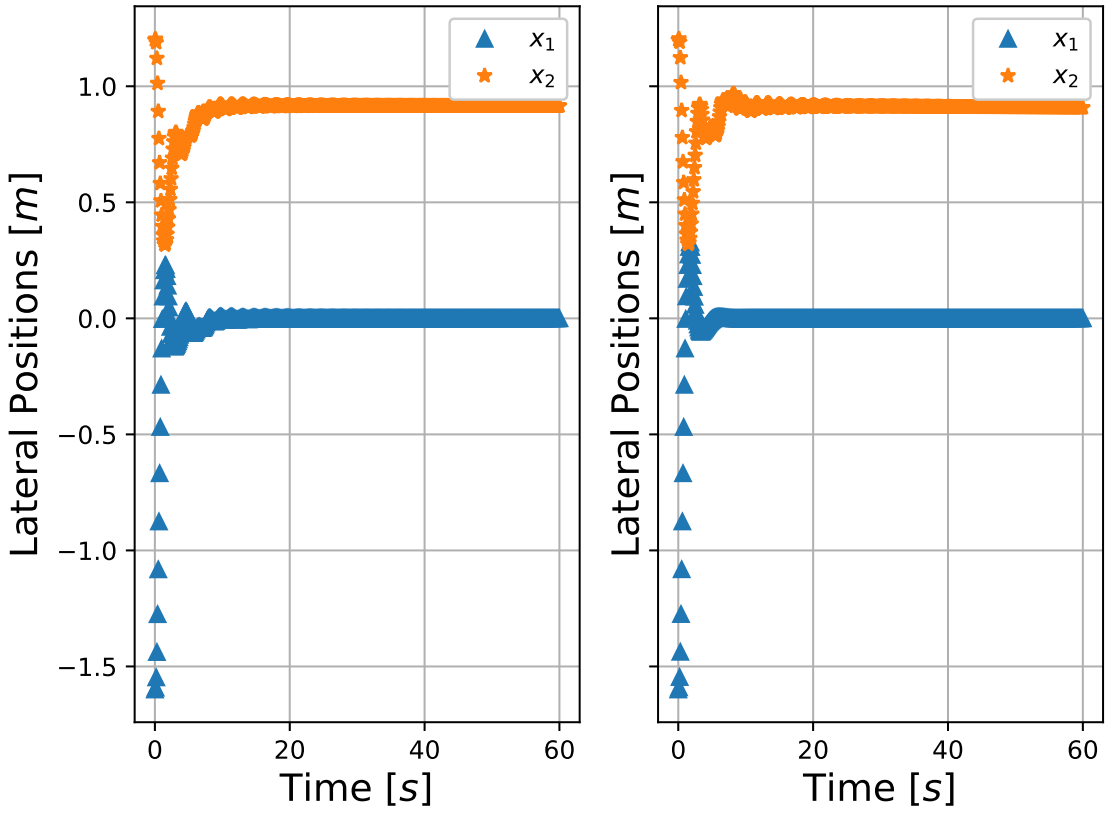

Figure 4-3: The lateral position of each of the agents. Left is the proposed controller

Figure 4-3 shows that the lateral position of each vehicle tends towards

$$x_1 \approx 0, x_2 \approx 2l \sin\left[\arccos\left(\frac{l_1 - l_2}{2l}\right)\right] \approx 0.9177 \tag{4.53}$$

on both plots. It can be seen that the control objective has been accomplished for the lateral position of the first vehicle.

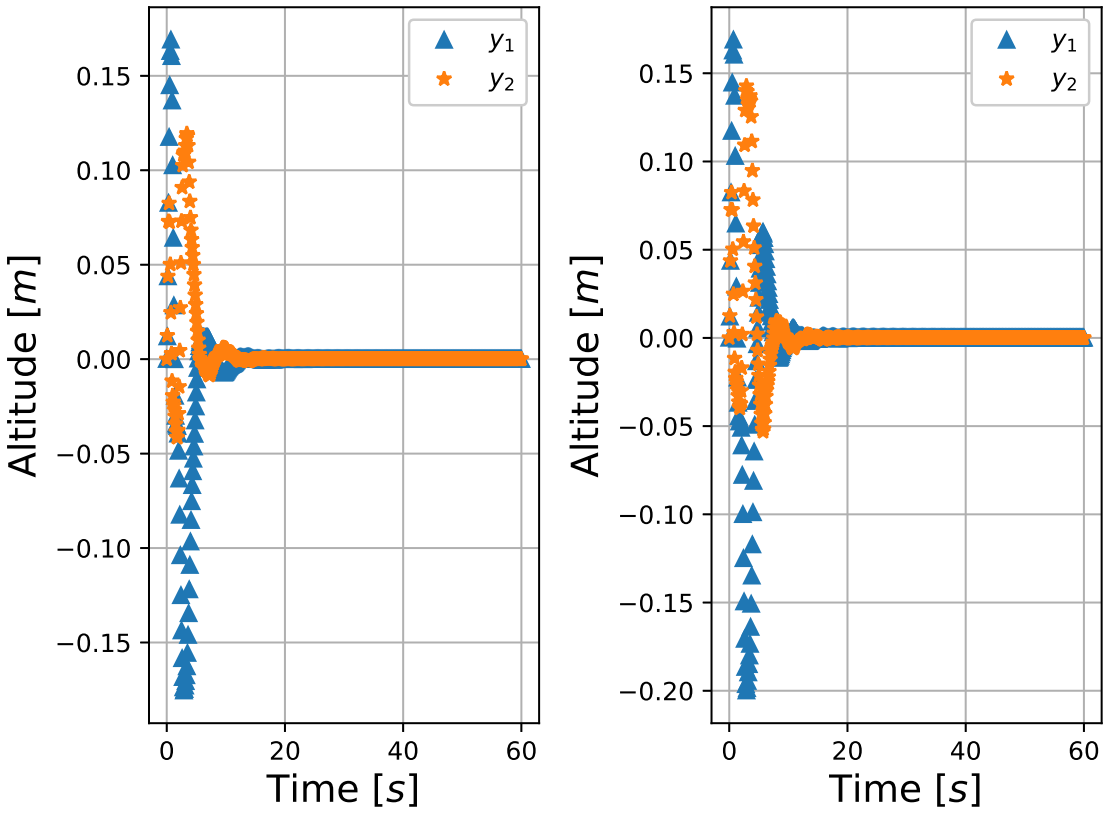

Figure 4-4: The altitude of each of the agents. Left is the proposed controller

Another control objective was to maintain a zero altitude in both vehicles. Figure 4-4 shows that this objective is accomplished in both plots.

The position of the bar is plotted in Figure 4-5. It can be seen that both plots converge asymptotically towards the values

$$p_l \approx \left[\begin{array}{c|c} \frac{l_1 - l_2}{2} & l_1 + l \sin\left\{\arccos\left(\frac{l_1 - l_2}{2l}\right)\right\} \end{array}\right]^T \approx [0.4588, -0.9018]^T \tag{4.54}$$

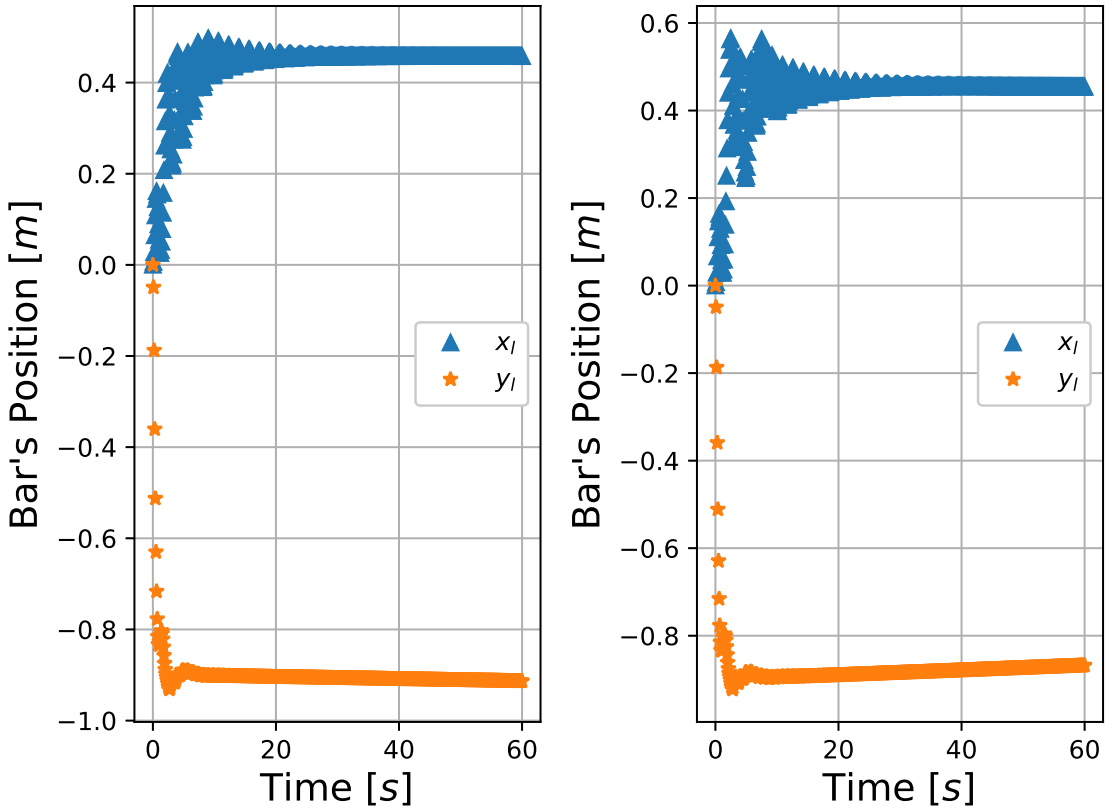

Figure 4-5: The position of the load in the plane. Left is the proposed controller

The bar's attitude also tends towards the constant value of

$$\theta_l \approx \arccos\left(\frac{l_1 - l_2}{2l}\right) \approx 0.40825 \tag{4.55}$$

as seen in Figure 4-6 for both plots.

The velocities of both vehicles tend to dissipate for the proposed control law as the velocity feedback term of the control acts as a damper of the kinetic energy and is reflected in the passivity properties that have been previously proved. The impedance control also added a dampening term for the vehicles' velocities. These velocities are shown in Figure 4-7 and Figure 4-8.

Even though both control algorithms do not depend on the bar's state (which is the bar's position, attitude, velocity and angular velocity), it can be seen that their kinetic energy (velocity) tends towards zero as seen in Figure 4-9 and Figure 4-10. This in turn implies

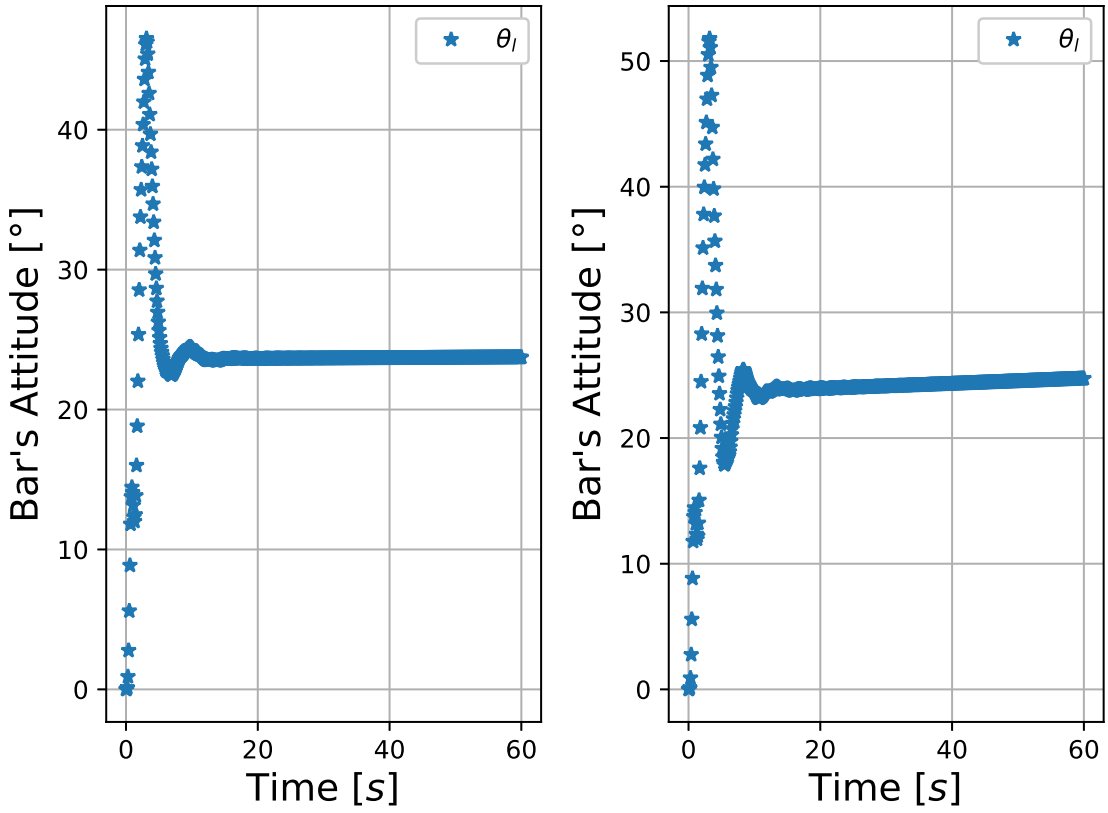

Figure 4-6: The orientation of the load w.r.t. time. Left is the proposed controller

that the velocity converges to zero and the position tends to the desired value.

Both control schemes have similar performance under the proposed simulation conditions. However, it should be noted that the impedance control law requires more direct knowledge of the state of the vehicles.

4.4 Summary

The aim of this chapter was to solve the problem of cooperative slung-load transportation on a plane using two modified PVTOL vehicles. For this purpose, a decentralized cooperative control law design methodology was devised using the physical connection of the system to establish what is known as implicit communication. The vehicles and the load are guaranteed to be locally asymptotically stable towards a desired state set using very little system information. In this way, the Control Objective 2.2.1 can be achieved as seen in Fig-

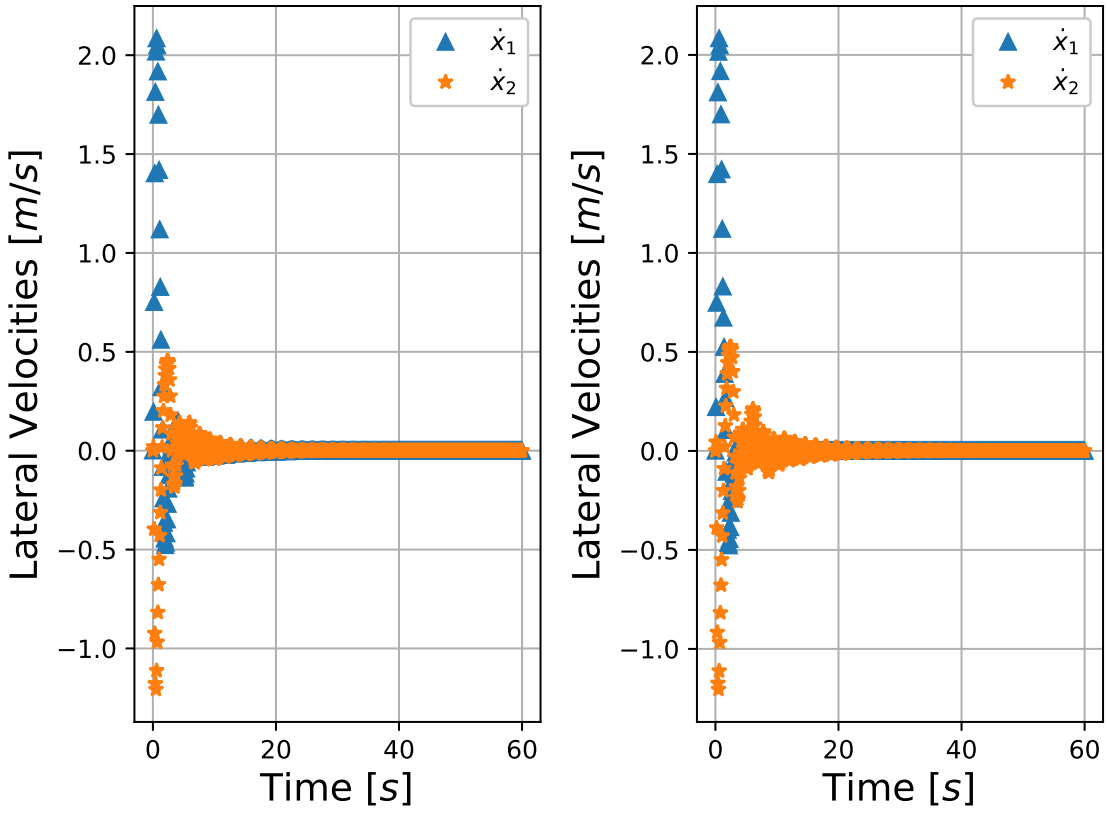

Figure 4-7: The lateral velocity of each of the agents. Left is the proposed controller

ure 2-4. The algorithm in its minimum expression only requires the velocity information of each vehicle as demonstrated by the fail-safe example in Section 4.2.4. The proposed approach was based on passivity, which adds robustness by dissipating any energy that may enter the system via a perturbation. The design using an objective function allows the proposed control scheme to be used as a basis for more complex algorithms, even a bounded one as shown in Section 4.2.4.

The method was displayed using a numeric simulation as an academic example with a formation objective, as described in Section 4.3.1, and the results analyzed in Section 4.3.4. A cooperative impedance control law was formulated in order to have comparative simulation results. It can be seen that the control was able to asymptotically stabilize the system using the proposed methodology in an similar manner as the impedance control. The key advantage of this method comes from the fact that the proposed control does not require the estimation of the external forces acting on each platform, unlike the ones

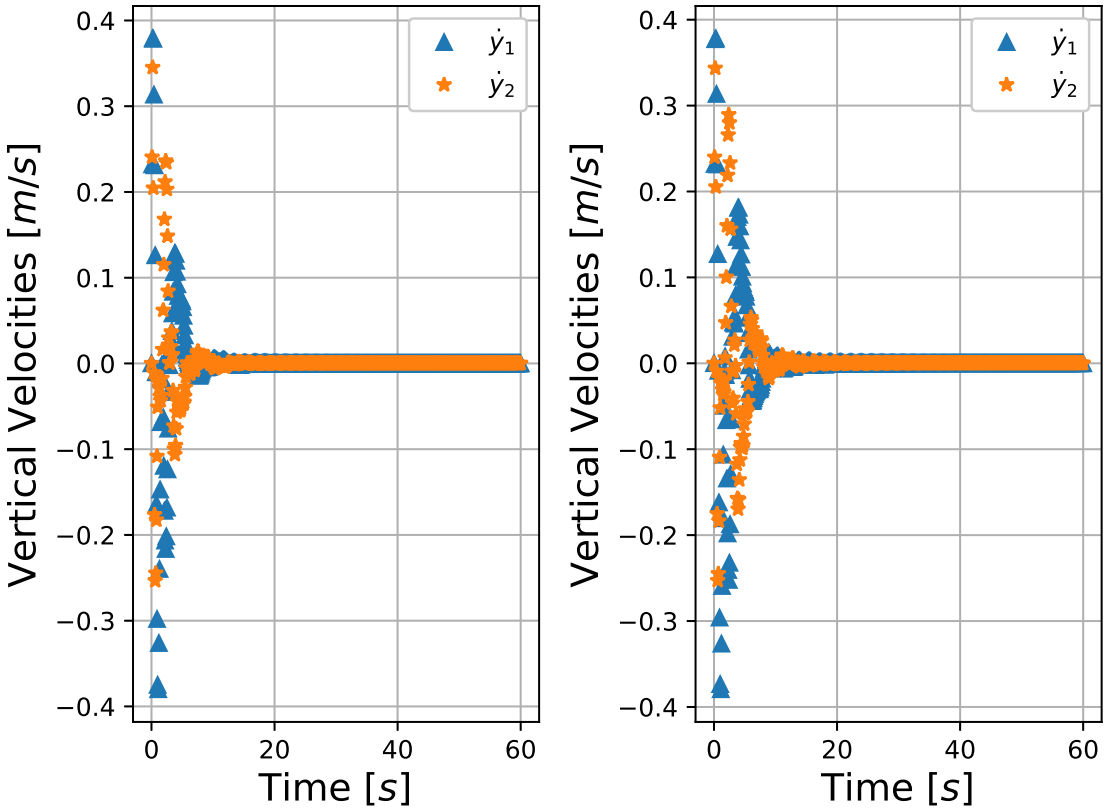

Figure 4-8: The vertical velocity of each of the agents. Left is the proposed controller proposed in [Tognon et al., 2018] [Tagliabue et al., 2017] [Tagliabue et al., 2019]

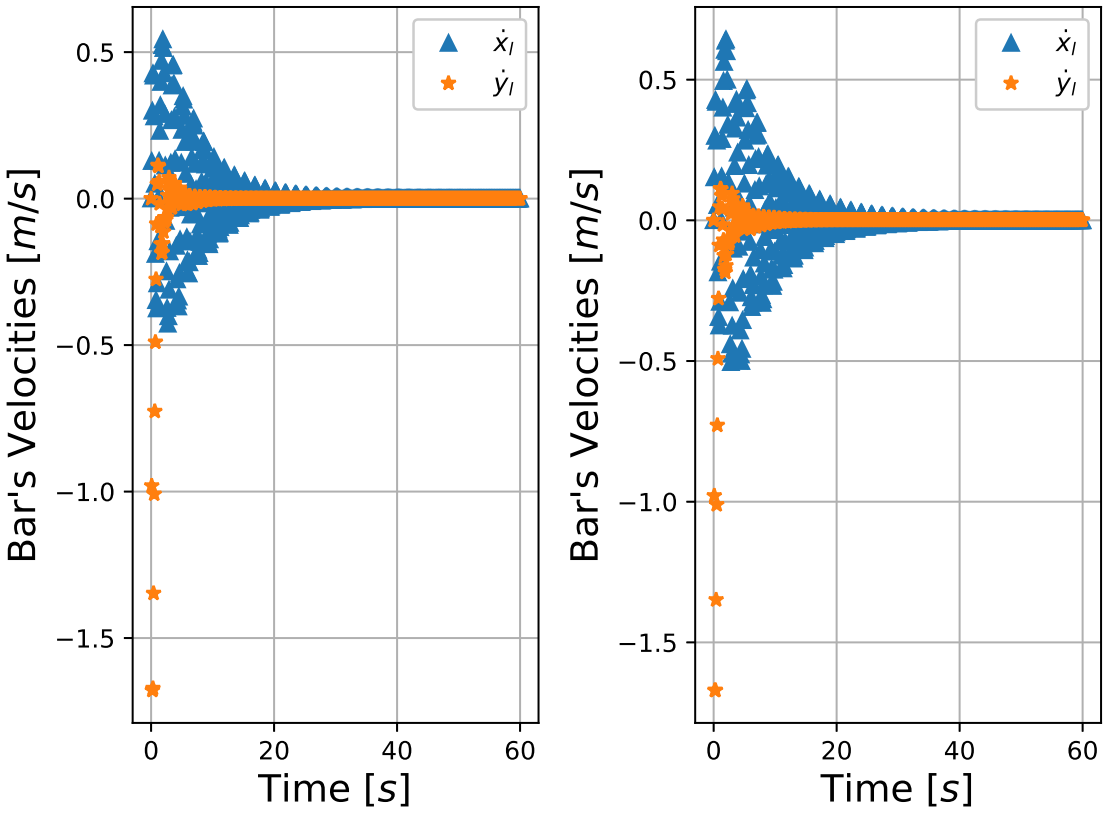

Figure 4-9: The velocity of the load in the plane. Left is the proposed controller

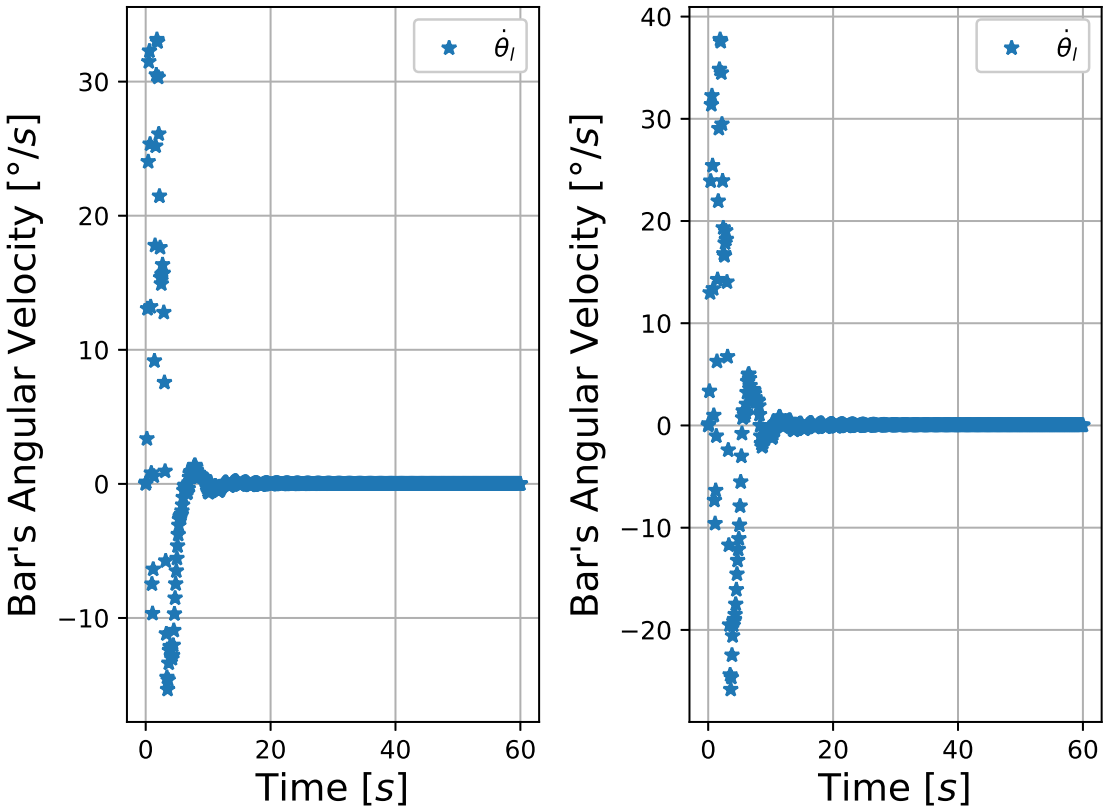

Figure 4-10: The change of angular velocity of the load w.r.t. time. Left is the proposed controller

Chapter 5

Indoor Experiments: Two Quadcopters Cooperative Slung-Load Transport Control

In this chapter the stability results and theorems developed in Chapter 4 were applied to a pair of quadcopter vehicles carrying a carbon fiber bar in order for them to achieve Control Objective 2.1.1. The theorems presented in the previous chapter, namely Theorem 4.2.4, do not directly translate into the quadcopter platform. However, the problem was divided into two separate cooperative control problems in two different planes. The resulting control algorithm was then fed into a quadrotor control law based on quaternions which was developed in [Carino et al., 2015], and it is summarized in Appendix D.

The chapter is divided in three main sections. The experimental setup is described in detail in Section 5.1, including the physical parameters of the system and the desired behavior of the cooperative system. Section 5.2 divides the control problem into two orthogonal planes; the design methodology from Chapter 4 is used to propose two separate cooperative controllers to achieve Control Objective 2.1.1 for each of the two different planes. Finally, the results are presented in Section 5.3. The proofs for this chapter are shown in Appendix E. An summary of the quadcopter controller used can be found in Appendix D.

5.1 Experimental Setup

The experimental setup consists of two quadcopter vehicles attached to a carbon fiber bar of one meter of length using nylon cables. The configuration can be seen in Figure 5-1

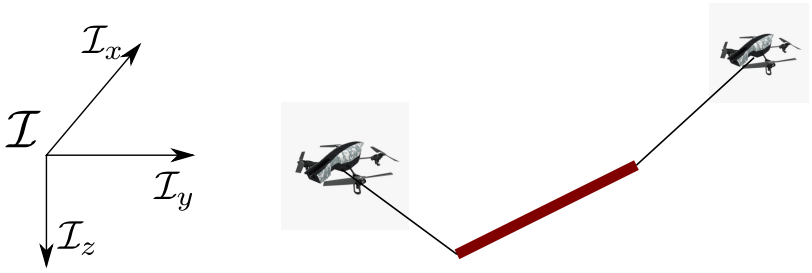

Figure 5-1: Slung-load configuration of the two quadcopters cooperatively carrying a bar. The inertial frame $\mathscr{I}$ can be separated into two perpendicular planes $x-z$ and $y-z$.

As was explained in Section 2.2.1, the movement of the quadcopters and the bar can be projected into two perpendicular planes $x-z$ and $y-z$. The planes and the quadcopter agent's projection can be seen in Figure 5-2 and Figure 5-3

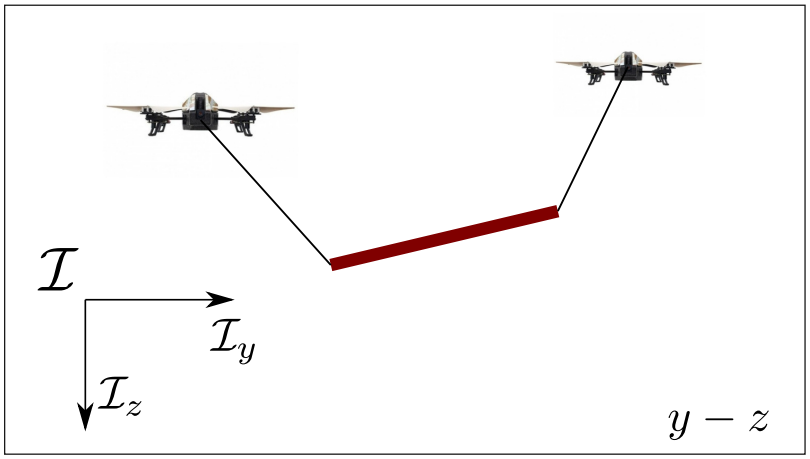

Figure 5-2: Slung-load configuration of the two quadcopters cooperatively carrying a bar in the $y-z$ plane

The objective of the experiment is to translate the bar from one point into another using both vehicles. One of the agents acts as the leader, receiving reference position commands from a human operator while the other agent is tasked with keeping a formation w.r.t. itself and its leader as closely as possible. In other words, the Control Objective 2.1.1 has been separated into two Control Objectives 2.2.1.

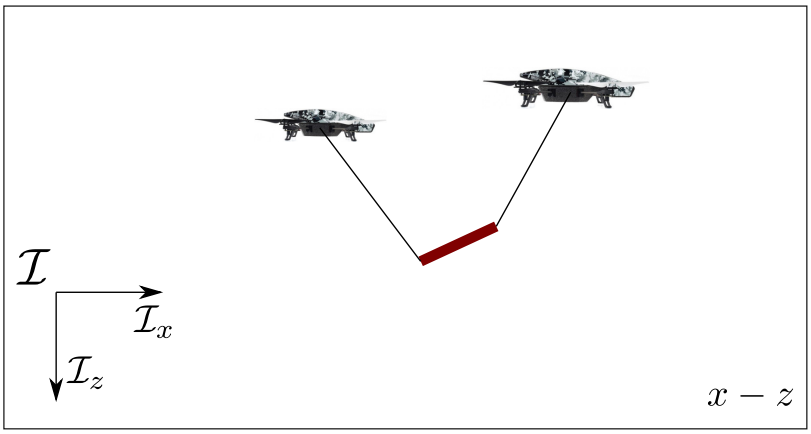

Figure 5-3: Slung-load configuration of the two quadcopters cooperatively carrying a bar in the $x-z$ plane

The quadcopter vehicles used were of the model Ar.Drone 2.0 platform by the company Parrot©. Its technical specifications can be seen in tables 5.1. The platform

Video Specifications [1]
720p 30fps HD camera
Wide-angle lens: 92 deg diagonal
Basic encoding profile: H264
Photo format: JPEG
Connection: Wi-Fi

Table 5.1: Video specifications of the Ar.Drone 2.0 platform [Parrot©, 2019]

[1] Not necessary for the experimental result

Electronics, Software and Sensors
Processor: ARM Cortex A8 1 GHz 32-bit processor
DSP video: 800 MHz TMS320DMC64x
OS: Linux 2.6.32
eq: Objective Function minimums RAM: DDR2 1 GB at 200 MHz
USB: High-speed USB 2.0 for extensions
Wi-Fi b g n
Gyroscope: 3 axles, accuracy of 2000 deg $/s$
Accelerometer: 3 axles, accuracy of $+/-50\,mg$
Magnetometer: 3 axles, accuracy of 6 deg
Pressure sensor: Accuracy of $+/-10\,Pa$
Altitude ultrasound sensor [2]
Vertical camera: QVGA 60 FPS to measure the ground speed

Table 5.2: Electronics, software and sensors specifications of the Ar.Drone 2.0 platform [Parrot©, 2019]

Motors and Weight
4 "inrunne" type brush-free motors: 14.5 $watts$ and 28500 rev/min
Micro ball bearing
Nylatron Gears
Bronze self-lubricating ball bearings
Weight with internal frame 380g

Table 5.3: Motors and weight specifications of the Ar.Drone 2.0 platform [Parrot©, 2019]

The platforms were programmed using the Fl-AIR programming platform, which "[...]is a framework written in C++ that aims at helping the development of applications for robots, and more specially for UAVs"[libre AIR, 2019], and the positions were obtained using.

an OptiTrack motion capture system [OptiTrack, 2019].

[2]Not enabled when the control law is active

5.2 Implemented Control Law

Let us define the desired objective sets $\Omega_{d,x-z} \subset \Omega_d$ and $\Omega_{d,y-z} \subset \Omega_d$ (see (4.26)) for each control objective on each of the planes $x-z$ and $y-z$, respectively, as

$$\Omega_{d,x-z} = \left\{ \left[\begin{array}{ccc} q^T & \dot{q}^T & \lambda^T \end{array} \right]^T \in \mathbb{R}^{16} \left| \begin{array}{l} \dot{q} = \overline{0}, e_{i,x} = 0, \\ \|e_{i,z}\| = l_i, \\ \|\lambda_i\| = \dfrac{m_l g}{2 l_i}, \\ e_{i,z} < 0, \lambda_i > 0, \\ z_1 = z_{1,d}, z_2 = z_{2,d} \neq z_{1,d} \\ x_1 = x_2 = x_{1,d} \end{array} \right. \right\} \tag{5.1}$$

and

$$\Omega_{d,y-z} = \left\{ \left[\begin{array}{ccc} q^T & \dot{q}^T & \lambda^T \end{array} \right]^T \in \mathbb{R}^{16} \left| \begin{array}{l} \dot{q} = \overline{0}, e_{i,y} = 0, \\ \|e_{i,z}\| = l_i, \\ \|\lambda_i\| = \dfrac{m_l g}{2 l_i}, \\ e_{i,z} < 0, \lambda_i > 0, \\ z_1 = z_{1,d}, z_2 = z_{2,d} \neq z_{1,d} \\ y_1 = y_{1,d}, y_2 - y_1 = d, y_1 \neq y_2 \end{array} \right. \right\} \tag{5.2}$$

where $x_{1,d}, z_{1,d}, z_{2,d} \in \mathbb{R}$ are reference positions in the x and z axes, respectively, given by the human operator; $y_{1,d} \in \mathbb{R}$ is a reference position in the y axis given by the human operator; $d \in \mathbb{R}_+$ is a reference distance between the first and second agents in the y axis The conditions $z_{2,d} \neq z_{1,d}$ and $y_1 \neq y_2$ are used to prevent collisions.

5.2.1 Implemented Objective Function

The objective functions of Section 4.2.1, $\psi_{x-z}\left(\vec{p}_{1,x-z}, \vec{p_{2,x-z}}\right)$ and $\psi_{y-z}\left(\vec{p}_{1,y-z}, \vec{p_{2,y-z}}\right)$ are defined for the planar positions $\vec{p}_{i,x-z}, \vec{p}_{i,y-z} \in \mathbb{R}^2$ for each of the planes $x-z$ and $y-z$, respectively. However, a problem becomes apparent from these definitions. The position reference is only available to the first of the agents. The other agent needs to follow the

former at a safe distance in order to ensure that the load remains at a constant altitude. In this case, the objective functions must only affect directly the state of the second agent, which poses a problem because of how these functions have been formulated up to this point (see the examples in Section 4.2.4). In simple terms, it is difficult to formulate an objective function explicitly that only affects one of the agents and achieves the proposed objectives.

Fortunately, the way the objective function was defined in Definition 4.2.1 is sufficiently general that it is not strictly necessary to know explicitly the objective function, only its characteristics. In particular, the properties

$$\psi(p_1,p_2):\begin{cases}\psi(p_1,p_2)>0 & ,p_i\notin\Omega_d\\ \psi(p_1,p_2)=0 & ,p_i\in\Omega_d\end{cases} \tag{5.3}$$

can be ensured by looking at the convexity of the objective function, which is a property of its partial differentiation w.r.t. each state $\vec{p}_i$.

This is shown in the following corollary

Corollary 5.2.1. *Let* $\psi(\vec{p}_1,\vec{p}_2):\begin{bmatrix}\mathbb{R}^2 & \mathbb{R}^2\end{bmatrix}\to\mathbb{R}$ *be an objective function with the properties shown in* (5.3) *if the partial differentiation function* $\dfrac{\partial\,\psi(\vec{p}_1,\vec{p}_2)}{\partial\begin{bmatrix}\vec{p}_1^T & \vec{p}_2^T\end{bmatrix}^T}$ *exists such that*

$$\left.\frac{\partial\,\psi(\vec{p}_1,\vec{p}_2)}{\partial\begin{bmatrix}\vec{p}_1^T & \vec{p}_2^T\end{bmatrix}^T}\right|_{\Omega_d}=\vec{0} \tag{5.4}$$

for some set Ω_d *and if the diagonal elements of the second partial differentiation function* $\dfrac{\partial^2\,\psi(\vec{p}_1,\vec{p}_2)}{\partial\begin{bmatrix}\vec{p}_1^T & \vec{p}_2^T\end{bmatrix}^{T,2}}$ *are positive*

Corollary 5.2.1 implies that the objective function is convex with a minimum in Ω_d. This is the same conditions used to prove Theorem B.3.1 in [Lozano et al., 2013, Lemma 7.3].

The objective functions can then be defined from its partial differentiation functions using the following theorem

Theorem 5.2.1. *Let there be two functions* $\psi_{x-z}(\vec{p}_{1,x-z}, \vec{p}_{2,x-z}) : \mathbb{R}^4 \to \mathbb{R}_+$ *and* $\psi_{y-z}\left(\vec{p}_{1,y-z}, \vec{p}_{2,y-z}\right) : \mathbb{R}^4 \to \mathbb{R}_+$ *whose partial differentiation w.r.t. each of their states be defined as*

$$\frac{\partial\, \psi_{x-z}(\vec{p}_{1,x-z}, \vec{p}_{2,x-z})}{\partial \begin{bmatrix} \vec{p}_{1,x-z}^T & \vec{p}_{2,x-z}^T \end{bmatrix}^T} := \begin{bmatrix} (x_1 - x_{1,d})\, k_{p,1} \\ (z_1 - z_{1,d})\, k_{p,1} \\ (x_2 - x_1)\, k_{p,2} \\ (z_2 - z_{2,d})\, k_{p,2} \end{bmatrix} \tag{5.5}$$

$$\frac{\partial\, \psi_{y-z}\left(\vec{p}_{1,y-z}, \vec{p}_{2,y-z}\right)}{\partial \begin{bmatrix} \vec{p}_{1,y-z}^T & \vec{p}_{2,y-z}^T \end{bmatrix}^T} := \begin{bmatrix} (y_1 - y_{1,d})\, k_{p,1} \\ (z_1 - z_{1,d})\, k_{p,1} \\ \left(\dfrac{y_2 - y_1}{d|y_2 - y_1|} - \dfrac{1}{y_2 - y_1}\right) k_{p,2} \\ (z_2 - z_{2,d})\, k_{p,2} \end{bmatrix} \tag{5.6}$$

for the planar positions $\vec{p}_{i,x-z}, \vec{p}_{i,y-z} \in \mathbb{R}^2$.

The functions $\psi_{x-z}(\vec{p}_{1,x-z}, \vec{p}_{2,x-z})$ *and* $\psi_{y-z}\left(\vec{p}_{1,y-z}, \vec{p}_{2,y-z}\right)$ *are candidate objective functions as described in Definition 4.2.1 with its minimums in* $\begin{bmatrix} \vec{p}_{1,x-z}^T & \vec{p}_{2,x-z}^T \end{bmatrix}^T \in \Omega_{d,x-z}$ *and* $\begin{bmatrix} \vec{p}_{1,y-z}^T & \vec{p}_{2,y-z}^T \end{bmatrix}^T \in \Omega_{d,y-z}$

□

The third term in equation (5.6) is of particular interest, as it helps to avoid the collision of both agents with a singularity when $y_1 = y_2$ and it is equal to zero when $|y_2 - y_1| = d$.

5.2.2 Implemented Control Law

The control law that was implemented in the quadcopter is explained in Appendix D by modeling the quadcopter as two PVTOL vehicles but on different planes. The reference force comes from applying Theorem 4.2.4 to the objective functions described in Theorem 5.2.1. Stability is ensured if the implemented controller [Carino et al., 2015, (12)] can guarantee that the error between the control law (4.33) and each of the quadcopter orientations q_i tends towards zero using Theorem D.1.1 in Appendix D. Therefore, Control Objective 2.3.1 is ensured for the implemented control scheme. This can be seen as a double implementation of the control law presented in Theorem 4.2.6.

The implemented control scheme can be seen in Figure 5-4. Comparing it with the one shown in Figure 2-4, it can be noted that the attitude control is now using the reference attitude provided by Theorem D.1.1 in Appendix D. However, the cooperative system structure remained the same.

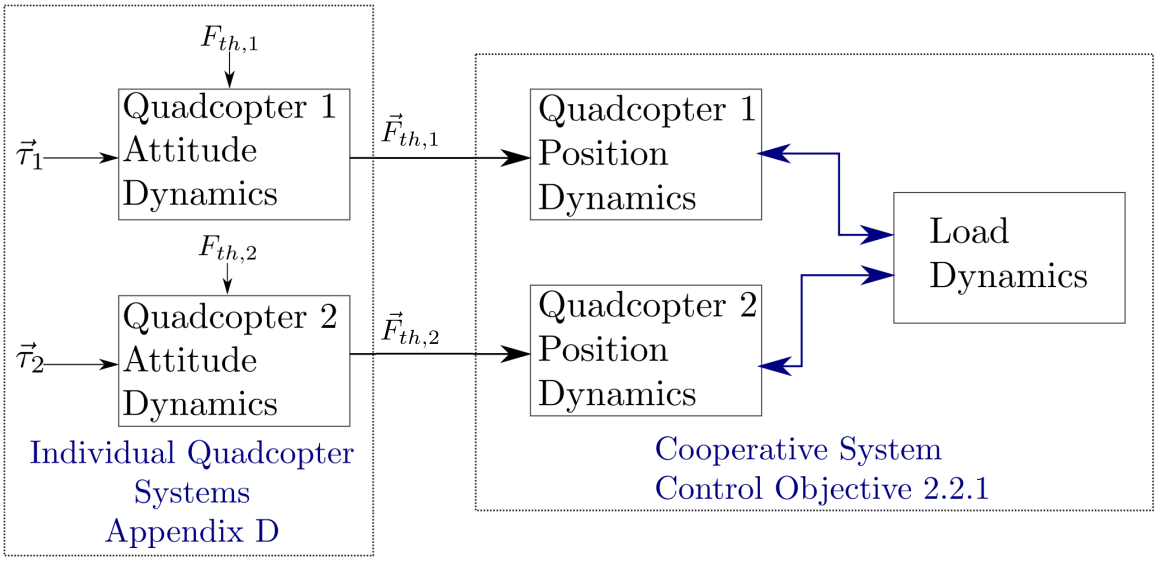

Figure 5-4: A block diagram that shows how the cooperative control using two quadcopters can be separated into two different specific control objectives

5.3 Experimental Results

Figure 5-5 shows the two quadcopter agents carrying the bar using nylon threads. The cables are not visible in the image.

Figures 5-6 and 5-7 show the position of the vehicles during the take-off part and the transportation part. It can be seen in Figure 5-6 that the vehicles try to remain in the x plane. Figure 5-7 shows that the drones keep their distance almost constant, which can also be seen in Figure 5-8, showing that the control is working.

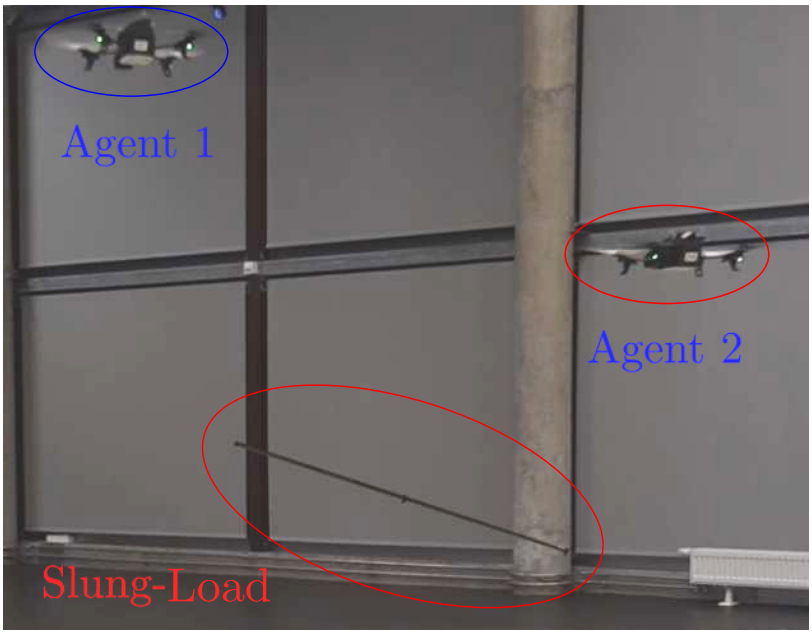

Figure 5-5: Two quadcopters transporting a slung-load

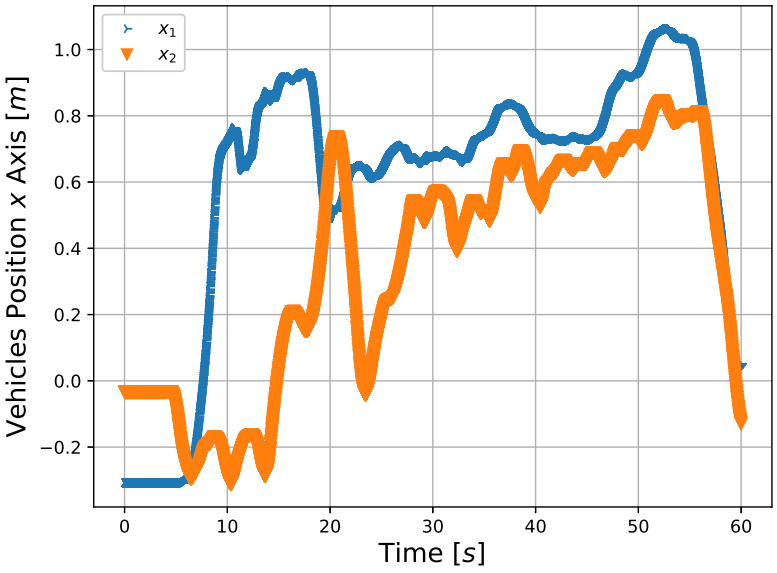

Figure 5-6: Position in the x axis of the transportation experiment

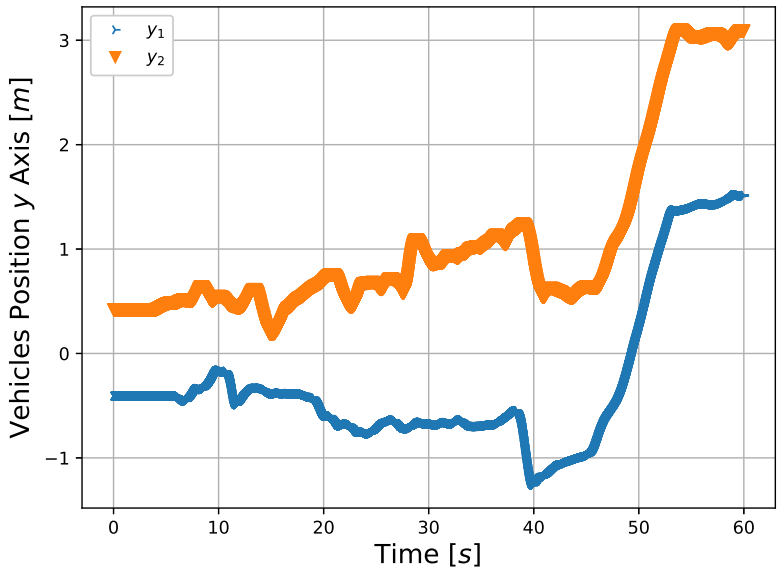

Figure 5-7: Position in the y axis of the transportation experiment

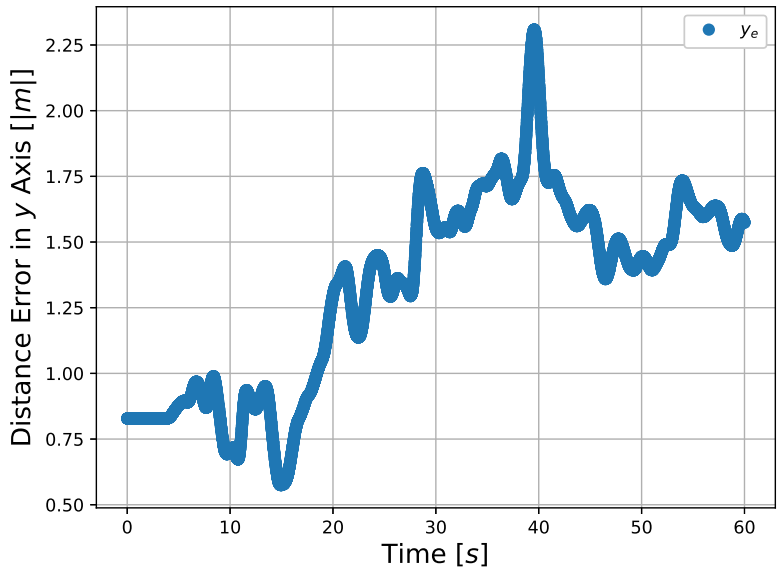

Figure 5-8: Distance between agents in the y axis in the transportation experiment

Figures 5-9 and 5-10 show the altitude of each vehicle along with the altitude reference. It can be seen that the first agent tracks the altitude better than the second one, but the error is still negligible.

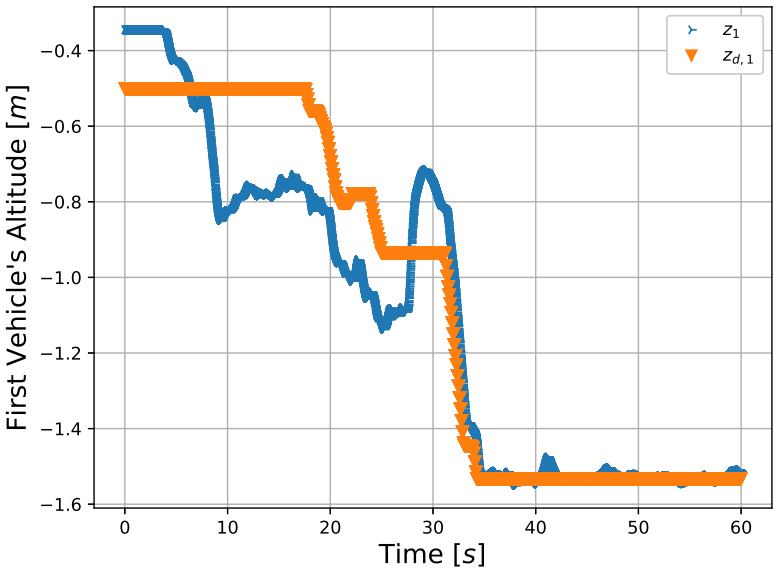

Figure 5-9: First drone's altitude of the transportation experiment

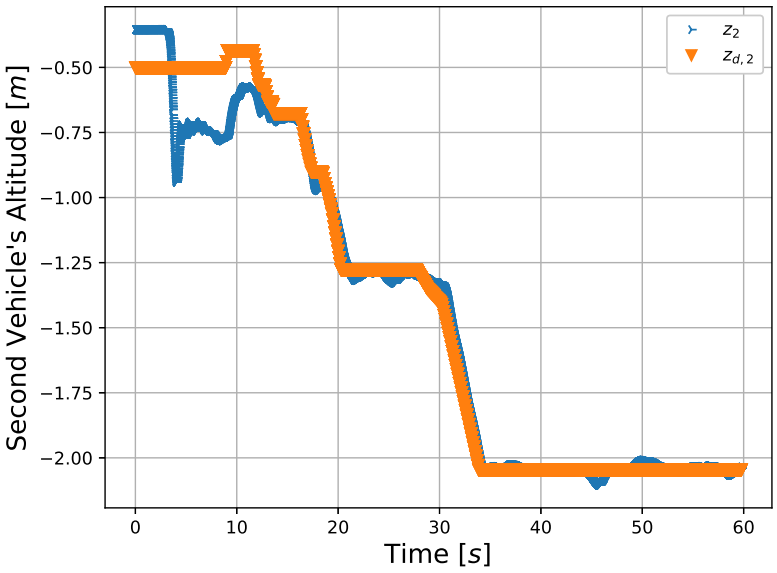

Figure 5-10: Second drone's altitude of the transportation experiment

Figures 5-11 and 5-12 display the velocity of each agent. It can be seen that there are some spikes but that could be because of the noise in the speed measurements of the OptiTrack, as it uses a low-pass filter in order to estimate the speeds.

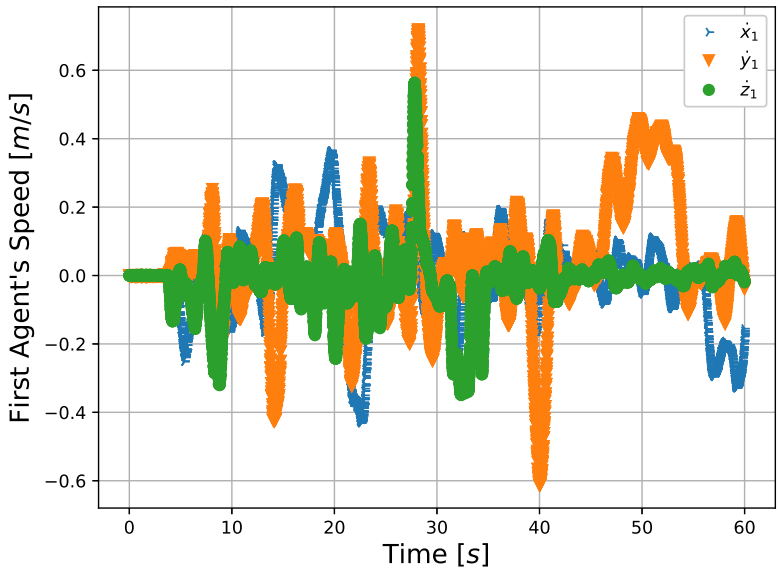

Figure 5-11: The first agent's speed in the transportation experiment

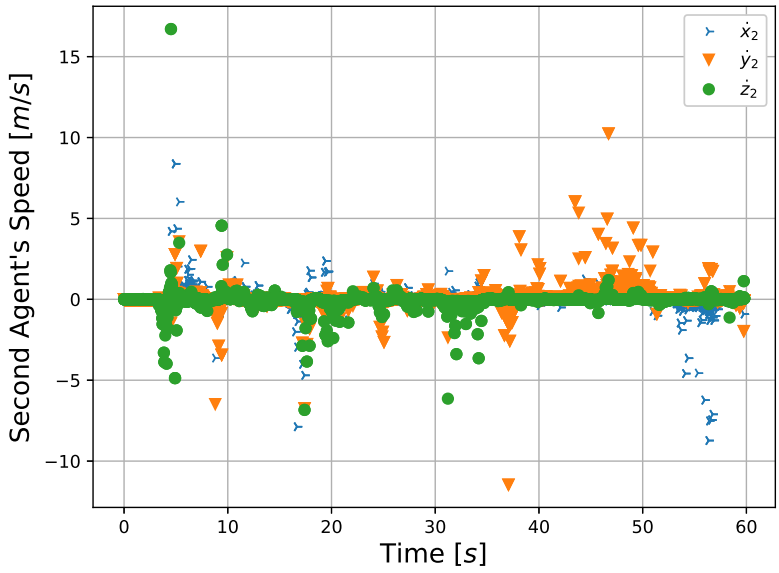

Figure 5-12: The second agent's speed in the transportation experiment

Figures 5-13 and 5-14 present the attitude of each drone. There are some spikes in the attitude due to the references shifting in order to enforce the desired position control.

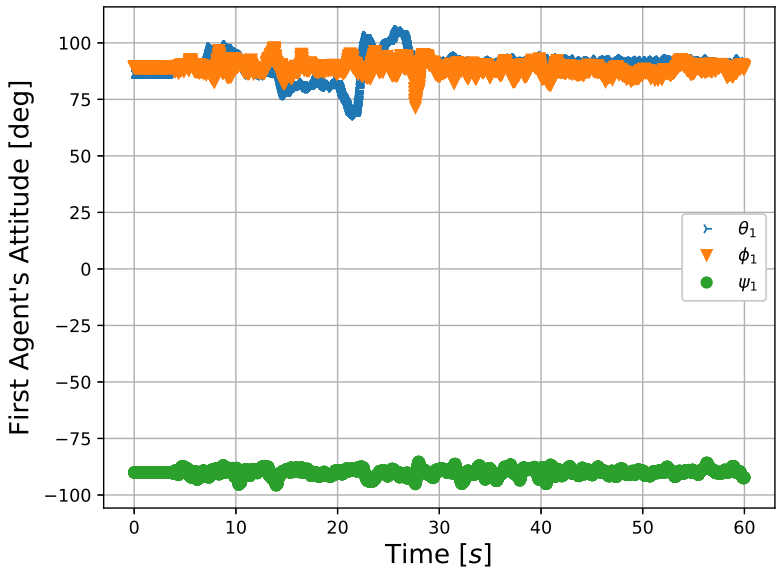

Figure 5-13: First agent's orientation in the transportation experiment

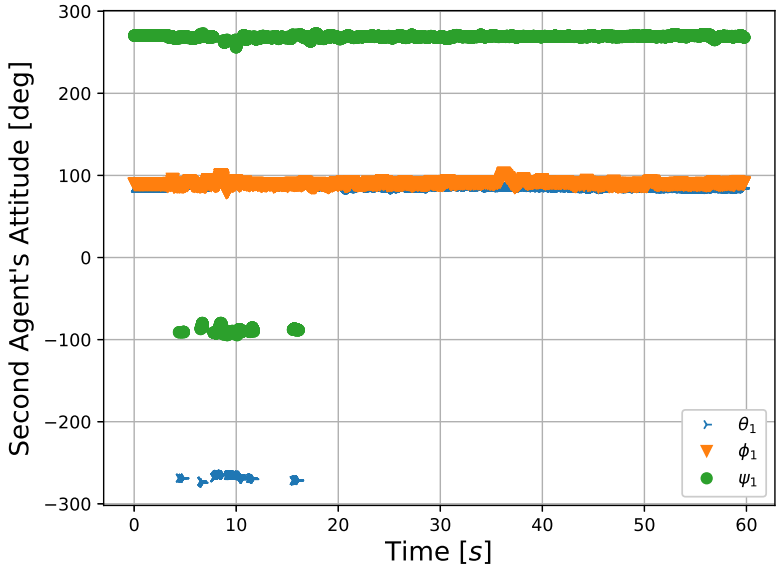

Figure 5-14: Second agent's orientation in the transportation experiment

Figures 5-15 and 5-16 present the angular velocity of each quadcopter. It is very noisy as it comes directly from the unfiltered IMU.

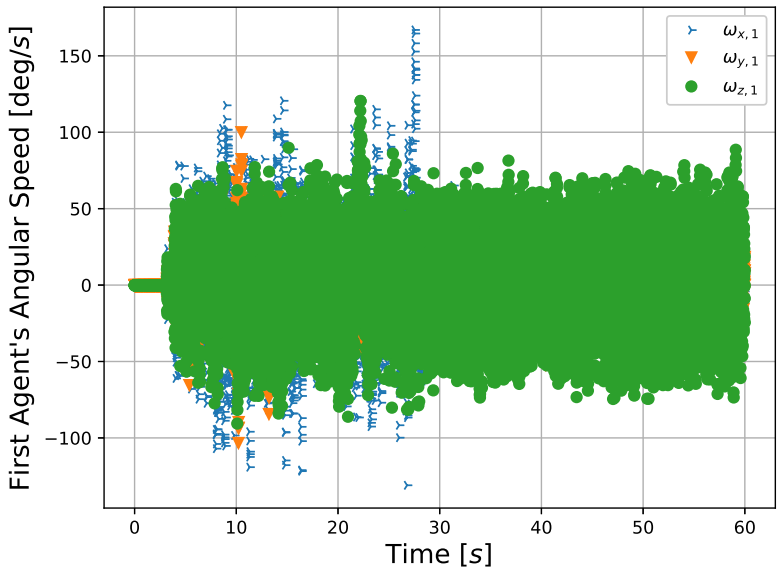

Figure 5-15: First agent's angular speed in the transportation experiment

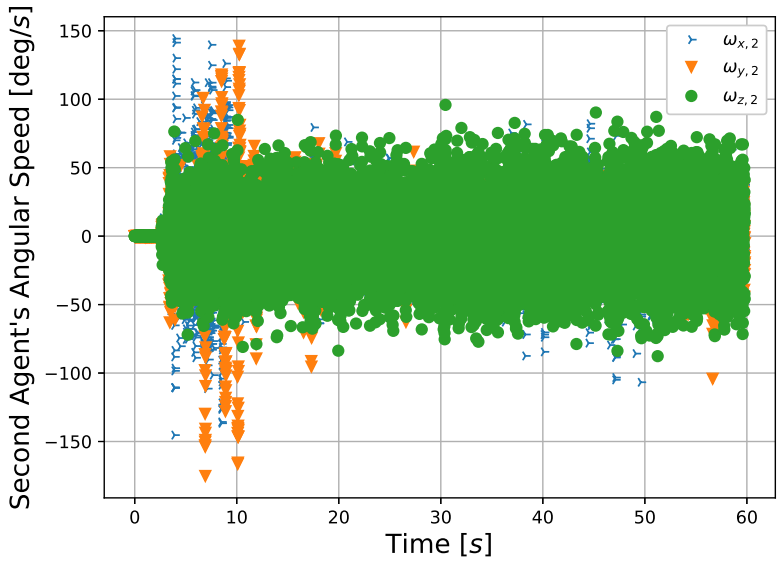

Figure 5-16: Second agent's angular speed in the transportation experiment

Finally, Figure 5-17 shows the full spatial trajectory of both agents in a 3D plot. It is worth noting that the distance in the x axis is relatively small compared to the altitude and the distance in the y axis.

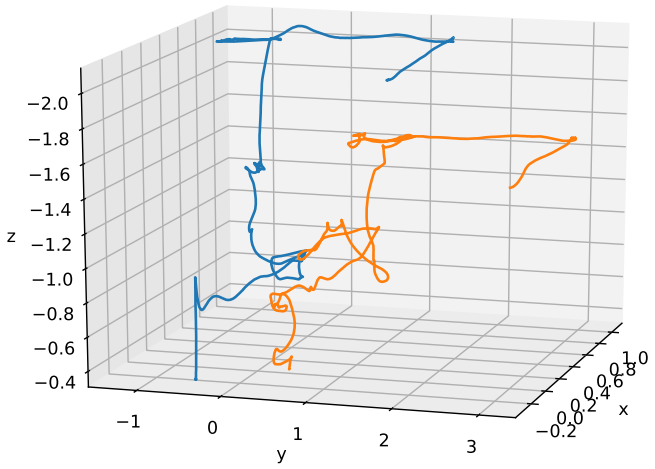

Figure 5-17: Trajectory of the transportation experiment

Chapter 6

Conclusions

In this thesis work, the design of a cooperative control scheme for slung-load transportation using UAV was developed and validated. The problem of transporting an object from one point into another using aerial vehicles is still being studied even though it started since the 1950's. Some of the most innovative advances in this field include the use of UAV, as they help to reduce the cost and to prevent any accidents involving human pilots. The interaction of UAV with the environment, which is called aerial manipulation, and is an area of opportunity that has picked the interest of a lot of researchers because it would allow for a wider array of applications of drones. The solutions in aerial manipulation for the transportation of an object usually fall in one of two categories: flying hands or tether mechanisms.

Flying hands allow for a very precise manipulation of a load, at the expense of a higher complexity, which often translates into a higher weight and less flight time. Configurations like the slung-load and tether mechanisms are simple and light-weight, but lack the dexterity to manipulate an object in a precise way. In some instances, the oscillations of the load could even destabilize the whole system if the vehicle is not able to compensate them.

Another way to increase the flight time is to distribute the load's weight among more than one UAV. These schemes that involve more than one vehicle, or agent, are from an area known as cooperative control. Some of the most well-known problems of cooperative control include the consensus problem and formation flight. There are many cooperative schemes for UAV, but there are not many that use them for aerial manipulation. One ex-

ample is the work presented in [Guerrero et al., 2015], which uses an interconnection and damping assignment passivity-based control (IDA-PBC) that allows a quadcopter to stabilize a slung-load. The IDA-PBC scheme is also used in [Valk and Keviczky, 2018] in order to cooperatively stabilize a group of mechanical and under-actuated agents. Most of these were analyzed in Chapter 1.

In Chapter 2, the cooperative transportation problem was introduced and then divided into three control objectives: Control Objective 2.1.1, Control Objective 2.2.1 and Control Objective 2.3.1. The first one can become quite complicated because there are many factors that can affect the stability of the system as a whole. Even adding agents increases the complexity and could make them be more inefficient due to errors in communications or bad state estimations. Because of this, the second control objective was developed such that it included various simplifications for the system. However, these objectives do not take into account the attitude dynamics of the vehicles, which play an important role because the quadcopters, or PVTOLs, have coupled orientation and position dynamics. This can be taken into account in the last control objective. A control design was developed in order to achieve these control objectives and, therefore, accomplish the original purpose of cooperative transport.

Control Objective 2.3.1 was mainly addressed in Chapter 3 by proposing a control algorithm for the PVTOL. The presented control design is based of feedback linearization and dynamic extension of the thrust force magnitude of the PVTOL model presented in Section 3.1. Many controllers were designed using this linearization, including the ones in Theorem 3.2.1, which asymptotically stabilizes the state towards the origin and Theorem 3.2.2, which stabilizes the state towards a desired trajectory. However, the main fault of these algorithms is that the feedback linearization has a singularity when the thrust force is null. This singularity prevents the linearization from being defined globally, but Theorem 3.2.3 and Theorem 3.2.4 give the basis to prove local asymptotic stability for the PVTOl platform by restricting the state to a region of attraction. An academic example of the proposed controller was given in Section 3.3. In Chapter 4, Control Objective 2.3.1 is solved by using Corollary 3.2.4.

Chapter 4 assumes that the agents used are particles, where the control inputs are the

forces that each particle exerts on the cooperative slung-load system presented in (4.22). The system model is obtained using an Euler-Lagrange approach, and the holonomic constraints due to the cables were addressed using Lagrange multipliers. The control design of the system model can be separated in three main parts. The first one consisted on adding a gravity compensation term in order to change the point of minimum mechanical energy of the system and to make it passive as seen in Theorem 4.2.1 and Theorem 4.2.2. The passivity is used to give some robustness to the system, as any perturbation can be considered as something that injects mechanical energy to the system. Theorem 4.2.3 shows how the controller takes advantage of this perspective based on energy consumption and adds a dissipation term that helps to reduce the mechanical energy of the system. Passivity also helps to implement feedback functions thanks to the properties explained in [Khalil, 2002, Theorem 6.1] (see Figure B-1), as was shown in the proof of Theorem 4.2.3.

Another key aspect of the proposed control design strategy is the definition of an objective function (as seen in Section 4.2.1, Definition 4.2.1). This objective function, along with Theorem 4.2.4, allows for the cooperative slung-load system to be asymptotically stable towards a desired set Ω_d. Thus, completing Control Objective 2.2.1. An academic example was given using an impedance control law as a comparison in Section 4.3. These results were combined with Control Objective 2.3.1 in Theorem 4.2.6.

Finally on Chapter 5, an indoor experiments was conducted using two quadcopters for the cooperative slung-load transport problem. In order to use the control design techniques developed in the previous chapters, the operational space was divided into two perpendicular planes as seen in Figure 5-1, Figure 5-2 and Figure 5-3. In the experimental configuration, it was decided that one of the agents would follow a reference position given by a human operator. In order to achieve this, two objective sets (5.1) and (5.2) were defined. A problem was encountered in the design of the objective function for both planes as seen in Section 4.2.1. This was because it was difficult to formulate an objective function explicitly that only affects one of the agents and achieves the proposed objective sets. In the end, the objective functions were successfully defined in Theorem 5.2.1 using Corollary 5.2.1. Figure 5-5 shows the quadcopters successfully carrying the load. Figures 5-6 through Figure 5-17 show the measurements of the tests made. The controller in [Carino et al., 2015, (12)]

and shown in Appendix D can guarantee that the error between the control law (4.33) and each of the quadcopter orientations q_i tends towards zero. Therefore, Control Objective 2.3.1 is ensured for the implemented control scheme, thus concluding that the proposed method works for the cooperative transport of a slung-load.

6.1 Future Works

The flexibility of the control scheme presented allows for the design and implementation of more complex control strategies. For example, the way the Rayleigh dissipation was applied in Theorem 4.2.3 makes it possible for other types of feedback functions to be used. These could be used to increase the robustness of the system or to add perturbation rejection directly in the control law. Another way to increase complexity is through the objective function design. In this work just a small amount of example objective functions were used, and even some that were not defined explicitly (see Theorem 5.2.1). It would be interesting to see what other design option could be used with this scheme.

An aspect that could be addressed is that the model presented has been simplified, but the methodology presented could be used for systems with added perturbations, like aerodynamic effects or even wind effects. This in turn would allow the study in more depth of the robustness of the proposed method. Also, a strong assumption made was that the cables were always tense. In real-world scenarios this might not always be the case, and in cooperative schemes this could be disastrous because the weight could stop being distributed among the agents. Maybe this could be addressed more thoroughly in the system model design or in the control design.

Another aspect that was not explored is that the movements of the platforms are constrained in the action plane. Even though the method presented in Chapter 5 found a way around this particular issue, it would be interesting to see if the proposed method could be extended to include more agents and to take into account the slacking of cables in the control design. This would eliminate the need to constrain the problem to few vehicles.

In practice, many of the physical parameters of the agents and the load are hard to estimate. The proposed control framework could be extended in order to estimate these

parameters online by means of an adaptive control scheme. This would be particularly useful in cases when different load weights need to use the same control law.

6.2 Publications

Published Journals Articles

- Escobar, J.C., Lozano, R. and Bonilla Estrada, M., 2019. PVTOL control using feedback linearisation with dynamic extension. *International Journal of Control*. DOI: 10.1080/00207179.2019.1676468.

- Escobar, J.C., Lozano, R. and Estrada, M.B., Two PVTOLs Cooperative Slung Load Transport Control Based on Passivity. *Advanced Control for Applications: Engineering and Industrial Systems.* DOI: 10.1002/adc2.22

Published Conference Articles

- Escobar, J.C., Estrada, M.B. and Lozano, R., 2017, June. Cooperative control for load transportation using two PVTOL vehicles with a passivity approach. In *2017 International Conference on Unmanned Aircraft Systems (ICUAS)* (pp. 1385-1391). IEEE. DOI: 10.1109/ICUAS.2017.7991470

- Escobar, J.C., Cabarbaye, A., Estrada, M.B. and Lozano, R., 2017, June. Quaternion Kalman filter for inertial measurement units. In *2017 International Conference on Unmanned Aircraft Systems (ICUAS)* (pp. 1037-1043). IEEE. DOI: 10.1109/ICUAS.2017.7991369

- Cabarbaye, A., Escobar, J.C., Lozano, R. and Estrada, M.B., 2017, June. Fast adaptive control of a 3-DOF inertial stabilised platforms based on quaternions. In *2017 International Conference on Unmanned Aircraft Systems (ICUAS)* (pp. 1463-1469). IEEE. DOI: 10.1109/ICUAS.2017.7991426

Published Book Chapters

- H. Abaunza, J. Carino, P. Castillo, chapter 2 *Modeling approaches*, Book: Indoor navigation strategies for aerial autonomous systems, P. Castillo, L. E. Munoz, P. Garcia, **ISBN**: 780128051894, Fev. 2017, Elsevier. DOI: 10.1016/B978-0-12-805189-4.00003-2

Appendices

Appendix A

PVTOL Control Demonstrations

A.1 Proof of Theorem 3.2.1

Proof of Theorem 3.2.1. First let us calculate the equilibrium points of both the lateral and altitude systems by substituting u_{tra} from equation (3.33) into (3.26) and u_{alt} from equation (3.33) into (3.29) as

$$\begin{aligned} \dot{\xi}_{tra} &= A\,\xi_{tra} - B\,K_{tra}\,\xi_{tra} \\ &= (A - B\,K_{tra})\,\xi_{tra} \end{aligned} \tag{A.1}$$

$$\begin{aligned} \dot{\xi}_{alt} &= A\,\xi_{alt} - B\,K_{alt}\,[\xi_{alt} - \gamma_u] + \gamma_{alt} \\ &= (A - B\,K_{alt})\,\xi_{alt} + \begin{bmatrix} 0 \\ -g \\ 0 \\ K_{alt,3}\,g \end{bmatrix} \end{aligned} \tag{A.2}$$

Solving equations (A.1) and (A.2) when $\dot{\xi}_{tra} = \overline{0}$ and $\dot{\xi}_{alt} = \overline{0}$ for ξ results in the state presented in equation (3.35).

Now, let us define the Lyapunov candidate function $V(\xi, t)$ as

$$V(\xi, t) \coloneqq \Delta\xi_{alt}^T\,P_{alt}\,\Delta\xi_{alt} + \xi_{tra}^T\,P_{tra}\,\xi_{tra} > 0 \tag{A.3}$$

where the altitude error $\Delta\xi_{alt}$ is defined as

$$\Delta\xi_{alt} \coloneqq \xi_{alt} - \begin{bmatrix} \overline{0}_{2\times 1} & g & 0 \end{bmatrix}^T \tag{A.4}$$

and its differentiation w.r.t. time, substituting from equations (3.26) and (3.33), which was partially developed in (A.2), is

$$\begin{aligned} \Delta\dot{\xi}_{alt} &= \dot{\xi}_{alt} \\ &= (A - BK_{alt})\,\xi_{alt} + \begin{bmatrix} 0 \\ -g \\ 0 \\ K_{alt,3}\,g \end{bmatrix} \\ &= (A - BK_{alt})\,\Delta\xi_{alt} \end{aligned} \tag{A.5}$$

It can be seen that substituting equation (3.35) into (A.3) results in $V(\xi^*, t) = 0$.

Differentiating (A.3) w.r.t. time results in

$$\dot{V}(\xi,t) = \Delta\xi_{alt}^T P_{alt}\,\Delta\dot{\xi}_{alt} + \Delta\dot{\xi}_{alt}^T P_{alt}\,\Delta\xi_{alt} + \xi_{tra}^T P_{tra}\,\dot{\xi}_{tra} + \dot{\xi}_{tra}^T P_{tra}\,\xi_{tra} \tag{A.6}$$

The term $\Delta\dot{\xi}_{alt}$ can be substituted from equation (A.5), and the term $\dot{\xi}_{tra}$ can be substituted from equation (A.1). This results in

$$\begin{aligned} \dot{V}(\xi,t) = {} & \Delta\xi_{alt}^T P_{alt}\,(A - BK_{alt})\,\Delta\xi_{alt} + \Delta\xi_{alt}^T\,(A - BK_{alt})^T\,P_{alt}\,\Delta\xi_{alt} + \\ & \xi_{tra}^T P_{tra}\,(A - BK_{tra})\,\xi_{tra} + \xi_{tra}^T\,(A - BK_{tra})^T\,P_{tra}\,\xi_{tra} \\ = {} & \Delta\xi_{alt}^T \left[P_{alt}\,(A - BK_{alt}) + (A - BK_{alt})^T\,P_{alt}\right]\Delta\xi_{alt} + \\ & \xi_{tra}^T \left[P_{tra}\,(A - BK_{tra}) + (A - BK_{tra})^T\,P_{tra}\right]\xi_{tra} \end{aligned} \tag{A.7}$$

which can be further simplified using equations (3.32) and (3.31), and results in

$$\dot{V}(\xi,t) = -\Delta\xi_{alt}^T Q_{alt}\,\Delta\xi_{alt} - \xi_{tra}^T Q_{tra}\,\xi_{tra} < 0 \tag{A.8}$$

Therefore, system (3.24) is proven to be asymptotically, exponentially stable to the state (3.35) using control law (3.33).

□

A.2 Proof of Theorem 3.2.2

Proof of Theorem 3.2.2. Let us use equations (3.38) and (3.39) to define the translation and altitude tracking errors as

$$e_{tra} \coloneqq \xi_{tra} - \xi_{tra,d} \tag{A.9}$$

$$e_{alt} \coloneqq \xi_{alt} - \xi_{alt,d} \tag{A.10}$$

The differentiation of these tracking errors w.r.t. time, using the control law (3.42) and systems (3.26), (3.29), (3.38) and (3.39), is

$$\dot{e}_{tra} = \dot{\xi}_{tra} - \dot{\xi}_{tra,d} = (A - BK_{tra})\, e_{tra} \tag{A.11}$$

$$\dot{e}_{alt} = \dot{\xi}_{alt} - \dot{\xi}_{alt,d} = (A - BK_{alt})\, e_{alt} + \begin{bmatrix} 0 \\ -g \\ 0 \\ K_{alt,2}\, g \end{bmatrix} \tag{A.12}$$

Let us now define an altitude difference as

$$\Delta e_{alt} \coloneqq e_{alt} - \begin{bmatrix} \overline{0}_{2\times 1} \\ g \\ 0 \end{bmatrix} \tag{A.13}$$

differentiating this altitude difference w.r.t. time using equation (A.12) results in

$$\Delta \dot{e}_{alt} = \dot{e}_{alt} = (A - BK_{alt})\, \Delta e_{alt} \tag{A.14}$$

The equilibrium point for the tracking error system can be obtained by solving the equations $\dot{e}_{tra} = \dot{e}_{alt} = \overline{0}$ for the tracking errors e_{tra} and e_{alt}, which was already solved in (A.1) and (A.2). Using the definition of the tracking errors in (A.9) and (A.10), it can be concluded that $\xi^*_{tra} = \xi_{tra,d}$ and $\xi^*_{alt} = \xi_{alt,d} + \begin{bmatrix} \overline{0}_{1\times 2} & g & 0 \end{bmatrix}^T$ which is the same state as the one defined in (3.43).

Now, let us define the Lyapunov candidate function $V_e(\xi, \xi_d, t)$ as

$$V_e(\xi, \xi_d, t) \coloneqq \Delta e_{alt}^T P_{alt} \Delta e_{alt} + e_{tra}^T P_{tra} e_{tra} > 0 \tag{A.15}$$

Substituting equation (3.43) into (A.15) results in $V_e(\xi^*, \xi_d, t) = 0$. Differentiating (A.15) w.r.t. time along the trajectories of the system results in

$$\dot{V}_e(\xi, \xi_d, t) = \Delta \dot{e}_{alt}^T P_{alt} \Delta e_{alt} + \Delta e_{alt}^T P_{alt} \Delta \dot{e}_{alt} + \dot{e}_{tra}^T P_{tra} e_{tra} + e_{tra}^T P_{tra} \dot{e}_{tra} \tag{A.16}$$

The term $\Delta \dot{e}_{alt}$ can be substituted from equation (A.14) and the term $\dot{e}_{tra}$ from equation (A.11). This results in

$$\begin{aligned} \dot{V}_e(\xi, \xi_d, t) = & \Delta e_{alt}^T P_{alt} \left(A - B K_{alt}\right) \Delta e_{alt} + \Delta e_{alt}^T \left(A - B K_{alt}\right)^T P_{alt} \Delta e_{alt} + \\ & e_{tra}^T P_{tra} \left(A - B K_{tra}\right) e_{tra} + e_{tra}^T \left(A - B K_{tra}\right)^T P_{tra} e_{tra} \\ = & \Delta e_{alt}^T \left[P_{alt} \left(A - B K_{alt}\right) + \left(A - B K_{alt}\right)^T P_{alt}\right] \Delta e_{alt} + \\ & e_{tra}^T \left[P_{tra} \left(A - B K_{tra}\right) + \left(A - B K_{tra}\right)^T P_{tra}\right] e_{tra} \end{aligned} \tag{A.17}$$

which can be further simplified using equations (3.32) and (3.31), that results in

$$\dot{V}_e(\xi, \xi_d, t) = -\Delta e_{alt}^T Q_{alt} \Delta e_{alt} - e_{tra}^T Q_{tra} e_{tra} < 0 \tag{A.18}$$

Therefore, system (3.24) is proven to be asymptotically, exponentially stable to the state (3.43) using control law (3.42). □

A.3 Proof of Theorem 3.2.3

Proof of Theorem 3.2.3. First, the maximum value of the region is obtained by substituting $u = 0$ into equation (3.4) and solving for $\ddot{z}$

$$\ddot{z} = \frac{u \cos\theta}{m} - g = -g \tag{A.19}$$

The stability proof of theorem 3.2.1 uses a Lyapunov candidate function made up of two different positive definite functions, one for the altitude dynamical system and another for the translational dynamical system. A new positive definite function can then be defined exclusively for the altitude system, which is independent from the translational system and even has different control input.

$$V(\xi,t) \geq V_{alt}(\xi_{alt},t) \coloneqq \xi_{alt}^T P_{alt}\, \xi_{alt} \tag{A.20}$$

Its differentiation w.r.t. time results in

$$\dot{V}_{alt}(\xi_{alt},t) = -\xi_{alt}^T Q_{alt}\, \xi_{alt} < 0 \tag{A.21}$$

which implies that the following inequality holds

$$V_{alt}(\xi_{alt},t) \leq \lambda_{max}(P_{alt}) \left|\left|\xi_{alt,0}\right|\right|^2 \leq V(\xi,t) \tag{A.22}$$

where $\xi_{alt,0} \in \mathbb{R}^4$ are the initial conditions of the altitude system.

In order to ensure that the control input $u > 0$, the initial conditions can be chosen such that

$$\begin{aligned} & \lambda_{max}(P_{alt}) \left|\left|\xi_{alt,0}\right|\right|^2 < \lambda_{max}(P_{alt})\, g^2 \\ \Longrightarrow \quad & \left|\left|\xi_{alt,0}\right|\right| < g \end{aligned} \tag{A.23}$$

which is the region presented in (3.44) and thus concluding the proof. □

A.4 Proof of Theorem 3.2.4

Proof of Theorem 3.2.4. First, the altitude error is defined as

$$\Delta z \coloneqq z - z_d \tag{A.24}$$

where the desired altitude is represented by z_d. Differentiating Δz w.r.t. time and using equations (3.4) and (3.37) results in

$$\Delta \ddot{z} = \ddot{z} - \ddot{z}_d = \frac{u \cos\theta}{m} - g - \frac{u_d \cos\theta_d}{m} \tag{A.25}$$

where $u_d, \theta_d \in \mathbb{R}$ are the desired thrust force and attitude angle, respectively. It is assumed that u_d is positive and constant.

The maximum value of the region of attraction can be acquired by obtaining the value of $||\Delta \ddot{z}||$ when $u = 0$. It is calculated from equation (A.25) as

$$||\Delta \ddot{z}|| = \left| \frac{u_d \cos\theta_d}{m} + g \right| \tag{A.26}$$

Taking a closer look at (A.11) and (A.14), the proof of the region of attraction is the same as in Theorem 3.2.3. In order to ensure that the control input $u > 0$, the initial conditions and the desired state can be chosen such that

$$\begin{aligned} & \lambda_{max}(P_{alt}) \left|\left|\xi_{alt,0}\right|\right|^2 < \lambda_{max}(P_{alt}) \left| \frac{u_d \cos\theta_d}{m} + g \right|^2 \\ \Longrightarrow \quad & \left|\left|\xi_{alt,0}\right|\right| < \left| \frac{u_d \cos\theta_d}{m} + g \right| \end{aligned} \tag{A.27}$$

which is the region presented in (3.45) and thus concluding the proof. □

Appendix B

Passivity Preliminaries

This section will introduce the definitions and theorems used for the remainder of this work. The passivity concepts can be found in [Lozano et al., 2013] [Khalil, 2002][Byrnes et al., 1991] [Willems, 1972b] [Willems, 1972a].

B.1 Passivity Definitions

Passivity is a property that depends exclusively on the relationship between the input and the output of a system. In simple terms, it is similar to the definition of a passive electric component in the fact that the property reflects that the amount of energy available in the system is finite. In a more formal description, passivity can be described using the following definition found in [Lozano et al., 2013, Definition 2.1].

Definition B.1.1. *A system* $H : \mathscr{L}_{2,e} \leftarrow \mathscr{L}_{2,e}$ *with input and output* $u(\cdot), y(\cdot) \in \mathbb{R}^m$*, respectively, is passive if* $\exists \beta \in \mathbb{R}$ *such that*

$$\int_{t_0}^{t} y^T(\tau) u(\tau)\, d\tau \geq \beta \tag{B.1}$$

$\forall u(\cdot)$ *and* $t, t_0 \in \mathbb{R}, t \geq t_0$

This definition can also be seen from the perspective of continuous positive functions, as stated in [Lozano et al., 2013, Theorem 2.2], as

Theorem B.1.1. *Assume that a continuous function $V(\cdot) \in \mathbb{R}_{\geq 0}$ exists such that*

$$V(t) - V(t_0) \leq \int_{t_0}^{t} y^T(\tau) u(\tau)\, d\tau \tag{B.2}$$

$\forall u(\cdot), t \geq t_0$ *and* $V(t_0)$. *Then the system with input* $u(\cdot)$ *and output* $y(\cdot)$ *is passive.*

Some nonlinear static functions are known to preserve the passivity properties when applied as a feedback gain or as inputs in certain dynamical systems. This can be seen in the following definition from [Bai et al., 2011, Definition 1.3]

Definition B.1.2. *A static nonlinearity* $y = h(u)$, *where* $h : \mathbb{R}^n \leftarrow \mathbb{R}^n$ *is a function with input* $u \in \mathbb{R}^n$ *is passive if*

$$u^T y = u^T h(u) \geq 0 \tag{B.3}$$

$\forall u(\cdot)$

B.2 Passivity Feedback Interconnection

A common result in passive systems that will be used for the stability analysis is that a feedback interconnection of passive systems preserves the passivity property as shown in [Khalil, 2002, Theorem 6.1]. The diagram of the connection can be seen in Figure B-1.

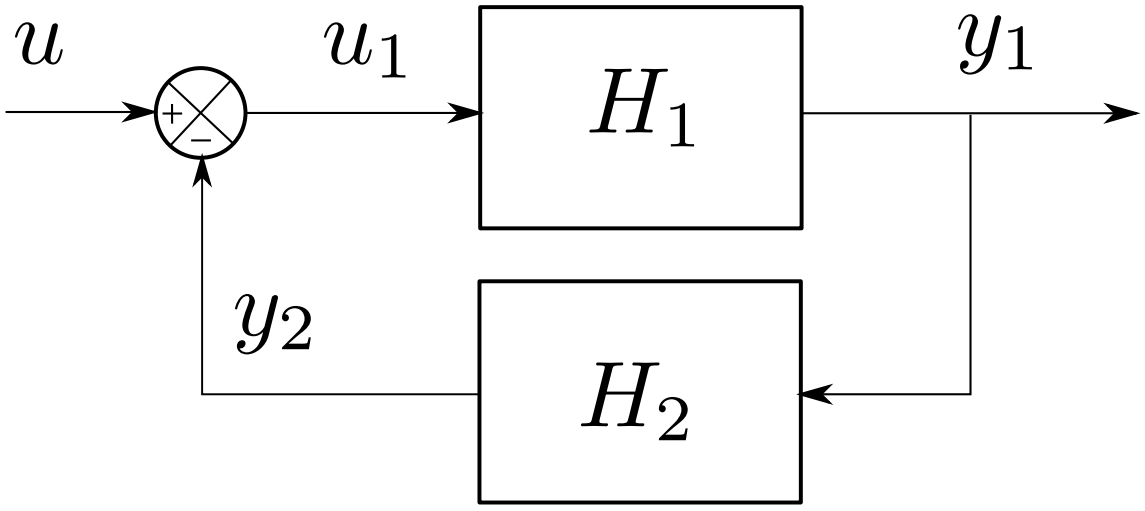

Figure B-1: Feedback interconnection diagram of two passive systems

B.3 Lagrange-Dirichlet Theorem

Finally, the Lagrange-Dirichlet theorem as presented in [Lozano et al., 2013, Lemma 7.3] is used to provide the basis of the asymptotic stability proof.

Theorem B.3.1. *Assume that a system's potential energy $U(q)$ is such that:*

- $\dfrac{\partial U}{\partial q}(q) = 0 \iff q = q^*$*, where q is the system's state in generalized coordinates (which will be defined in the following section) and q^* is a critical point of the potential energy.*
- $\dfrac{\partial^2 U}{\partial q^2}(q^*) > 0$*, which implies that $U(q)$ is locally convex around q^*.*

The unforced Euler-Lagrange dynamics with Rayleigh dissipation possesses a fixed point $(q, \dot{q}) = (q^*, 0)$ that is locally asymptotically stable.

Appendix C

Cooperative Slung-Load Transport Control Demonstrations

C.1 Proof of Theorem 4.2.1

Proof of Theorem 4.2.1. Substituting the control (4.29) into (4.22) results in

$$M\ddot{q}+A^T(q)\,\lambda+G(q)=E\begin{bmatrix}u_{1,p}+u_{1,g}\\ u_{2,p}+u_{2,g}\end{bmatrix} \tag{C.1}$$

$$M\ddot{q}+A^T(q)\,\lambda+G(q)-E\begin{bmatrix}u_{1,g}\\ u_{2,g}\end{bmatrix}=E\begin{bmatrix}u_{1,p}\\ u_{2,p}\end{bmatrix} \tag{C.2}$$

$$M\ddot{q}+A^T(q)\,\lambda+G'(q)=E\begin{bmatrix}u_{1,p}\\ u_{2,p}\end{bmatrix} \tag{C.3}$$

where

$$G'(q) \coloneqq \begin{bmatrix} 0 \\ m_l g \\ 0 \\ 0 \\ -\frac{m_l g}{2} \\ 0 \\ -\frac{m_l g}{2} \end{bmatrix} \tag{C.4}$$

The effect that the gravity compensation term has had on the system is that it has effectively changed the form of the potential energy of the resulting system (C.3). That is, a new potential energy term $U' \in \mathbb{R}$ exists such that $\frac{\partial U'}{\partial q} \coloneqq A^T(q)\,\lambda + G'(q)$. Following theorem B.3.1 description, the critical points of the potential energy $q^* \in \mathbb{R}^7$ and $\lambda^* \in \mathbb{R}^2$ can then be found by solving $A^T(q)\,\lambda + G'(q) = \overline{0}$, which will be expanded in the following equations

$$e_1 \lambda_1 + e_2 \lambda_2 + \begin{bmatrix} 0 \\ m_l g \end{bmatrix} = 0 \tag{C.5}$$

$$(e_2 \lambda_2 - e_1 \lambda_1)^T \begin{bmatrix} -\sin\theta_l \\ \cos\theta_l \end{bmatrix} l = 0 \tag{C.6}$$

$$-e_i \lambda_i + \begin{bmatrix} 0 \\ -\frac{m_l g}{2} \end{bmatrix} = 0 \tag{C.7}$$

Solving equations (C.5) through (C.7) results in the following solution set

$$\begin{bmatrix} q^* \\ \lambda^* \end{bmatrix} \in \Omega_g \coloneqq \left\{ q \in \mathbb{R}^7, \lambda \in \mathbb{R}^2 \;\middle|\; \begin{array}{l} e_{i,x} = 0, \left\| e_{i,y} \right\| = l_i, \\ \|\lambda_i\| = \frac{m_l g}{2 l_i}, \\ e_{i,y} \lambda_i > 0 \end{array} \right\} \tag{C.8}$$

Depending on the signs of $e_{i,y}$ and λ_i, there are four possible configurations of the crit-

ical points q^* and λ^*, which are shown on Figure C-1. From these possible configurations, only 1) (where $e_{i,y} < 0$ and $\lambda_i > 0$) is a stable critical point of the system, that is, the system tends to drift away from all the other possible configurations. This can be shown by analyzing the convexity of all the configurations.

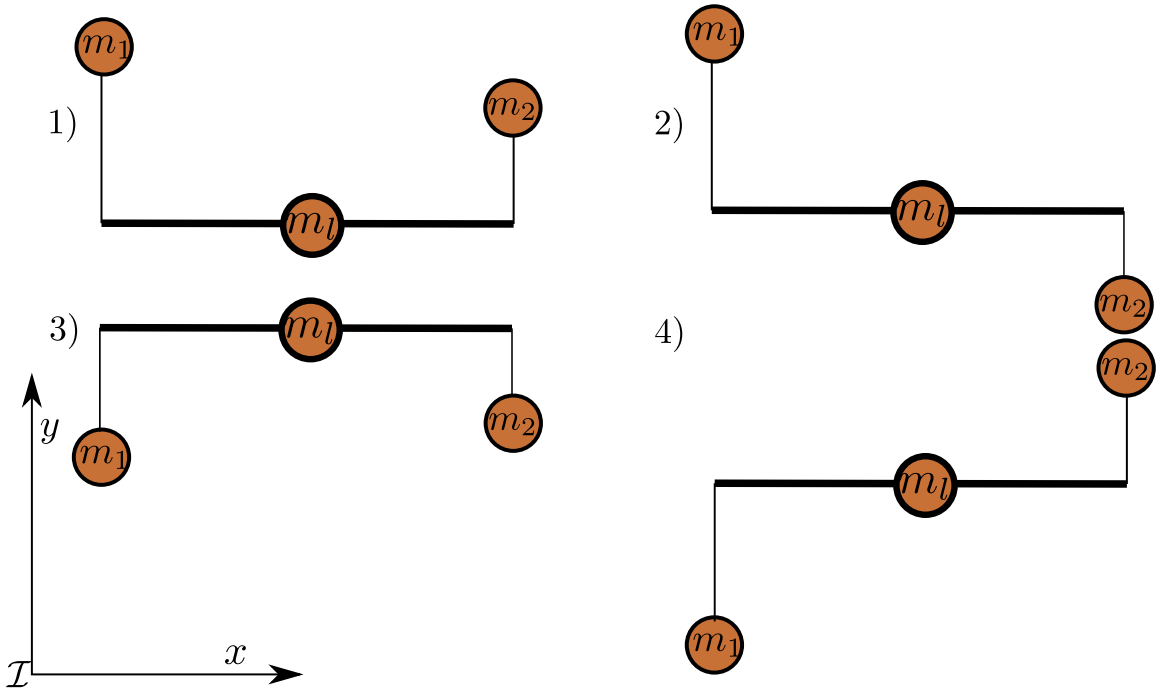

Figure C-1: Possible configurations for the solution set Ω_g

In order to determine that $\dfrac{\partial^2 U'}{\partial q^2}(q^*, \lambda^*) > 0$, it is sufficient to determine that its diagonal elements are nonnegative. The diagonal elements are obtained from equations (C.5) through (C.7) as

$$\frac{\partial^2 U'}{\partial p_l^2}(q^*, \lambda^*) = \lambda_1 + \lambda_2 \tag{C.9}$$

$$\begin{aligned}\frac{\partial^2 U'}{\partial \theta_l^2}(q^*, \lambda^*) = \; & -(e_2\lambda_2 - e_1\lambda_1)^T \begin{bmatrix} \cos\theta_l \\ \sin\theta_l \end{bmatrix} l \\ & + \left(\begin{bmatrix} -\sin\theta_l \\ \cos\theta_l \end{bmatrix} \lambda_2 l + \begin{bmatrix} -\sin\theta_l \\ \cos\theta_l \end{bmatrix} \lambda_1 l \right)^T \begin{bmatrix} -\sin\theta_l \\ \cos\theta_l \end{bmatrix} l \end{aligned} \tag{C.10}$$

$$\frac{\partial^2 U'}{\partial p_i^2}(q^*,\lambda^*) = \lambda_i \tag{C.11}$$

Equation (C.11) is only positive when $\lambda_i > 0$, which implies that the only possible configuration that could be convex is 1). In order to conclude the convexity of configuration 1), equations (C.9) and (C.10) are evaluated for this configuration

$$\left.\frac{\partial^2 U'}{\partial p_l^2}(q^*,\lambda^*)\right|_{e_{i,y}<0,\lambda_i>0} = \lambda_1 + \lambda_2 > 0 \tag{C.12}$$

$$\left.\frac{\partial^2 U'}{\partial \theta_l^2}(q^*,\lambda^*)\right|_{e_{i,y}<0,\lambda_i>0} = -\overbrace{(e_2\,\lambda_2 - e_1\,\lambda_1)^T}^{0} \begin{bmatrix} \cos\theta_l \\ \sin\theta_l \end{bmatrix} l + (\lambda_1+\lambda_2)\, l^2 > 0 \tag{C.13}$$

which implies that the only convex configuration of the critical points is 1).

Therefore, the new point of minimal potential energy is located in the set

$$\Omega_g = \left\{ q \in \mathbb{R}^7, \lambda \in \mathbb{R}^2 \;\middle|\; \begin{array}{l} e_{i,x} = 0, \left\| e_{i,y} \right\| = l_i, \\ \|\lambda_i\| = \dfrac{m_l\, g}{2\, l_i}, \\ e_{i,y} > 0, \\ \lambda_i > 0 \end{array} \right\} \tag{C.14}$$

□

C.2 Proof of Theorem 4.2.2

Proof of Theorem 4.2.2. Firstly, system (4.22) is changed into system (C.3) because of the gravity compensation term and Theorem 4.2.2. In order to prove that system (C.3) is passive from the input $u_{i,p}$ to the velocity vector $\begin{bmatrix} \dot{p}_1^T & \dot{p}_2^T \end{bmatrix}^T$, it is necessary to note that the potential energy $U' \geq U'_{min}$ is also limited from below from the assumption that the poten-

tial energy U was also limited from below and the fact it is convex with minimum in Ω_g (see Theorem 4.2.1). The proposed storage function is the total energy function

$$V_s(q,\dot{q},t) := \frac{\dot{q}^T M \dot{q}}{2} + U' - U'_{min} \geq 0 \tag{C.15}$$

Its differentiation w.r.t. time results in

$$\dot{V}_s(q,\dot{q},t) = \frac{\ddot{q}^T M \dot{q} + \dot{q}^T M \ddot{q}}{2} + \dot{U}' \tag{C.16}$$

Substituting $\ddot{q} = M^{-1}\left(-A^T(q)\,\lambda - G'(q) + E\begin{bmatrix} u_{1,p} \\ u_{2,p} \end{bmatrix}\right)$ from (C.3) into (C.16) results in

$$\begin{aligned} \dot{V}_s(q,\dot{q},t) = & \left[-A^T(q)\,\lambda - G'(q) + E\begin{bmatrix} u_{1,p} \\ u_{2,p} \end{bmatrix}\right]^T \dot{q} \\ & + \frac{\partial U}{\partial q}\dot{q} \\ = & \begin{bmatrix} u_{1,p} & u_{2,p} \end{bmatrix}^T E^T \dot{q} - \lambda^T A(q)\,\dot{q} \\ & - G'^T(q)\,\dot{q} + \lambda^T A(q)\,\dot{q} + G'^T(q)\,\dot{q} \\ = & \begin{bmatrix} u_{1,p} & u_{2,p} \end{bmatrix} E^T \dot{q} = u_{1,p}^T \dot{p}_1 + u_{2,p}^T \dot{p}_2 \end{aligned} \tag{C.17}$$

Integrating both sides of (C.17) w.r.t. time results in

$$\begin{aligned} & \int_{t_0}^{t} \dot{V}_s(q,\dot{q},\tau)\,d\tau \\ = & V_s(q,\dot{q},t) - V_{s,0}(q,\dot{q},t) \\ = & \int_{t_0}^{t} u_{1,p}^T \dot{p}_1 + u_{2,p}^T \dot{p}_2\,d\tau \end{aligned} \tag{C.18}$$

Since $V_s(q,\dot{q},t) - V_{s,0}(q,\dot{q},t) \geq -V_{s,0}(q,\dot{q},t)$ from (C.15), and the fact that $-V_{s,0}(q,\dot{q},t)$ denotes the total energy of the system at time t_0, which is constant, this implies that

$$\int_{t_0}^{t} u_1^T\,\dot{p}_1 + u_2^T\,\dot{p}_2\,\tau \geq -V_{s,0}(q,\dot{q},t) \tag{C.19}$$

which proves that system (C.3) is passive from the input $u_{i,p}$ to the velocity vector $\begin{bmatrix} \dot{p}_1^T & \dot{p}_2^T \end{bmatrix}^T$

□

C.3 Proof of Theorem 4.2.3

Proof of Theorem 4.2.3. Because of theorem B.1.1, and the fact that the Rayleigh dissipation term $u_{i,v} = -k_{v,i}\dot{p}_i$ from (4.32) is also passive (because it is just a proportional feedback gain), the system

$$M\ddot{q} + A^T(q)\,\lambda + G'(q) + E\begin{bmatrix} k_{v,1}\,\dot{p}_1 \\ k_{v,2}\,\dot{p}_2 \end{bmatrix} = E\begin{bmatrix} u_{1,\psi} \\ u_{2,\psi} \end{bmatrix} \tag{C.20}$$

is passive from the inputs $u_{i,\psi}$ to the generalized velocities $\dot{q}$. This is illustrated in Figure 4-2.

□

C.4 Proof of Theorem 4.2.4

Proof of Theorem 4.2.4. Using theorem B.3.1, it can be concluded that system (C.20) is locally asymptotically stable to the set

$$\Omega_v := \left\{ \begin{bmatrix} q^T & \dot{q}^T \end{bmatrix}^T \in \mathbb{R}^{14}, \lambda \in \mathbb{R}^2 \;\middle|\; \begin{array}{l} \dot{p}_i = \overline{0}, e_{i,x} = 0, \\ \left\| e_{i,y} \right\| = l_i, \\ \|\lambda_i\| = \dfrac{m_l\, g}{2\, l_i}, \\ e_{i,y} < 0, \lambda_i > 0 \end{array} \right\} \tag{C.21}$$

if the inputs $u_{i,\phi} = \overline{0}$

The stability is local because system (C.20) may start in one of the unstable configurations exposed in Figure C-1. In order to guarantee stability of the system, and have a more realistic practical approximation of the behavior of the cables, the initial conditions will be restricted to the states where the cables are not experiencing any compression (where $\lambda_i < 0$) and with zero kinetic energy in order to ensure that the velocities stay small. The resulting set of viable initial conditions is depicted in (4.34).

In order to prove stability in the case when the control inputs $u_{i,\phi} \neq \overline{0}$, the candidate Lyapunov function used is defined as

$$V(q,\dot{q},t) \coloneqq V_s(q,\dot{q},t) + \psi(q_1,q_2) \geq 0 \tag{C.22}$$

Differentiating with respect to time through the trajectories of system (C.20) using control law (4.33) and equation (C.17) results in

$$\begin{aligned}
\dot{V}(q,\dot{q},t) = \;& u_{1,p}^T \dot{p}_1 + u_{2,p}^T \dot{p}_2 + \dot{\psi}(q_1,q_2) \\
= \;& -k_{v,1}\, \dot{p}_1^T\, \dot{p}_1 - k_{v,2}\, \dot{p}_2^T\, \dot{p}_2 - u_{1,\phi}^T\, \dot{p}_1 - u_{2,\phi}^T\, \dot{p}_2 \\
& + \frac{\partial \psi^T(p_1,p_2)}{\partial q}\, \frac{\partial q}{\partial t} \\
= \;& -k_{v,1}\, \dot{p}_1^T\, \dot{p}_1 - k_{v,2}\, \dot{p}_2^T\, \dot{p}_2 - \frac{\partial \psi^T(p_1,p_2)}{\partial p_1}\, \dot{p}_1 \\
& - \frac{\partial \psi^T(p_1,p_2)}{\partial p_2}\, \dot{p}_2 + \frac{\partial \psi^T(p_1,p_2)}{\partial q}\, \dot{q} \\
= \;& -k_{v,1}\, \dot{p}_1^T\, \dot{p}_1 - k_{v,2}\, \dot{p}_2^T\, \dot{p}_2 \leq 0
\end{aligned} \tag{C.23}$$

It can be seen that (C.23) is negative semi-definite. The Krasovskii-LaSalle's invariant set theorem, along with a look at definition 4.2.1 , allows us to conclude that system (C.20) is locally asymptotically stable to the set $\Omega_d \subset \Omega_v$ thus concluding the proof.

□

C.5 Proof of Theorem 4.2.5

Proof of Theorem 4.2.5. Without any loss of generality, the proof is the same as the one presented for theorem 4.2.4, except that the definitions of the separated control law become

$$u_{i,v} \coloneqq -\overline{\sigma}_{\beta_i}(k_{v,i}\dot{p}_i) \tag{C.24}$$

$$u_{i,\psi} \coloneqq -\frac{\partial \psi_b(p_1,p_2)}{\partial p_i} \tag{C.25}$$

and the candidate Lyapunov function used is

$$V(q,\dot{q},t) \coloneqq V_s(q,\dot{q},t) + \psi_b(q_1,q_2) \geq 0 \tag{C.26}$$

Differentiating (C.26) w.r.t. time results in

$$\dot{V}(q,\dot{q},t) = -k_{v,1}\,\dot{p}_1^T\,\overline{\sigma}_{\beta_1}(k_{v,1}\dot{p}_1) - k_{v,2}\,\dot{p}_2^T\,\overline{\sigma}_{\beta_2}(k_{v,2}\dot{p}_2) \tag{C.27}$$

The derivative of the Lyapunov function (C.27) is negative semi-definite if the term

$$-k_{v,i}\,\dot{p}_i^T\,\overline{\sigma}_{\beta_i}(k_{v,i}\dot{p}_i) \tag{C.28}$$

is negative semi-definite.

If the function $\overline{\sigma}_{\beta_i}(k_{v,i}\dot{p}_i)$ is saturated, that is, $\|k_{v,i}\dot{p}_i\| \geq \beta_i$, the term (C.28) becomes

$$-k_{v,i}\,\beta_i\,\dot{p}_i^T\,sign(k_{v,i}\dot{p}_i) = -k_{v,i}\,\beta_i\,\dot{p}_i^T\,sign(\dot{p}_i) \leq -k_{v,i}\,\beta_i\,\|\dot{p}_i\| \leq 0 \tag{C.29}$$

which is negative semi-definite.

In the case when the term (C.28) is on the linear part, the case is the same as the one in theorem 4.2.4. This proves that (C.27) is negative semi-definite, and the rest of the proof follows the one in theorem 4.2.4 without any loss of generality.

□

C.6 Proof of Theorem 4.2.6

Proof of Theorem 4.2.6. Let us define a new Lyapunov candidate function as

$$V \coloneqq V(q,\dot{q},t) + \sum_{i=1}^{n} V_{att,i}(\xi_i) \tag{C.30}$$

where $V(q,\dot{q},t)$ is defined as in (C.22)

The difference of V w.r.t. time results in

$$
\begin{aligned}
\dot{V} = & \dot{V}(q,\dot{q},t) + \sum_{i=1}^{n} \dot{V}_{att,i}(\xi_i) \\
= & \vec{F}_{th,1}^{T}\dot{p}_1 + \vec{F}_{th,2}^{T}\dot{p}_2 + \dot{\psi}(q_1,q_2) - \sum_{i=1}^{n} \upsilon_i \left(\vec{F}_{th,i} - u_i\right) \\
= & \left(\vec{F}_{th,1} - u_1 + u_1\right)^{T}\dot{p}_1 + \left(\vec{F}_{th,2} - u_2 + u_2\right)^{T}\dot{p}_2 + \dot{\psi}(q_1,q_2) - \sum_{i=1}^{n} \upsilon_i \left(\vec{F}_{th,i} - u_i\right) \\
= & u_1^{T}\dot{p}_1 + u_2^{T}\dot{p}_2 + \dot{\psi}(q_1,q_2) + \sum_{i=1}^{n}\left[\left(\vec{F}_{th,i} - u_i\right)^{T}\dot{p}_1 - \upsilon_i\left(\vec{F}_{th,i} - u_i\right)\right]
\end{aligned}
\tag{C.31}
$$

which can be simplified using the results from equation (C.23). This results in

$$
\begin{aligned}
\dot{V} \leq & \sum_{i=1}^{n}\left(\vec{F}_{th,i} - u_i\right)^{T}\dot{p}_1 - \upsilon_i\left(\vec{F}_{th,i} - u_i\right) \\
\leq & -\sum_{i=1}^{n}\upsilon_i\left(\vec{F}_{th,i} - u_i\right) - \left(\vec{F}_{th,i} - u_i\right)^{T}\dot{p}_1 \\
\leq & -\sum_{i=1}^{n}\left|\upsilon_i\left(\vec{F}_{th,i} - u_i\right)\right| - \left\|\dot{\vec{p}}_i\right\|\left\|\vec{F}_{th,i} - u_i\right\|
\end{aligned}
\tag{C.32}
$$

Using the condition (4.39) and the result in (C.32), it can be seen that $\dot{V} \leq 0$. Without any loss of generality, the results can be extended with the saturated control law following the same methodology as the proof of Theorem 4.2.5, thus concluding the proof.

□

Appendix D

Quadcopter Control

This section describes the theory and control law used for the stability of a quadcopter vehicle. The results presented here are a summary of the ones published in [Carino et al., 2015] for a better understanding on how they were used in the experimental results presented in Chapter 5.

The quadcopter vehicle can be seen as an underactuated rigid body platform. This is because the position dynamics depend on the attitude dynamics. In other terms, it is not possible to change the position of the platform without having to alter its orientation. The solution presented separates the problem into designing two independent control laws, one for the position dynamics and one for the attitude, and then connect the output of one into the input of the other one (see Figure D-1).

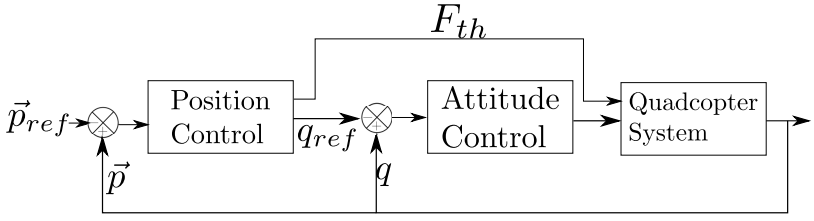

Figure D-1: A diagram that shows how the quadcopter control is connected in [Carino et al., 2015]

D.1 Desired Attitude

The following theorem comes from [Carino et al., 2015, (14)]

Theorem D.1.1. *Let $\vec{F}_{th} \in \mathbb{R}^3$ be a desired thrust force in the inertial frame, $\vec{b} \in \mathbb{R}^3; ||\vec{b}|| = 1$ be a unitary vector denoting the axis in which the thrust acts in the body frame, and $q_{ref}, q'_{ref} \in \mathbb{H}$ be quaternion variables defined as*

$$q'_{ref} \coloneqq \left(\vec{b} \cdot \vec{F}_{th} + \left\|\vec{F}_{th}\right\|\right) + \vec{b} \times \vec{F}_{th} \tag{D.1}$$

$$q_{ref} \coloneqq \frac{q'_{ref}}{\left\|q'_{ref}\right\|} \tag{D.2}$$

If the quadcopter attitude is the same as q_{ref}, then the thrust force's direction is the same as the desired thrust force.

Theorem D.1.1 and Figure D-1 show that a reference attitude $q_{ref} \in \mathbb{H}, \quad \left\|q_{ref}\right\|$ can be constructed from a reference thrust force, either from Theorem 4.2.4 or Theorem 4.2.5 in this particular case. If the attitude of the quadcopter is the same as this reference orientation, then the thrust force of the quadcopter is guaranteed to be the same as the one from Theorem 4.2.4 or Theorem 4.2.5 (considering that the thrust force of the quadcopter is a control input). This bears a striking resemblance to the function of the control law proposed in Chapter 3, but for the PVTOL platform.

In [Carino et al., 2015], the orientation control used is a PD controller based on a quaternion model. The one used for the attitude dynamics of the quadrotor platforms in Chapter 5 has the same structure.

Appendix E

Experimental Validation Demonstrations

E.1 Proof of Theorem 5.2.1

Proof of Theorem 5.2.1. It can be seen that equations (5.5) and (5.6) are equal to zero when $\begin{bmatrix} \vec{p}_{1,x-z}^T & \vec{p}_{2,x-z}^T \end{bmatrix}^T \in \Omega_{d,x-z}$ and $\begin{bmatrix} \vec{p}_{1,y-z}^T & \vec{p}_{2,y-z}^T \end{bmatrix}^T \in \Omega_{d,y-z}$, respectively.

The differentiation of each of the diagonal elements of the matrix $\dfrac{\partial^2 \psi_{x-z}(\vec{p}_{1,x-z}, \vec{p}_{2,x-z})}{\partial \begin{bmatrix} \vec{p}_{1,x-z}^T & \vec{p}_{2,x-z}^T \end{bmatrix}^{T,2}}$ w.r.t. each position are calculated in the following equations

$$\frac{\partial^2 \psi_{x-z}(\vec{p}_{1,x-z}, \vec{p}_{2,x-z})}{\partial x_1^2} = k_{p,1} > 0 \tag{E.1}$$

$$\frac{\partial^2 \psi_{x-z}(\vec{p}_{1,x-z}, \vec{p}_{2,x-z})}{\partial z_1^2} = k_{p,1} > 0 \tag{E.2}$$

$$\frac{\partial^2 \psi_{x-z}(\vec{p}_{1,x-z}, \vec{p}_{2,x-z})}{\partial x_2^2} = k_{p,2} > 0 \tag{E.3}$$

$$\frac{\partial^2 \psi_{x-z}(\vec{p}_{1,x-z}, \vec{p}_{2,x-z})}{\partial z_2^2} = k_{p,2} > 0 \tag{E.4}$$

The differentiation of each of the diagonal elements of the matrix $\frac{\partial^2 \psi_{y-z}\left(\vec{p}_{1,y-z}, \vec{p}_{2,y-z}\right)}{\partial \begin{bmatrix} \vec{p}_{1,y-z}^T & \vec{p}_{2,y-z}^T \end{bmatrix}^{T,2}}$ w.r.t. each position are calculated in the following equations

$$\frac{\partial^2 \psi_{y-z}\left(\vec{p}_{1,y-z}, \vec{p}_{2,y-z}\right)}{\partial y_1^2} = k_{p,1} > 0 \tag{E.5}$$

$$\frac{\partial^2 \psi_{y-z}\left(\vec{p}_{1,y-z}, \vec{p}_{2,y-z}\right)}{\partial z_1^2} = k_{p,1} > 0 \tag{E.6}$$

$$\frac{\partial^2 \psi_{y-z}\left(\vec{p}_{1,y-z}, \vec{p}_{2,y-z}\right)}{\partial y_2^2} = \frac{k_{p,2}}{\left(y_2 - y_1\right)^2} > 0 \tag{E.7}$$

$$\frac{\partial^2 \psi_{y-z}\left(\vec{p}_{1,y-z}, \vec{p}_{2,y-z}\right)}{\partial z_2^2} = k_{p,2} > 0 \tag{E.8}$$

Using Corollary 5.2.1 and equations (E.1) through (E.4) and equations (E.5) through (E.8), the functions $\psi_{x-z}\left(\vec{p}_{1,x-z}, \vec{p}_{2,x-z}\right)$ and $\psi_{y-z}\left(\vec{p}_{1,y-z}, \vec{p}_{2,y-z}\right)$ are valid objective functions according to Definition 4.2.1. □

Bibliography

[Aghdam et al., 2016] Aghdam, A. S., Menhaj, M. B., Barazandeh, F., and Abdollahi, F. (2016). Cooperative load transport with movable load center of mass using multiple quadrotor uavs. In *2016 4th International Conference on Control, Instrumentation, and Automation (ICCIA)*, pages 23–27. IEEE.

[Aguilar-Ibañez, 2017] Aguilar-Ibañez, C. (2017). Stabilization of the pvtol aircraft based on a sliding mode and a saturation function. *International Journal of Robust and Nonlinear Control*, 27(5):843–859.

[Aguilar-Ibanez et al., 2019] Aguilar-Ibanez, C., Sira-Ramirez, H., Suarez-Castanon, M. S., and Garrido, R. (2019). Robust trajectory-tracking control of a pvtol under crosswind. *Asian Journal of Control*.

[Aguilar-Ibañez et al., 2018] Aguilar-Ibañez, C., Suarez-Castanon, M. S., Mendoza-Mendoza, J., de Jesus Rubio, J., and Martínez-García, J. C. (2018). Output-feedback stabilization of the pvtol aircraft system based on an exact differentiator. *Journal of Intelligent & Robotic Systems*, pages 1–12.

[ASME, 2013] ASME, editor (2013). *Avian-Inspired Grasping for Quadrotor Micro UAVs*, volume Volume 6A: 37th Mechanisms and Robotics Conference of *International Design Engineering Technical Conferences and Computers and Information in Engineering Conference*. ASME. V06AT07A014.

[Augugliaro and D'Andrea, 2013] Augugliaro, F. and D'Andrea, R. (2013). Admittance control for physical human-quadrocopter interaction. In *2013 European Control Conference (ECC)*, pages 1805–1810. IFAC.

[Backus et al., 2014] Backus, S. B., Odhner, L. U., and Dollar, A. M. (2014). Design of hands for aerial manipulation: Actuator number and routing for grasping and perching. In *2014 IEEE/RSJ International Conference on Intelligent Robots and Systems*, pages 34–40. IEEE.

[Bai et al., 2011] Bai, H., Arcak, M., and Wen, J. (2011). *Cooperative control design: a systematic, passivity-based approach*. Springer Science & Business Media.

[Belokon et al., 2019] Belokon, S., Derishev, D., Zolotukhin, Y. N., Nesterov, A., and Filippov, M. (2019). Control of hybrid unmanned aerial vehicle motion in transitional modes. *Optoelectronics, Instrumentation and Data Processing*, 55(4):346–355.

[Byrnes et al., 1991] Byrnes, C. I., Isidori, A., and Willems, J. C. (1991). Passivity, feedback equivalence, and the global stabilization of minimum phase nonlinear systems. *IEEE Transactions on automatic control*, 36(11):1228–1240.

[Cano et al., 2013] Cano, R., Pérez, C., Pruano, F., Ollero, A., and Heredia, G. (2013). Mechanical design of a 6-dof aerial manipulator for assembling bar structures using uavs. In *2nd RED-UAS 2013 workshop on research, education and development of unmanned aerial systems*, volume 218. ARCAS.

[Carino et al., 2015] Carino, J., Abaunza, H., and Castillo, P. (2015). Quadrotor quaternion control. In *Unmanned Aircraft Systems (ICUAS), 2015 International Conference on*, pages 825–831. IEEE.

[Castillo et al., 2005] Castillo, P., Lozano, R., and Dzul, A. E. (2005). The pvtol aircraft. In *Modelling and Control of Mini-Flying Machines*, pages 23–37. Springer London, London.

[Chen, 1998] Chen, C.-T. (1998). *Linear system theory and design*. Oxford University Press, Inc.

[Cronin, 2019] Cronin, W. E. (2019). Aerodynamic analysis of a fixed rotor hybrid vtol uav in transitional flight using cfd. *The UNSW Canberra at ADFA Journal of Undergraduate Engineering Research*, 12(2).

[Cruz and Fierro, 2014] Cruz, P. and Fierro, R. (2014). Autonomous lift of a cable-suspended load by an unmanned aerial robot. In *2014 IEEE Conference on Control Applications (CCA)*, pages 802–807. IEEE.

[Cruz and Fierro, 2017] Cruz, P. J. and Fierro, R. (2017). Cable-suspended load lifting by a quadrotor uav: hybrid model, trajectory generation, and control. *Autonomous Robots*, 41(8):1629–1643.

[Danko and Oh, 2013] Danko, T. W. and Oh, P. Y. (2013). A hyper-redundant manipulator for mobile manipulating unmanned aerial vehicles. In *2013 International Conference on Unmanned Aircraft Systems (ICUAS)*, pages 974–981. IEEE.

[Dorf and Bishop, 2011] Dorf, R. C. and Bishop, R. H. (2011). *Modern control systems*. Pearson.

[Foehn et al., 2017] Foehn, P., Falanga, D., Kuppuswamy, N., Tedrake, R., and Scaramuzza, D. (2017). Fast trajectory optimization for agile quadrotor maneuvers with a cable-suspended payload. In *Robotics: Science and Systems*, pages 1–10. NCCR.

[Gabellieri et al., 2018] Gabellieri, C., Tognon, M., Pallottino, L., and Franchi, A. (2018). A study on force-based collaboration in flying swarms. In *International Conference on Swarm Intelligence*, pages 3–15. Springer.

[Garcia et al., 2006] Garcia, P. C., Lozano, R., and Dzul, A. E. (2006). *Modelling and control of mini-flying machines*. Springer Science & Business Media.

[Guerrero et al., 2015] Guerrero, M. E., Mercado, D., Lozano, R., and García, C. (2015). Passivity based control for a quadrotor uav transporting a cable-suspended payload with minimum swing. In *2015 54th IEEE Conference on Decision and Control (CDC)*, pages 6718–6723. IEEE.

[Heredia et al., 2019] Heredia, G., Cano, R., Jimenez-Cano, A., and Ollero, A. (2019). *Modeling and Design of Multirotors with Multi-joint Arms*, pages 15–33. Springer International Publishing, Cham.

[Hernández-Castañeda et al., 2018] Hernández-Castañeda, F., Santibáñez, V., and Jurado, F. (2018). Priority altitude pvtol aircraft control via immersion and invariance. *International Journal of Control*, pages 1–12.

[Joshi et al., 2019] Joshi, A., Tripathi, A., and Ponnalgu, R. (2019). Modelling and design of a hybrid aerial vehicle combining vtol capabilities with fixed wing aircraft. In *2019 6th International Conference on Instrumentation, Control, and Automation (ICA)*, pages 47–51. IEEE.

[Khalil, 2002] Khalil, H. (2002). *Nonlinear Systems*. Prentice Hall, third edition edition.

[Khalil, 2015] Khalil, H. K. (2015). *Nonlinear control*. Pearson New York.

[Khamseh et al., 2018] Khamseh, H. B., Janabi-Sharifi, F., and Abdessameud, A. (2018). Aerial manipulation-a literature survey. *Robotics and Autonomous Systems*, 107:221 – 235.

[Kim et al., 2013] Kim, S., Choi, S., and Kim, H. J. (2013). Aerial manipulation using a quadrotor with a two dof robotic arm. In *2013 IEEE/RSJ International Conference on Intelligent Robots and Systems*, pages 4990–4995. IEEE.

[libre AIR, 2019] libre AIR, F. (2019). Fl-air - framework libre air. `https://devel.hds.utc.fr/software/flair/wiki`. Accessed: 2019-12-28.

[Lozano et al., 2013] Lozano, R., Brogliato, B., Egeland, O., and Maschke, B. (2013). *Dissipative systems analysis and control: theory and applications*. Springer Science & Business Media.

[Manubens et al., 2013] Manubens, M., Devaurs, D., Ros, L., and Cortés, J. (2013). Motion planning for 6-d manipulation with aerial towed-cable systems. In *Robotics: Science and Systems (RSS)*, page 8p. Robotics: Science and Systems (RSS).

[Masone et al., 2016] Masone, C., Bülthoff, H. H., and Stegagno, P. (2016). Cooperative transportation of a payload using quadrotors: A reconfigurable cable-driven parallel robot. In *2016 IEEE/RSJ International Conference on Intelligent Robots and Systems (IROS)*, pages 1623–1630. IEEE.

[Maza et al., 2009] Maza, I., Kondak, K., Bernard, M., and Ollero, A. (2009). Multi-uav cooperation and control for load transportation and deployment. In *Selected papers from the 2nd International Symposium on UAVs, Reno, Nevada, USA June 8–10, 2009*, pages 417–449. Springer.

[Mellinger et al., 2011] Mellinger, D., Lindsey, Q., Shomin, M., and Kumar, V. (2011). Design, modeling, estimation and control for aerial grasping and manipulation. In *2011 IEEE/RSJ International Conference on Intelligent Robots and Systems*, pages 2668–2673. IEEE.

[Mellinger et al., 2013] Mellinger, D., Shomin, M., Michael, N., and Kumar, V. (2013). Cooperative grasping and transport using multiple quadrotors. In *Distributed autonomous robotic systems*, pages 545–558. Springer.

[Munoz et al., 2010] Munoz, L. E., Santos, O., and Castillo, P. (2010). Robust nonlinear real-time control strategy to stabilize a pvtol aircraft in crosswind. In *2010 IEEE/RSJ International Conference on Intelligent Robots and Systems*, pages 1606–1611. IEEE.

[Nikou et al., 2015] Nikou, A., Gavridis, G. C., and Kyriakopoulos, K. J. (2015). Mechanical design, modelling and control of a novel aerial manipulator. In *2015 IEEE International Conference on Robotics and Automation (ICRA)*, pages 4698–4703. IEEE.

[Notter et al., 2016] Notter, S., Heckmann, A., Mcfadyen, A., and Gonzalez, F. (2016). Modelling, simulation and flight test of a model predictive controlled multirotor with heavy slung load. *IFAC-PapersOnLine*, 49(17):182 – 187. 20th IFAC Symposium on Automatic Control in AerospaceACA 2016.

[OptiTrack, 2019] OptiTrack (2019). Optitrack - motion capture systems. `https://optitrack.com/`. Accessed: 2019-12-28.

[Orsag et al., 2014] Orsag, M., Korpela, C. M., Bogdan, S., and Oh, P. Y. (2014). Hybrid adaptive control for aerial manipulation. *Journal of Intelligent & Robotic Systems*, 73(1):693–707.

[Parrot©, 2019] Parrot© (2019). Parrot ar.drone 2.0 elite edition. `https://www.parrot.com/us/drones/parrot-ardrone-20-elite-edition`. Accessed: 2019-12-28.

[Pereira et al., 2016] Pereira, P. O., Herzog, M., and Dimarogonas, D. V. (2016). Slung load transportation with a single aerial vehicle and disturbance removal. In *2016 24th Mediterranean Conference on Control and Automation (MED)*, pages 671–676. IEEE.

[Puga et al., 2015] Puga, S., Bonilla, M., Moog, C. H., Malabre, M., and Lozano, R. (2015). Singularly perturbed feedback linearization for siso nonlinear systems with measurement of the state. In *2015 European Control Conference (ECC)*, pages 3250–3255. IEEE.

[Qu, 2009] Qu, Z. (2009). Cooperative control of dynamical systems: applications to autonomous vehicles. In *Cooperative control of dynamical systems: applications to autonomous vehicles*, chapter 5, page 202. Springer Science & Business Media.

[Ramon Soria et al., 2019] Ramon Soria, P., Arrue, B. C., and Ollero, A. (2019). A 3d-printable docking system for aerial robots: Controlling aerial robotic manipulators in outdoor industrial applications. *IEEE Robotics Automation Magazine*, 26(1):44–53.

[Rezaee and Abdollahi, 2013] Rezaee, H. and Abdollahi, F. (2013). A decentralized cooperative control scheme with obstacle avoidance for a team of mobile robots. *IEEE Transactions on Industrial Electronics*, 61(1):347–354.

[Ruggiero et al., 2018] Ruggiero, F., Lippiello, V., and Ollero, A. (2018). Aerial manipulation: A literature review. *IEEE Robotics and Automation Letters*, 3(3):1957–1964.

[SAYYAADI and SOLTANI, 2018] SAYYAADI, H. and SOLTANI, A. (2018). Modeling and control for cooperative transport of a slung fluid container using quadrotors. *Chinese Journal of Aeronautics*, 31(2):262 – 272.

[Shirani et al., 2019] Shirani, B., Najafi, M., and Izadi, I. (2019). Cooperative load transportation using multiple uavs. *Aerospace Science and Technology*, 84:158 – 169.

[Sreenath and Kumar, 2013] Sreenath, K. and Kumar, V. (2013). Dynamics, control and planning for cooperative manipulation of payloads suspended by cables from multiple quadrotor robots. *rn*, 1(r2):r3.

[Suarez et al., 2015] Suarez, A., Heredia, G., and Ollero, A. (2015). Lightweight compliant arm for aerial manipulation. In *2015 IEEE/RSJ International Conference on Intelligent Robots and Systems (IROS)*, pages 1627–1632. IEEE.

[Suarez et al., 2019] Suarez, A., Heredia, G., and Ollero, A. (2019). *Compliant Aerial Manipulators with Dual Arms*, pages 83–95. Springer International Publishing, Cham.

[Tagliabue et al., 2019] Tagliabue, A., Kamel, M., Siegwart, R., and Nieto, J. (2019). Robust collaborative object transportation using multiple mavs. *The International Journal of Robotics Research*.

[Tagliabue et al., 2017] Tagliabue, A., Kamel, M., Verling, S., Siegwart, R., and Nieto, J. (2017). Collaborative transportation using mavs via passive force control. In *2017 IEEE International Conference on Robotics and Automation (ICRA)*, pages 5766–5773. IEEE.

[Thomas et al., 2014] Thomas, J., Loianno, G., Sreenath, K., and Kumar, V. (2014). Toward image based visual servoing for aerial grasping and perching. In *2014 IEEE International Conference on Robotics and Automation (ICRA)*, pages 2113–2118. IEEE.

[Tognon et al., 2018] Tognon, M., Gabellieri, C., Pallottino, L., and Franchi, A. (2018). Aerial co-manipulation with cables: The role of internal force for equilibria, stability, and passivity. *IEEE Robotics and Automation Letters*, 3(3):2577–2583.

[Valavanis and Vachtsevanos, 2015] Valavanis, K. P. and Vachtsevanos, G. J. (2015). Introduction to the handbook on uavs. *Handbook of Unmanned Aerial Vehicles*, pages 5–42.

[Valk and Keviczky, 2018] Valk, L. and Keviczky, T. (2018). Distributed control of heterogeneous underactuated mechanical systems. *IFAC-PapersOnLine*, 51(23):325 – 330. 7th IFAC Workshop on Distributed Estimation and Control in Networked Systems NECSYS 2018.

[Villani and De Schutter, 2016] Villani, L. and De Schutter, J. (2016). *Force Control*, pages 201–205. Springer Berlin Heidelberg, Berlin, Heidelberg.

[Willems, 1972a] Willems, J. (1972a). Dissipative dynamical systems-part 1: general theory. *Archive for mechanics analysis*, 45(5):321–351.

[Willems, 1972b] Willems, J. C. (1972b). Dissipative dynamical systems part ii: Linear systems with quadratic supply rates. *Archive for rational mechanics and analysis*, 45(5):352–393.

[Yu et al., 2019] Yu, P., Wang, Z., and Wong, K. (2019). Exploring aerial perching and grasping with dual symmetric manipulators and compliant end-effectors. *International Journal of Micro Air Vehicles*, 11:1756829319877416.